

**APPLICATION OF THE PHOTOACOUSTIC TECHNIQUE
FOR IMAGING AND THERMAL
CHARACTERISATION OF SOLID SAMPLES**

*Thesis submitted to the
COCHIN UNIVERSITY OF SCIENCE AND TECHNOLOGY
for the award of the degree of
DOCTOR OF PHILOSOPHY*

By
A. A. SUDHAKARAN

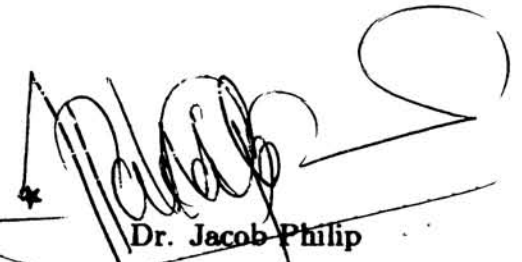
**DEPARTMENT OF PHYSICS
COCHIN UNIVERSITY OF SCIENCE AND TECHNOLOGY
COCHIN - 682 022, INDIA**

DECEMBER 1996

CERTIFICATE

Certified that the work presented in this thesis is based on the bona fide work done by Mr. A. A. Sudhakaran under my guidance in the Department of Physics, Cochin University of Science and Technology, and has not been included in any other thesis submitted previously for the award of any degree.

Kochi 682022
12th December 1996


Dr. Jacob Philip
Supervising Guide

INSTRUMENTATION
OF
DEPARTMENT
OF
Cochin University of Science & Technology
Kochi-682 022

DECLARATION

Certified that the work presented in this thesis is based on the original work done by me under the guidance of Dr. Jacob Philip, Professor and Head, Department of Instrumentation, Cochin University of Science and Technology, and has not been included in any other thesis submitted previously for the award of any degree.

Kochi 682022
12th December 1996


A. A. Sudhakaran

PREFACE

The photoacoustic/ photothermal technique is recognised as a sensitive and convenient method to determine optical and thermal properties of solid samples. It is also a convenient spectroscopic technique with significantly larger detection sensitivity compared to conventional techniques. Recently, the technique is being applied to do microscopy as well as imaging. The power of the technique lies in the fact that it detects the radiation absorbed by the sample and can be adopted to samples in any form. The technique works well for samples in the gaseous, liquid as well as solid forms of matter. It has also been used to investigate thermodynamic changes such as phase transitions in materials as well as in calorimetry.

The photoacoustic (PA) effect is the generation of an acoustic signal in an enclosed volume when a sample, kept inside the volume, is irradiated by an intensity modulated beam of radiation. The radiation absorbed by the sample is converted into thermal waves by nonradiative deexcitation processes. The propagating thermal waves cause a corresponding expansion and contraction of the gas medium surrounding the sample, which in turn can be detected as sound waves by a sensitive microphone. These sound waves have the same frequency as the initial modulation frequency of light. Lock-in detection method enables one to have a sufficiently high signal to noise ratio for the detected signal. The PA signal amplitude depends on the optical absorption coefficient of the sample and its thermal properties. The PA signal phase is a function of the thermal diffusivity of the sample. Measurement of the PA amplitude and phase enables one to get very valuable information about the optical and thermal properties of the sample.

Since the PA signal amplitude and phase depend on the thermal properties of the sample, any variation in thermal conductivity within any region in the sample should get reflected in the output PA signal. This fact is the basic principle behind using photoacoustic effect for imaging and nondestructive testing of solid samples. Photoacoustic

surface imaging and depth profiling lead to estimation of surface and subsurface features of solid samples. We have carried out systematic investigations on the use of the photoacoustic technique in surface imaging and depth profiling of solid samples. The details of the experimental work done and the results obtained are given in this thesis.

The photoacoustic technique has emerged of late as a convenient method to determine thermal parameters such as thermal conductivity, diffusivity and effusivity of solid samples. The established techniques involve a frequency analysis of the photoacoustic amplitude or phase. We have developed a new photoacoustic scanning technique to undertake thermal effusivity measurements. The technique can be adopted to measure thermal effusivity of samples in the thin film form as well. Details of the method, theoretical background, experimental details, and results are given in the thesis.

In the following paragraphs, we give a chapter wise description of the contents of the thesis.

An overall introduction to various aspects of the photoacoustic technique is given in chapter 1. An outline of the Rosencwaig- Gersho theory, which is a well established and tested theory of the photoacoustic phenomenon, is outlined in this chapter. Applications of the method in spectroscopy, optical and thermal characterisation of solid samples, microscopy and imaging are outlined. All the important works done so far in this area are cited and references given. The existing techniques for measuring thermal parameters such as thermal conductivity, diffusivity and effusivity are also outlined in this chapter.

The second chapter of the thesis describes the details of the instrumentation developed by us for carrying out the work described in the subsequent chapters of the thesis. We have designed and fabricated a microprocessor based two dimensional scanning unit for photoacoustic scanning of solid surfaces. The technical details of the hardware, software and mechanical assembly are outlined. We have designed and fabricated a room temperature photoacoustic cell in which the sample can be kept and

scanned. Its details are also given in this chapter.

Photoacoustic imaging technique has been applied to silicon wafer, nylon disc, brass disc and teflon disc samples in which surface scratches and buried voids have been artificially made to test the power of the photoacoustic technique as a nondestructive testing method. The details of the experiment, results obtained and a discussion of the results are given in chapter 3 of the thesis. We have carried out systematic and extensive experiments on the use of the photoacoustic technique in depth profiling of solid samples. The method has been applied to solid multilayer sample made with silicon and brass. We have systematically studied the influence of interfaces on photoacoustic amplitude and phase. Depth profiling is accomplished by varying the thermal thickness of the top layer by varying the chopping frequency. Details of the experiment and results obtained are outlined in chapter 4 of the thesis.

The fifth chapter of the thesis is devoted to a detailed description of the principle and theoretical background of the photoacoustic scanning method developed by us to determine the thermal parameters of solid samples. The method involves keeping the experimental sample in close contact with a reference sample and coating the top surfaces of both the samples with a light absorber film such as carbon black. As one optically scans the surface with a chopped beam of light, one can detect a distinct change in photoacoustic amplitude as well as phase as the backing is changed from the experimental sample to the reference sample. We have derived expressions for the photoacoustic amplitude ratio as well as phase difference for such an experimental situation and expressed them in terms of the thermal effusivities of the experimental and reference samples. It is shown that the thermal effusivity of the experimental sample can be determined if the effusivities of the reference sample and the absorbing layer are known.

We have carried out detailed experimentation on the technique described in chapter 5. Measurements have been carried out on a number of sample combinations pre-

pared with materials of various thermal parameters. It is found that the technique works very well. One distinct advantage of the technique is that measurements are carried out at a single modulation frequency. Details of the measurements, results obtained and discussion of the results are given in chapter 6 of the thesis.

In chapter 7, we demonstrate that the technique described in chapters 5 and 6 can very well be adapted to measure thermal effusivity of thin films. Obviously, the technique works only with light absorbing films. We have carried out measurements on polyacetal and different brands of black enamel paints coated in the form of thin film over a specific substrate with two regions made of different materials. Details of the measurements and the results obtained are outlined in this chapter.

In the last chapter we provide an overall conclusion to the work done in this thesis. Suggestions and scope for doing further work in this direction are also outlined in this chapter.

During the course of this work, the following papers have been published/ submitted for publication.

- (1) Photothermal imaging- An emerging nondestructive testing method (General article)
Phys. News **23**, 91- 96 (1993)
- (2) A microprocessor controlled scanning unit for photoacoustic imaging of solids,
J. Instrum. Soc. of India, **23** (3 & 4) 152- 157 (1995)
- (3) A photoacoustic scanning technique to measure thermal effusivity of solids,
Rev. Sci. Instrum. (in press)
- (4) Determination of thermal effusivity of solids by a photoacoustic scanning technique,
Pramana - J. Phys. (in press)

- (5) A one dimensional photoacoustic scanning technique to measure thermal effusivity of thin films,
Meas. Sci. & Tech. (UK) (submitted)
- (6) A photoacoustic scanning technique for thermal characterisation of solid samples,
Proc. of the 9th Int. Conf. on Photoacoustic and photothermal phenomena,
Nanjing, China, (June 1996)
- (7) A Photoacoustic scanning technique to determine thermal properties of thin/ thick films,
Proc. of the Int. Conf. on Instrumentation, 92 August 1996, Bangalore (Allied Pub. New Delhi 1996)

CONTENTS

Preface		i
Acknowledgment		vii
Chapter 1	The photoacoustic effect : An introduction	
1.1	A glimpse of the history of the photoacoustic effect	1
1.2	Principle and theory of photoacoustic effect	4
1.3	Application of the photoacoustic effect	14
1.3.1	Photoacoustic spectroscopy	14
1.3.2	PA monitoring of deexcitation processes	16
1.3.3	PA sensing of physical properties of materials	19
1.3.3.a	Photoacoustic imaging	20
1.3.3.b	PA depth profiling	20
1.3.4.c	PA microscopy	21
1.3.5.d	Thermal characterisation of solids	23
	References	26
Chapter 2	Instrumentation	
2.1	General aspects of the PA spectrometer	33
2.1.1	Source of radiation	33
2.1.2	Modulation	35

2.1.3	Photoacoustic cell	36
2.1.4	Acoustic detectors	38
2.1.5	Signal processing	39
2.2	Present experimental setup	39
2.2.1	Construction and standardisation of the PA cell	41
	Microprocessor controlled scanning unit	46
2.2.2.a	Mechanical assembly of the scanning unit	46
2.2.2.b	Description of the stepper motors and driving circuit	48
2.2.2.c	Description of microprocessor interfacing	51
2.2.2.c 1	Hardware	51
2.2.2.c 2	Software	56
2.3	Automated photoacoustic imaging unit	61
	References	63
Chapter 3	Photoacoustic imaging of solid samples	
3.1	Introduction	65
3.2	Experimental details	66
3.2a	PA imaging of silicon wafer samples	66
3.2a.1	Results and discussion	67
3.2b	PA imaging of nylon sample	69
3.2b.1	Results and discussion	75

3.2c	PA imaging of brass disc	77
3.2d	Subsurface PA imaging in teflon sample	77
3.3	Conclusion	81
	References	84
Chapter 4	Photoacoustic depth profiling in multilayer solid structure	
4.1	Introduction	86
4.2	Principle of the technique	87
4.3	Experimental method	89
4.4	Sample structure	91
4.5	Results and discussion	96
4.6	Conclusions	102
	References	103
Chapter 5	Thermal characterisation of solids by a photoacoustic scanning technique : Principle	
5.1	Introduction	104
5.2	Principle of the technique	106
5.3	Application of R-G theory to the present sample configuration	109
	References	123

Chapter 6	Thermal characterisation of solids by a PA scanning technique : Experiment	
6.1	Introduction	125
6.2	Sample preparation	125
6.3	Experimental method	127
6.4	Results	129
6.5	Discussion and conclusion	141
Chapter 7	A one dimensional photoacoustic scanning technique to measure thermal effusivity of thin films	
7.1	Introduction	143
7.2	Principle of the method	146
7.3	Experimental method	153
7.4	Results and discussion	155
7.5	Conclusions	164
	References	165
Chapter 8	Summary and conclusion	166
	Appendix 1	170

Chapter 1

THE PHOTOACOUSTIC EFFECT : AN INTRODUCTION

1.1 A glimpse of the history of the Photoacoustic effect

Photoacoustic effect refers to the generation of acoustic waves in a medium when it is irradiated by an intensity modulated optical radiation. In its broad sense, photoacoustics now covers the generation of acoustic waves or other thermoelastic waves by any type of energetic radiation, including electromagnetic radiation from radio frequency waves to X - rays, electrons and other particles. The effect was discovered by Alexandar Graham Bell[1] way back in 1880, who observed that audible sound was produced when chopped sun light was incident on light absorbing materials

In the nineteenth century itself, a few experiments were reported on liquids, but no attempt was made by the investigators to explain the mechanism of generation of photoacoustic signals in liquids. On the other hand, even though several attempts have been made to account for the phenomenon in solids, only recently a satisfactory quantitative theory could be formulated. But, one should not ignore the hypotheses of Mercadier[2] and Preece[3] in 1881, which came quite close to the present understanding of the photoacoustic effect. Mercadier[2], who also experimented with the photoacoustic effect, suggested that the sound originates from vibrating movements caused by the alternate heating and cooling produced by the intermittent radiation, principally in the gaseous layer adhering to the solid surface hit by the radiation. Preece[3] wrote that the photoacoustic effect is "purely an effect of radiant heat and it is essentially due to the changes of volume in vapors or gases produced by the degradation and absorption of this heat in a confined space".

No further experiments in photoacoustics were reported in the nineteenth century. This was mainly due to two reasons: first, the effect was considered just as an interesting physical phenomenon of no great scientific or practical value; second, the experiments were difficult to perform quantitatively, since no sensitive sound detectors were available at that time.

The photoacoustic effect lay completely dormant for nearly 50 years, until the advent of the microphone. In 1938, Viengerove[4] used photoacoustic effect for the study of infrared light absorption in gases and to evaluate concentrations of gaseous species in gas mixtures. He could measure CO_2 concentrations in N_2 down to $\approx 0.2\text{vol}\%$ using the technique. Measurement of concentration lower than this was limited both by the relatively low sensitivity of his microphone and by background absorption of incident radiation by cell windows and walls. A year later, Pfund[5] reported a gas analyser system for measuring concentrations of CO and CO_2 . Pfund's experiments were of additional interest because, instead of detecting pressure - volume changes with a microphone, he measured the corresponding changes in the gas temperature directly, using a thermopile shielded from the direct optical radiation.

In 1943 Luft[6] designed an automatically recording gas analyser which employed two photoacoustic cells in a differential configuration. One cell contained the gas mixture to be analysed, while the other contained the gas mixture minus the particular species of interest. In this instrument, therefore, the microphone output was proportional to the pressure difference between the two cells. Luft's differential analyzer had two major improvements over Viengrov's[4] original design. First, it minimized the signal due to background absorption in the cell windows and walls, since the same background signal was present in both the cells. Second, it permitted analysis of gas mixtures containing more than two species. This instrument had a sensitivity that

permitted measurement of CO_2 in N_2 down to a few parts per million as compared to Viengerov's early capability of only a few parts per thousand.

The strong rebirth of the photoacoustic effect in the years following 1938 was apparently limited entirely to gases. It was not until early 1970s, some 90 years after Bell's original discovery, that the phenomenon in nongaseous matter was rediscovered.

The renaissance of photoacoustic effect in the early 1970s with the advent of lasers and phase lock-in amplifier techniques opened the modern history of PA effect. The modern theory is still not complete, although considerable progress has been made during the past 20 years. According to the modern concept, thermal waves are generated in the sample due to nonradiative deexcitation of atoms, when the sample is irradiated by an intensity modulated beam of light[17]. The thermal waves possess a frequency that is the same as the frequency with which the incident beam of light is modulated. If the sample placed in an enclosed volume of gas is irradiated by a chopped beam of light, the thermal waves produced in the sample diffuses into the adhering layer of gas producing heating and cooling alternately. This alternate heating and cooling produces corresponding expansion and contraction of the gas layer. As a result acoustic waves are generated in the enclosed gas with the same frequency as that of the modulation frequency of the incident beam of light.

The basic physics of generation of photoacoustic and photothermal signals is the same, the only difference being in the method of detection. In photoacoustic effect the detection is performed by acoustic means whereas in photothermal effect the detection is by one of the thermal detection techniques.

Quantitative developments of photoacoustic or photothermal effects during the last two decads have made these effects suitable techniques for measuring optical

and thermal properties of solid samples. They also make convenient spectroscopic techniques with significantly larger detection sensitivities compared to their conventional counterparts. Nowadays the techniques are being used to do even microscopy as well as imaging. The power of these techniques lie in the fact that they detect the radiation absorbed by the sample in any form. The techniques work well for samples in the gaseous, liquid as well as solid forms of matter. They have also been used successfully to investigate thermodynamic changes such as phase transitions in materials as well as in calorimetry.

1.2 Principle and theory of photoacoustic effect in solids

As has been mentioned already, several theoretical explanations for photoacoustic (PA) effect have been put forward in the nineteenth century itself. But the present explanation of the PA effect in solids is based on modern theories developed during the 1970s. The evolution of modern theory started with the attempt of Parker[8] in 1973. He developed a theory to give a quantitative explanation for the PA signal emanating from the cell windows while conducting photoacoustics experiments in gases. Later, Rosencwaig and Gersho[9,10] put forward a more general theory for PA effect in solid samples. This theory has been found to be very successful in interpreting most of the experimental results. According to Rosencwaig - Gersho (R-G) theory, the PA signal produced in a gas - microphone PA cell depends both on the generation of pressure disturbance at the sample - gas interface and on the transport of this pressure disturbance through the gas to the microphone. The pressure disturbance at the sample - gas interface is the result of periodic heat flow from the sample to adjoining gas layer as determined by thermal diffusion equations. The R - G theory gives an exact equation for the amplitude and phase of the PA signal as a function of the optical, thermal and geometrical properties of the sample, the cell and the gas within the cell. Although the

R-G theory do have certain limitations, it is found to be very successful in interpreting most of the experimental results[11- 15]. We have followed R-G theory as the basic theory for interpreting our experimental findings described in this thesis. Therefore, we think it is necessary to give a brief outline of the R - G theory here.

The R - G theory is a one dimensional analysis of the production of photoacoustic signal based on thermal diffusion equation in the sample, the backing material and surrounding gas in a simple cylindrical cell as shown in Fig. 1.1. The cell has a diameter D and length L. It is assumed that the length L is small compared to the wavelength of the acoustic signal. A microphone (not shown in the figure) is used to detect the acoustic signal produced in the cell. The solid sample is assumed to be in the form of a disc of diameter D and thickness l_s . The sample is mounted on a poor thermal conductor of thickness l_b which acts as a backing. The length of the gas column in the cell is represented by l_g . In the sample geometry under consideration, it is assumed that the gas and the backing material do not absorb light.

The following physical parameters of the sample, backing material and the gas medium have an important role in the theoretical formulation.

k : the thermal conductivity ($Cal\ cm^{-1}secs^{-1}\ deg\ C^{-1}$)

ρ : the density ($gm\ cm^{-3}$)

C : specific heat ($Cal\ gm^{-1}$)

$\alpha = k/\rho C$: the thermal diffusivity (cm^2secs^{-1})

$a = (\omega/2\alpha)^{1/2}$: the thermal diffusion coefficient (cm^{-1}) where ω (sec^{-1}) is the modulation frequency (angular)

$\mu = 1/a$: the thermal diffusion length (cm)

β : the optical absorption coefficient.

The suffixes s, b and g refer to the sample, the backing medium and the gas in front of

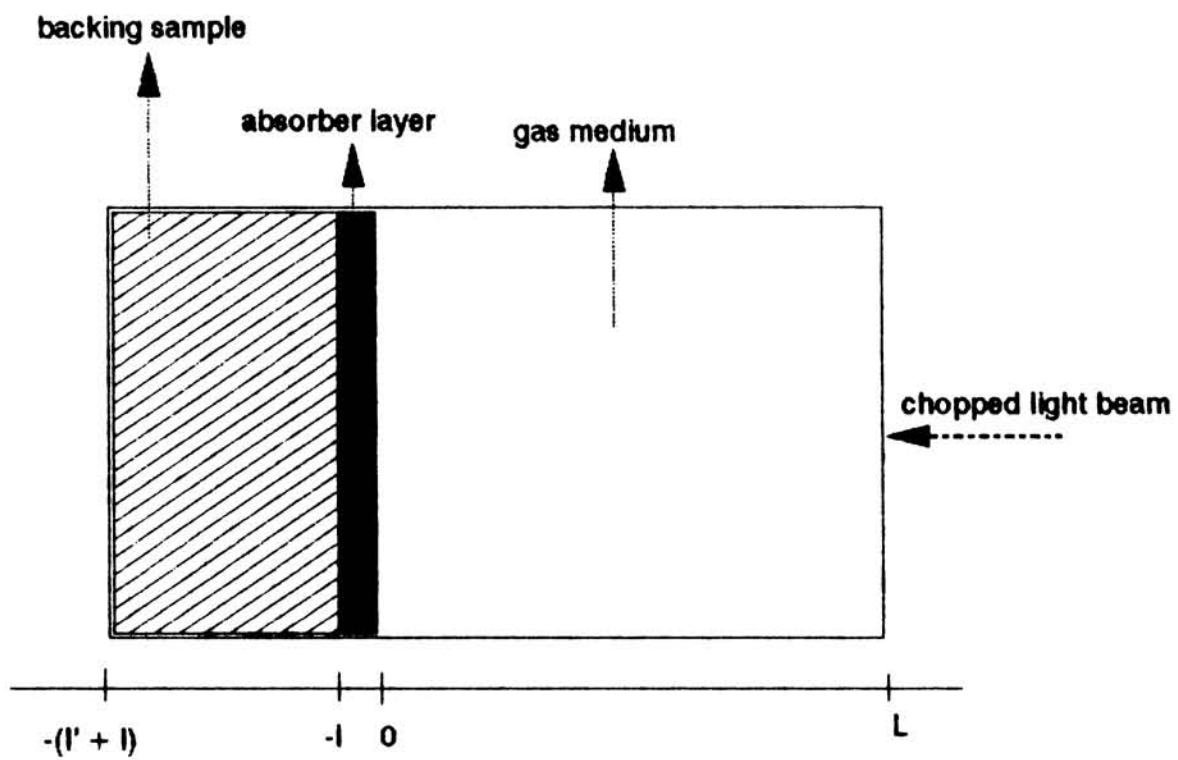


Fig 1.1 : Configuration of a cylindrical sample cell

the sample respectively.

The intensity of the sinusoidally chopped beam of monochromatic light with wavelength λ incident on the sample can be expressed as

$$I = \frac{1}{2} I_0 (1 + \cos \omega t) \quad (1.1)$$

where I_0 is the incident light flux ($W\text{ cm}^{-2}$) and ω is the chopping frequency in rad sec^{-1} . The density of heat produced at a point x within the sample due to absorption of light at this point is given by

$$H = \frac{1}{2} \beta I_0 e^{\beta x} (1 + \cos \omega t) \quad (1.2)$$

where x is negative since the solid extends from $x = 0$ to $x = -l_s$ (see Fig. 1.1).

The thermal diffusion equation in the solid, taking into account the distributed heat source, can be written as

$$\frac{\partial^2 \theta}{\partial x^2} = \frac{1}{\alpha_s} \frac{\partial \theta}{\partial t} - A e^{\beta x} (1 + e^{i\omega t}) \quad (1.3)$$

$$\text{for } -l_s \leq x \leq 0$$

where $A = \beta I_0 \eta / 2k_s$, θ is the temperature and η is the efficiency with which the absorbed light is converted into heat by nonradiative deexcitation process. The value of η is assumed to be unity in the calculations that follow. The thermal diffusion equations for the backing material and the gas are given, respectively, by

$$\frac{\partial^2 \theta}{\partial x^2} = \frac{1}{\alpha_b} \frac{\partial \theta}{\partial t} \quad (1.4)$$

$$\text{for } -l_b - l_s \leq x \leq -l_s$$

$$\frac{\partial^2 \theta}{\partial x^2} = \frac{1}{\alpha_g} \frac{\partial \theta}{\partial t} \quad (1.5)$$

$$\text{for } 0 \leq x \leq l_g$$

The real parts of the complex valued solutions $\theta(x, t)$ of equation (1.3) to (1.5) are the solutions of physical interest and represent the temperature in the cell relative to ambient temperature as a function of position and time. The general solution of $\theta(x, t)$ in the cell, neglecting transients, can be written as

$$\begin{aligned} & l_b(x + l_s + l_b)W_0 + We^{\sigma_b(x+l_s)}e^{kx} && \text{for } -l_s - l_b \leq x \leq -l_s \\ \theta(x, t) = & b_1 + b_2x + b_3e^{\beta x} + (Ue^{\sigma_s x} + Ve^{-\sigma_s x} - Ee^{\beta x})e^{kx} && \text{for } -l_s \leq x \leq 0 \quad (1.6) \\ & (1 - x/l_g)F + \theta_0 e^{-\sigma_s x} e^{kx} && \text{for } 0 \leq x \leq l_g \end{aligned}$$

where W, U, V, E and θ are complex valued constants, b_1, b_2, b_3, W_0 and F are real valued constants and $\sigma = (1 + i)a$. θ_0 and W represent the complex amplitude of periodic temperatures at the sample - gas boundary ($x = 0$) and the sample - backing boundary respectively. The terms b_3 and E are determined by the forcing function in equation (1.3) and are given by

$$b_3 = -A/\beta^2 \quad (1.7)$$

$$E = \frac{A}{(\beta^2 - \sigma_s^2)} = \frac{\beta I_0}{2k_s(\beta^2 - \sigma_s^2)} \quad (1.8)$$

By applying the appropriate boundary conditions, all the constants of equation (1.6) and hence the d.c and a.c components of the solution can be obtained. Then the explicit solution for θ , the complex amplitude of the periodic temperature at the solid - gas boundary ($x = 0$), is given by

$$\theta_0 = \frac{\beta I_0}{2k_s(\beta^2 - \sigma_s^2)} \left[\frac{(r-1)(b+1)e^{\sigma_s l_s} - (r+1)(b-1)e^{-\sigma_s l_s} + 2(b-r)e^{-\beta l_s}}{(g+1)(b+1)e^{\sigma_s l_s} - (g-1)(b-1)e^{-\sigma_s l_s}} \right] \quad (1.9)$$

where

$$b = \frac{k_b a_b}{k_s a_s} \quad (1.10)$$

$$g = \frac{k_g a_g}{k_s a_s} \quad (1.11)$$

$$r = (1 - i) \frac{\beta}{2a_s} \quad (1.12)$$

The acoustic signal originates from the periodic heat flow from the solid sample to the surrounding gas medium. This periodic heat flow causes a periodic temperature fluctuation in the gas as given by the sinusoidal (a.c) component of solution (1.6),

$$\theta_{a.c}(x, t) = \theta_0 e^{-\sigma_s x} e^{i\omega t} \quad (1.13)$$

The actual physical temperature variation in the gas medium is given by the real part of eq. (1.13) as

$$T_{a.c}(x, t) = e^{-\sigma_s x} [\theta_1 \cos(\omega t - a_s x) - \theta_2 \sin(\omega t - a_s x)] \quad (1.14)$$

where θ_1 and θ_2 are the real and imaginary parts of θ_0 , as given by eq. (1.9)

Since the periodic temperature variation in the gas is effectively fully damped out at a distance of $2\pi\mu_g$, only the boundary layer of the gas having thickness upto $2\pi\mu_g$ is capable of responding thermally to the periodic temperature at the surface of the sample. This boundary layer of gas expands and contracts periodically, thus acting as an acoustic piston on the rest of the gas column. The displacement of this gas piston can be estimated as

$$\delta x(t) = 2\pi\mu_g \frac{\bar{\theta}(t)}{T_0} = \frac{\theta_0 \mu_0}{\sqrt{2} T_0} e^{i(\omega t - \pi/4)} \quad (1.15)$$

Here $\bar{\theta}(t)$ is the spatially averaged temperature of the gas within the boundary layer given by

$$\bar{\theta}(t) = \frac{1}{2\pi\mu_g} \int_0^{2\pi\mu_g} \theta_{a.c}(x, t) dx \approx \frac{1}{2\sqrt{2}\pi} \theta_0 e^{i(\omega t - \pi/4)} \quad (1.16)$$

If we assume that the rest of the gas responds to the acoustic piston adiabatically, then the acoustic pressure in the cell due to the displacement of the piston is

derived from the adiabatic gas law,

$$PV^\gamma = \text{constant}$$

where P is the pressure, V is the gas volume in the cell and γ is the ratio of the specific heats of the gas. Therefore the incremental pressure is given by

$$\delta P(t) = \frac{\gamma P_0}{V_0} \delta V = \frac{\gamma P_0}{l_g} \delta x(t) \quad (1.17)$$

where P_0 and V_0 are the ambient pressure and volume respectively and δV is the incremental volume. Substituting for $\delta x(t)$ from eq. (1.15),

$$\delta P(t) = Q e^{(\omega t - \pi/4)} \quad (1.18)$$

where

$$Q = \frac{\gamma P_0 \beta_0}{\sqrt{2} l_g a_g T_0} \quad (1.19)$$

The real part of $\delta P(t)$ represents the actual physical pressure variation $\Delta P(t)$ as

$$\Delta P(t) = Q_1 \text{Cos}(\omega t - \pi/4) - Q_2 \text{Sin}(\omega t - \pi/4) \quad (1.20)$$

or

$$\Delta P(t) = q \text{Cos}(\omega t - \psi - \pi/4) \quad (1.21)$$

where Q_1 and Q_2 are the real and imaginary parts of Q , and q and ψ are the amplitude and phase of Q respectively, that is

$$Q = Q_1 + iQ_2 = q e^{i\psi} \quad (1.22)$$

Thus Q specifies the complex envelope of the sinusoidal pressure variation, and the explicit formula for Q is obtained by combining eq.(1.9) and (1.19) as

$$Q = \frac{\beta l_0 \gamma P_0}{2\sqrt{2} T_0 k_s l_g a_g (\beta^2 - \sigma^2)} \left[\frac{(r-1)(b+1)e^{\sigma l_0} - (r+1)(b-1)e^{-\sigma l_0} + 2(b-r)e^{-\beta l_0}}{(g+1)(b-1)e^{\sigma l_0} - (g-1)(b+1)e^{-\sigma l_0}} \right] \quad (1.23)$$

Special cases:

The complicated expression given above can be made simple by considering the following special cases. These case are arrived at on the basis of relative magnitudes of the optical absorption length $l = 1/\beta$, the thermal diffusion length μ_s and thickness l_s of the sample respectively. It is also assumed that $k_g a_g \leq k_b a_b$ and $k_b a_b \approx k_s a_s$. Moreover, it is convenient to define the constant

$$Y = \frac{\gamma P_0 I_0}{2\sqrt{2} T_0 l_g} \quad (1.24)$$

Case 1: Optically transparent solids ($l > l_s$)

In this case the light is absorbed throughout the length of the sample and also some light is transmitted through the sample. Here, depending upon thermal diffusion length three separate cases can be considered as follows:

Case 1a: Thermally thin solids ($\mu_s \gg l_s$; $\mu_s > l_g$)

Assuming $e^{-\beta l_s} \approx 1 - \beta l_s$, $e^{\pm \sigma_s l_s} \approx 1$ and $|r| > 1$ in eqn. (1.23), the expression for Q reduces to

$$Q = \frac{(1-i)\beta l_s}{2a_g} (\mu_b/k_b) Y \quad (1.25)$$

The acoustic signal is proportional to βl_s and it has an ω^{-1} dependence.

Case 1b: Thermally thin solids ($\mu_s > l_s$; $\mu_s < l_g$)

Setting $e^{\beta l_s} \approx (1 - \beta l_s)$, $e^{\pm \sigma_s l_s} \approx (1 + \sigma_s l_s)$ and $|r| < 1$, the expression for Q becomes

$$Q = \frac{(1-i)\beta l_s}{2a_g} (\mu_b/k_b) Y \quad (1.26)$$

Here also the acoustic signal varies directly with βl_s and has ω^{-1} dependence. That is, in above two cases, the thermal properties of the backing material come into play in the

expression for Q .

Case 1c: Thermally thick solids ($\mu_s < l_s$; $\mu_s \ll l_\beta$)

Here one can assume $e^{-\beta l_s} \approx (1 - \beta l_s)$, $e^{-\sigma l_s} \approx 0$ and $|r| \ll 1$. Then the expression for Q reduces to

$$Q = \frac{-i\beta\mu_s}{2a_g}(\mu_s/k_s)Y \quad (1.27)$$

In this equation the acoustic signal is proportional to $\beta\mu_s$. Therefore only the light absorbed within the first thermal diffusion length contributes to the signal. In this case the signal has got an $\omega^{-3/2}$ frequency dependence.

Case 2: Optically opaque solids ($l_\beta \ll l_s$)

In this case most of the light is absorbed within a distance that is small compared to the thickness l_s of the sample. Here also, depending upon the thermal diffusion length, three separate cases can be considered as follows.

Case 2a: Thermally thin solids ($\mu_s \gg l_s$; $\mu_s \gg l_\beta$)

Admitting the approximations $e^{\beta l_s} \approx 0$, $e^{\pm\sigma l_s} \approx 1$ and $|r| \gg 1$ in eqn(1.23), we get

$$Q = \frac{(1-i)}{2a_g}(\mu_b/k_b)Y \quad (1.28)$$

Here, the acoustic signal is independent of the absorption coefficient and varies as ω^{-1} . This would be the case applicable to a very good absorber such as carbon black.

Case 2b: Thermally thick solids ($\mu_s < l_s$; $\mu_s > l_g$)

Setting $e^{-\beta_s} \approx 0$, $e^{-\sigma_s l_s} \approx 0$ and $|r| > 1$, we have

$$Q = \frac{(1-i)}{2a_g} (\mu_s/k_s) Y \quad (1.29)$$

Here also, the acoustic signal is independent of the absorption coefficient β and varies as ω^{-1} .

Case 2c: Thermally thick solids ($\mu_s \ll l_s$; $\mu_s \gg l_g$)

Applying the approximations $e^{-\beta_s} \approx 0$, $e^{-\sigma_s l_s} \approx 0$ and $|r| < 1$ in equation (1.23), we get

$$Q = \frac{-i\beta\mu_s}{2a_g} (\mu_s/k_s) Y \quad (1.30)$$

This is a very important and interesting case because even though the sample is optically opaque it is not photoacoustically opaque as long as $\mu_s < l_g$, that is, the PA signal is proportional to β . The signal is also dependent on the thermal properties of the sample and varies as $\omega^{-3/2}$.

The R-G theory as discussed in equation (1.23) to (1.30) has successfully been verified by several subsequent workers [16-18]. After the formulation of the R-G theory several improvements have been made on it by treating the transport of acoustic signals in the gas more exactly with Navier - Stokes equations[19-21].

McDonald and Wetsel[20] modified the theory by taking the contribution to the signal from thermally induced vibrations in the sample into account. Although these modifications did not change the basic results of the R-G theory for most experimental conditions, they were able to account for the observed deviations from R-G theory at very low modulation frequencies.

1.3 Applications of the photoacoustic effect

Wide ranging applications for PA effect in various branches of science, technology and medicine have been reported in recent years[21-25]. The applications of PA effect can be divided into the following four classes, based on the properties of the materials under study.

(a) Photoacoustic spectroscopy, (b) PA monitoring of de-excitation processes, (c) PA sensing of physical properties of materials and (d) PA generation of mechanical motion[26].

1.3.1 Photoacoustic spectroscopy

Photoacoustic spectroscopy (PAS) is the most fundamental and earliest application of the PA effect. Based on the method of detection and the source of energy used for excitation of samples, photoacoustic spectroscopy is known in different names like Gas - microphone PAS, Photothermal deflection PAS, Pizelectric PAS, Photopyroelectric spectroscopy, Fourier transform photoacoustic spectroscopy, Photoacoustic X-ray absorption spectroscopy, Laser induced PAS etc[27]. One of the remarkable advantages of PA spectroscopy is that, it is able to provide absorption spectra of materials just like conventional optical absorption spectra. It is also capable of dealing with (i) samples of very low optical density, (ii) samples of very high optical density (iii) light scattering samples and (iv) specularly reflecting samples[9-22]. That means this technique can provide spectroscopic information over a wide range of absorption coefficients ranging from weakly absorbing transparent materials to highly absorbing opaque materials.

With the advent of laser PA systems, the sensitivity of PA spectroscopy has risen by several orders of magnitude higher than conventional spectroscopic techniques[28]. This enhancement in the sensitivity of PA spectroscopy has made it a compe-

tent technique in overtone spectroscopy, trace analysis, pollution monitoring etc[29-33]. The PA technique can also be used to study insulators, semiconductors and even metallic systems that cannot readily be studied by conventional absorption techniques. In the case of insulators, PA spectra can provide information on the optical absorption bands in the material and in semiconductors both direct and indirect transitions can be detected.

Recently, several investigators[34-49] have exploited the PA technique to study the variation of optical band gap with composition in semiconducting chalcogenide glasses. Madhusoodanan *et al.*[34-38] have determined the optical energy gap of different semiconducting binary glass samples like As-Se, Ge-Se, Ge-Te, Ge-As-Te, etc at different compositions and at various temperatures by measuring the normalized PA signal as a function of wavelength of the incident light beam. Similar method has been adopted by Nandakumar *et al.*[39-41] to analyse the variation of optical band gap in ternary glasses with composition as well as temperature. Zegadi *et al.*[48] adopted the same method, but applied in a slightly different way, to evaluate the band gaps of a series of $CuIn_xGa_{1-x}Se_2$ alloys.

PA monitoring of weak absorption in solids with high detection sensitivity of the order of $10^{-5}cm^{-1}$ using piezoelectric detection has been reported on highly transparent solids like CaFe, SrFe etc.[16]. The high sensitivity of the technique has made it a suitable tool for determining absorptions in thin film as well. In thin film, weak absorption may be caused by a low absorption coefficient for the optical wavelength or may be caused by short path length. Therefore this method has found a high degree of application in thin film optical coatings like laser mirrors, absorption by glass surfaces, thin layer chromatography, surface chemistry, surface catalysis etc.[27]. PAS can be used effectively for studying absorbed or chemisorbed molecular species and compounds as

well as surface passivation, surface oxidation or reduction on metals, semiconductors and insulators.

Another important application of PA spectroscopy is the optical characterisation of highly opaque samples. This is achieved by irradiating the sample with a light beam chopped at high frequency such that $\mu_s < l_\beta$. In a similar manner one can record the power spectrum of the excitation source with an optically opaque sample using high chopping frequency such that $\mu_s > l_\beta$. Following this principle one can fabricate a power meter with a wide wavelength range easily with an absorber sample. Moreover, it can also be used to study Urbach tail, excitations and other fine structures in crystalline, powder and amorphous semiconductors[33,43,50-52], which in turn helps to study the effect of impurities, dopants, electromagnetic fields etc. on the material.

1.3.2 PA monitoring of deexcitation processes

Here the thermal decay branch is monitored to provide information on competing decay branches. After optical excitation, four decay branches are generally possible. They are luminescent, photochemical, photoelectric and thermal which may be generated directly or through energy transfer processes. For example, if luminescence and heat are the only two competing branches, PA monitoring of heat branch can provide the quantum efficiency of luminescence under suitable circumstances. That is when a luminescent material that is optically excited can decay only by fluorescence or by heat generation, the measurement of the absolute heat energy generated provides the fluorescence quantum efficiency. There are several publications[53-58] which report measurement of fluorescent quantum efficiency by PA effect.

The measurement of luminescence quantum efficiency by PA method can be very useful for studying laser materials. For example, the fluorescence quantum yield

of laser dyes in various solvents at various concentrations can be measured to understand the effect of solvent quenching and concentration quenching. New laser solid materials in the form of powders can be tested without the necessity of growing macroscopic crystals as conventional methods of measuring luminescence quantum efficiency would require[26]. PA effect has effectively been utilized for deexcitation studies in rare earth oxides and in doped crystals[59,60,61]. It gives information about the lifetime of various states and deexcitation channels. A combination of conventional fluorescent spectroscopy and PAS can provide information about the relative strengths of the radiative and nonradiative deexcitation processes in solids.

PA monitoring can provide a new and sensitive way to study or to monitor photochemical processes. Photochemical effects can produce characteristic acoustic signals due to different mechanisms. The simplest mechanism by which photochemistry influences the magnitude of the PA signal or a photothermal signal, in general, is that of complementarity. When the two branches are complementary (assuming the luminescence and photoelectric branches to be zero), the increase of one branch must mean decrease of the other. The complementary effect is well demonstrated in the important photosynthesis work of Cahen and co-workers[62,63]. They observed that for samples with active photosynthesis, the PA spectrum and the optical absorption spectrum actually differed by an amount corresponding to the conversion into chemical energy (called the "photochemical loss").

It has been reported by different authors [62-65] that PA technique is very suitable for studying some other photochemical effect like energetics in the purple membrane of *Halobacterium halobrium*, photochemically induced acoustic generation (photochemical gas evolution and consumption) and photochemical chain reactions.

PA monitoring of deexcitation is found to be very useful to study the effi-

ciency of photovoltaic materials[66]. In a photovoltaic or photoconductive device, the thermal energy produced in the optical excitation will be less than the absorbed light energy since part of the light energy is converted into electrical energy. That is, the observed PA signal from the sample should be smaller when the sample is photoelectrically active. Tam[67] extended Cahen's idea of PA monitoring of photoelectricity to other systems. Tam used a PA method for the first time to study the photoconductive quantum efficiency of a thin organic dye film.

There are several other recent papers on the use of photoacoustic monitoring of photoelectric carrier generation or related effects in semiconductors and organic dyes. Thielmann and Neumann[68] have applied a photoacoustic technique similar to Cahen's[66] to determine the photocarrier generation quantum efficiency in a Schottky diode. Wasa *et al.*[69] have investigated nonradiative states in *GaAs* and *InP* by PA technique. Tokumoto *et al.*[70] have used PA spectroscopy to study *Si*, *Ge*, *INSb*, *GaAs* and *GaP* in the region above the fundamental absorption edge. Iwasaki *et al.*[71] have used laser PA spectroscopy to examine voltage- dependent electron recombination processes at a semiconductor electrode dye solution interface. Iwasaki *et al.*[72] have also used the PA technique to study spectral sensitization effects by dyes on *ZnO* powder.

PA monitoring technique has proved its ability for measuring energy transfer processes in excited molecules. There are at least two ways to achieve energy transfer. The most commonly used way is by collisions either self- collision of the excited molecules with the ground state of the same molecules, or collision of the excited state molecules with foreign molecules. Another less common but very powerful way is stimulated transition by light. Parker and Ritke[73] performed some of the pioneering work on the PA measurement of collisional deactivation time of the electronic state of O_2 , and obtained a pressure x life time product of pure oxygen. Robin and co- workers[74-76]

performed a series of experiments in organic vapors which beautifully demonstrate the use of PA technique to measure energy transfer processes when various triplet or singlet excited states are produced.

Using PA monitoring technique a series of experiments on energy transfer processes in vapors of organic materials has been performed by Hunter and co-workers[77] Huetz- aubert and Tripodi[78] used PA technique to investigate vibrational relaxations of CO_2 in collision with itself or with other molecules like N_2 , H_2 , CO_2 etc. Subsequently, Lepoutre and co- workers[79] investigated in detail the collisional deactivation rates of vibrationally excited CO_2 with a host of other molecules at temperatures ranging from 170 to 400 K. In succession with the work of Huetz- Aubert[78] several investigators have applied the PA technique for the determination of relaxation rates in solids as well as gases. Energy transfer due to stimulated transition by light has also been studied by PA technique.

1.3.3 PA sensing of physical properties of materials

The generation and propagation of acoustic waves in a sample depend critically on the thermoelastic and physical properties of the sample. By monitoring the PA signal, one is able to probe or measure such properties as acoustic velocities, elasticity, density, thickness, specific heat, thermal conductivity, material discontinuities, crystallinity, phase transitions and so on. By focusing the light beam, some of these physical properties may be measured locally and hence by scanning the beam over the sample, PA imaging of the property concerned can be realised. A review of pulsed PA methods for material characterisation is given by Hutchins and Tam[80].

1.3.3.a Photoacoustic imaging

The technique of PA imaging is concerned with the detection of variations in surface and subsurface thermoelastic properties in a sample. In particular, if little lateral resolution is desired and PA imaging is mainly concerned with the property variations in the thickness direction, the technique is usually called "PA depth profiling". On the other hand, if high lateral resolution is required, the technique is called "PA microscopy". PA imaging rely on the detection of variations in magnitude or phase of the PA signal as the sample surface is scanned with the modulated beam of light.

1.3.3.b PA depth profiling

PA depth profiling is a technique of using the PA signal from a sample to determine its depth dependent properties. Such a technique can be destructive or nondestructive.

An example for destructive PA depth profiling is given by Yeack *et al.*[56], who monitored the PA signal due to laser ablation of a composite, layered sample. They used the PA monitoring technique to control the optical ablation and was stopped after a desired depth was reached. Their method of PA monitoring of stepwise ablation by laser pulses may be extended to many other novel technological or medical applications where optical ablation, evaporation, coagulation, polymerization, or other chemical or physical changes need to be performed stepwise with light pulses. In these applications, the PA pulse signal can be continuously monitored and the completion of the desired operation (eg. drilling through a certain layer) can be indicated by a characteristic change in the pulsed PA signal.

Nondestructive depth profiling techniques are more important and useful. Usually, depth profiling is obtained by a chopping - frequency dependent measurement

of the PA signal with a gas - coupled microphone. The qualitative idea for an opaque sample is simple. The modulated thermal coupling at the gas - sample interface occurs between a sample thermal diffusion length μ_s and a gas thermal diffusion length μ_g . Since the diffusion lengths depends on the chopping frequency f as $f^{-1/2}$, a higher chopping frequency corresponds to probing the sample closer to the surface. A good example is the chopping frequency dependence of the visible PA spectra of an apple peel or of a spinach leaf reported by Rosencwaig[81], Adams and Kirkbright[82] and others. At a comparatively high chopping frequency (eg. $f \approx 300$ Hz , $\mu_s \approx 10\mu m$), the PA spectrum corresponds to the optical absorption of the top layer of the plant matters while at a lower chopping frequency (eg. $f \approx 30$ Hz , $\mu_s \approx 33\mu m$), the PA spectrum corresponds to absorption by the pigment below the top layer.

Various PA cells using gas microphone system for depth profiling studies of solid samples are described in literature. For example, Adams and Krikbright[82], Tam and Wong[83] etc have described PA cells for which the coupling gas and its thickness can be changed so that the PA signal for a depth - profiling experiment can be optimized. Depth profiling with the use of direct coupling is also possible, in which case the PA signal with piezoelectric detection is usually preferred over microphone detection due to higher magnitude of the signal and better signal to noise ratio.

1.3.3.c PA microscopy

PA microscopy is a field that is fast expanding and is being actively pursued by many research groups because of its potential applications in thin film technology, chemical engineering, biology, medical diagnostics etc. It provides a unique method for obtaining subsurface images of irregularities, flaws, doping nonuniformities etc which cannot normally be obtained by other nondestructive techniques.

A number of papers have been published in this field [84-90]. Von Gutfeld and Melcher[84] were the first to demonstrate that subsurface voids in an Al cylinder could affect the pulsed PA signal detected by a piezoelectric transducer. Wong *et al.*[85,86] first reported actual PA images of subsurface structure in solids.

Ash *et al.*[87], Busse and Rosencwaig[88], Busse and Ograbeck[89] and Perkowitz and Busse[90] have also demonstrated that PA microscopy can be used to map out subsurface features such as in integrated circuits, ceramic substrates etc. The PA phase image is usually more informative than the PA amplitude image because the former is much less affected by the variations in optical absorption, rather it depends mainly on the variations in thermoelastic properties. The PA imaging of compositional variation in $Hg_{1-x}Cd_xTe$ semiconductors reported by McClelland *et al.*[91] is a good example of an application of PA detection for industrial quality control. The $Hg_{1-x}Cd_xTe$ semiconductors are very useful for mid - IR detection. The compositional uniformity of the $Hg_{1-x}Cd_xTe$ can be ensured by PA scanning microscopy before its fabrication into IR detector arrays. Using a CW Nd:YAG laser for excitation, Macfarlane *et al.*[92] have demonstrated PA mapping of damages due to ion implantation and subsequent recrystallization due to annealing in Si and GaAs. In most PA microscopy experiments the image obtained is either due to variations in optical absorption or due to variations in thermoelastic properties. But, the PA microscopy experiment of Wickramasinghe *et al.*[93] is an exception. They used a mode - locked Q switched Nd:YAG laser to excite a sample of metal film with optical pulse trains of duration 0.2ns at 210MHz repetition rate. In this experiment PA image is formed by sensing the PA ultrasonic waves generated in the sample. Consequently ultrasonic scattering would also affect the PA imaging in this experiment.

PA microscopy techniques has been used for nondestructive imaging of various

subsurface features like voids in metals, flaws in ceramics, absorption sites in laser windows and water content in porous materials. It also can be used for determining inhomogeneities in layered materials, foreign material inclusions in biological samples, defects in integrated circuits and substrates, compositional variations in alloys, ion - implantation damages in semiconductors etc.

1.3.3.d Thermal characterisation of solids

The PA effect depends not only on the optical properties of the sample, but also on its thermal and geometric properties and in some cases on its elastic properties as well. Most commonly encountered thermal parameters in PAS are the thermal diffusivity, $\alpha = k/\rho C$ and the thermal effusivity, $e = \sqrt{k\rho C}$, where K is the thermal conductivity, ρ is the density and C is the specific heat of the sample. The thermal diffusivity α is of direct relevance in heat flow studies. It determines the rate of periodic or transient heat transportation through a medium. Because of its controlling nature and common occurrence in heat flow problems, its determination is very often necessary. Moreover, a knowledge of thermal diffusivity enables one to determine thermal conductivity of a sample. An extensive review on thermal parameters of solids has been published by Touloukian *et al.*[94].

Adams and Kirkbright[95] measured the thermal diffusivities of copper, aluminium and polymer samples from the phase lag measured in the frequency dependent photoacoustic signal from these samples. An alternate method of measuring the thermal diffusivity of solid materials have been reported independently by two groups. Lepoutre *et al.*[96] and Sugitani *et al.*[97] measured the thermal diffusivity of materials by analysing the variation of photoacoustic signal amplitude with chopping frequency.

Of late the later method has gained popularity among the investigators in this

filed. Philp *et al.*[98] have used this chopping frequency analysis technique to determine the thermal diffusivity of samples belonging to the $A_x^{IV}B_{1-x}^{VI}$ family of semiconducting chalcogenide glasses at different compositions. The technique has been used by Madhusoodanan *et al.*[34,37,99-102] and Nandakumar *et al.*[39,40,103] for demonstrating the variation of thermal diffusivity with composition or temperature in binary and ternary semiconducting chalcogenide glasses respectively. One can determine the thermal diffusivity of a sample using the expression, $\alpha = f_c l_s^2$, where f_c is the critical chopping frequency at which a sample of thickness l_s goes from thermally thin to thermally thick regime. The chopping frequency analysis enables one to evaluate the critical frequency f_c . Madhusoodanan *et al.*[104] have also evaluated the thermal conductivity of some bulk polymer samples by the same method. Isaac *et al.*[105] have used this method to show that there is an abrupt increase in thermal diffusion below T_c in the high T_c superconductor $YBa_2CuO_{7-\delta}$.

Swimm[106] determined the average thermal properties of a multilayer thin film optical coating using both front and rear surface illumination techniques. Lachaine *et al.*[107] performed front surface measurements on a thin polymer film by changing the backing material.

Another important technique put forward by Lachaine[108] involves determination of thermal diffusivity by measuring the photoacoustic phase variation as a function of sample thickness. Thomas *et al.*[109] have demonstrated a single beam photoacoustic phase lag measurement for determining the thermal diffusivity of solid samples. They measured the phase difference of PA signals from front and rear surfaces of a solid sample by rotating the PA cell by 180° illuminating the both surfaces by same chopped beam of light.

Phase transition studies on solids is another important aspect of thermal char-

acterization of solids. The thermal parameters of a material generally undergo changes when the material undergoes a phase transition. Therefore by monitoring the PA signal as a function of temperature one can get information about features of phase transitions. During last ten years, many investigators have employed the PA technique for phase transition studies in many materials[100,101,106,110,111]. Madhusoodanan *et al.*[100,101] measured the glass transition temperature of As_xTe_{1-x} glass by measuring the PA amplitude and phase as a function of temperature. A similar method has been adopted by Isaac *et al.*[105,110] for determining the T_c of the high T_c superconductor $YB_2Cu_3O_7$. Isaac *et al.* have also applied the PA technique to study the stability of the ferroelectric phase in polycrystalline KNO_3 [112].

1.4 Work presented in this thesis

PA sensing of physical properties of a material has potential uses in nondestructive testing and thermal characterization of bulk as well as thin film samples. In this work a realization of PA imaging of surface and subsurface features of solid samples and an analysis of the depth profiling ability of PA technique have been performed. We have developed a new and simple PA scanning technique for the thermal characterization of bulk solid as well as thin film samples. The details of the principle, theoretical formulation, experimental realization and the results obtained are presented in the following chapters of this thesis.

References

- [1] A. G. Bell, *Am. J. Science* **20**, 305 (1880)
- [2] M. E. Mercadier, *C. R. Hebd. Serv. Acad. Sci.* **92**, 409 (1881)
- [3] W. H. Preece, *Proc. Royal Soc.(Lond)* **31**, 506 (1881)
- [4] M. L. Viengerov, *Dokl. Akad. Nauk. SSSR* **19**, 687 (1938)
- [5] A. H. Pfund, *Science* **90**, 326 (1939)
- [6] K. F. Luft, *Z. Tech. Phys.* **24**, 97 (1943)
- [7] A. Rosencwaig, *Photoacoustics and Photoacoustic Spectroscopy*, (Wiley, New York 1980)
- [8] J. G. Parker, *Appl. Opt.* **12**, 2974 (1973)
- [9] A. Rosencwaig and A. Gersho, *J. Appl. Phys.* **47**, 64 (1976)
- [10] A. Rosencwaig and A. Gersho, *Science* **190**, 556 (1975)
- [11] L. C. Aamodt, J. C. Murphy and J. G. Parker *J. Appl. Phys.* **48**, 927 (1977)
- [12] M. J. Adams, G. F. Kirkbright and K. R. Menon, *Anal. Chem.* **51**, 508 (1979)
- [13] F. A. Mc Clelland and R. N. Kniseley, *Appl. Phys. Lett.* **28** 467 (1976)
- [14] E. M. Monahan, Jr. and A. W. Nolle, *J. Appl. Phys.* **48**, 3519 (1977)
- [15] A. Rosencwaig, in *Advances in Electronics and Electron Physics* **46**, 207 (1978)
- [16] A. Hordvik and H. Schlossberg, *Appl. Opt.* **16**, 101 (1976)
- [17] A. Rosencwaig, *Rev. Sci. Instrum.* **48**, 113 (1977)

- [18] G. C. Wetsel, Jr. and F. A. Mc Donald, **Appl. Phys. Lett.** **30**, 252 (1977)
- [19] H. S. Bennett and R. A. Forman, **Appl. Opt.** **15**, 2405 (1976)
- [20] F. A. Mc Donald, G. C. Wetsel, Jr., **J. Appl. Phys.** **49**, 2313 (1978)
- [21] G. C. Wetsel, Jr. and F. A. Mc Donald, **Bull. Am. Phys. Soc.** **22**, 295 (1977)
- [22] A. Rosencwaig, **Opt. Commun.** **7**, 305 (1973)
- [23] A. Rosencwaig, **Phys. Today** **28**, 23 (1975)
- [24] A. Rosencwaig, **Science** **181**, 657 (1973)
- [25] A. Rosencwaig and S. S. Hall, **Anal. Chem.** **47**, 548 (1978)
- [26] A. C. Tam, **Rev. Mod. Phys.** **58**, 381 (1986)
- [27] P. Hess and J. Pelze (eds), **Photoacoustic and Photothermal Phenomena**
58,2 (Springer - Verlag 1988)
- [28] C. K. N. Patel and R. J. Kerl, **Appl. Phys. Lett.** **30**, 578 (1977)
- [29] R. G. Bray and M. J. Berry, **J. Chem. Phys.** **71**, 4909 (1979)
- [30] G. Stella, J. Gelfand and W. H. Smith, **Chem. Phys. Lett.** **39**, 146 (1976)
- [31] C. K. N. Patel, **Science** **220**, 157 (1978)
- [32] T. H. Vansteenkiste, F. R. Faxvog and D. M. Rossler, **Appl. Spectroscopy** **35**,
194 (1981)
- [33] P. C. Claspy, C. Ha and Y. H. Pao, **Appl. Opt.** **16**, 2972 (1977)
- [34] K. N. Madhusoodanan and J. Philip, **Pramana- J. Phys.** **33**, 705 (1989)

- [35] K. N. Madhusoodanan, A. Srinivasan, E.S.R. Gopal, K. Nandakumar and J. Philip, **Indian J. Phys.** **65A(4)**, 306 (1991)
- [36] K. N. Madhusoodanan, J. Philip, S. Asokan, G. Parthasarathy and E.S.R. Gopal, **J. Non-cryst. Solids** **109**, 225 (1989)
- [37] K. N. Madhusoodanan, J. Philip, G. Parthasarthy, S. Asokan and E.S.R. Gopal, **Phil. Mag.** **B58**, 123 (1988)
- [38] K. N. Madhusoodanan and J. Philip, **Phys. Stat. Sol. (a)** **108**, 775 (1988)
- [39] K. Nandakumar and J. Philip, **Indian J. Phys.** **69A**, 595 (1995)
- [40] K. Nandakumar and J. Philip, **J. Non-cryst. Solids** **144** 247 (1992)
- [41] K. Nandakumar and J. Philip, **Bull. Mater. Sci.** **11**, 297 (1988)
- [42] J. H. Harris and M. A. Tenhover, **J. Non-cryst. Solids** **83**, 272 (1986)
- [43] T. Ikari, S. Shigetoni and Y. Koga, **J. Phys. C: Solid state Phys.** **17**, L969 (1984)
- [44] R. S. Ram, O. Prakash and A. N. Pandey, **Pramana- J. Phys.** **28**, 293 (1987)
- [45] A. Srinivasan, K. N. Madhusoodanan, E.S.R. Gopal and J. Philip, **J. Non-cryst. Solids** **155**, 267 (1993)
- [46] A. Srinivasan, K. N. Madhusoodanan, E.S.R. Gopal and J. Philip, **Phil. Mag.** **B65**, 99 (1992)
- [47] T. Somasundaram, P. Ganguly and K. J. Rao, **Proc. Indian Acad. Sci. (Chem. Sci.)****92**, 65 (1983)
- [48] Zegadi, M. A. Slifkin, M. Danin, A. E. Hill and R. D. Tomlinson, **Phys. Stat. Sol. (a)** **133**, 533 (1992)

- [49] C. S. Sunandana and A. K. Bhatnagar, **Solid state Commun.** **51**, 143 (1984)
- [50] P. Rochon and T. J. Racey, **J. Photoacoustics** **1**, 475 (1983)
- [51] L. Baldassarre and A. Cingolani, **Solid state Commun.** **44**, 705 (1982)
- [52] M. Fathallah and M. Zouaghi, **Solid state Commun.** **54**, 317 (1985)
- [53] R. G. Stearne and G. S. Kino, **Appl. Phys. Lett.** **47**, 1048 (1985)
- [54] W. G. Adams, J. G. Highfield and G. F. Kirkbright, **Anal. Chem.** **49**, 1850 (1977)
- [55] J. C. Murphy and L. C. Aamodt, **J. Appl. Phys.** **48**, 3502 (1977)
- [56] R. S. Quimby and W. N. Yen, **Opt. Lett.** **3**, 181 (1978)
- [57] W. Lahaman and H. J. Ludwing, **Chem. Phys. Lett.** **45**, 177 (1977)
- [58] A. Rosencwaig and E. A. Hildum, **Phys. Rev. B** **23**, 3301 (1981)
- [59] C. D. Merkle and R. C. Powell, **Chem. Phys. Lett.** **46**, 303 (1977)
- [60] R. G. Peterson and R. C. Powell, **Chem. Phys. Lett.** **53**, 366 (1978)
- [61] J. Etxebarria and J. Fernandez, **J. Phys. C: Solid state Phys.** **16**, 3803 (1983)
- [62] D. Cahen, H. Garty and S. R. Caplen, **FEBS Lett.** **91**, 131 (1978)
- [63] D. Cahen, S. Malkin and E. J. Lerner, **FEBS Lett.** **91**, 339 (1978)
- [64] G. J. Diebold, **J. Phys. Chem.** **84**, 2213 (1980)
- [65] R. C. Gray and A. J. Bard, **Anal. Chem.** **50**, 1262 (1978)
- [66] D. Cahen, **Appl. Phys. Lett.** **33**, 810 (1978)
- [67] A. C. Tam, **Appl. Phys. Lett.** **37**, 978 (1980)

- [68] W. Thielemann and H. Neumann, *Phys. Stat. Solidi A* **61**, K123 (1980)
- [69] K. Wasa, K. Tsubouchi and N. Mikoshiba, *Jap. J. Appl. Phys.* **19**, L653 (1980)
- [70] H. Tokumoto, M. Tokumoto and T. Ishiguro, *J. Phys. Soc. Jpn.* **50**, 602 (1981)
- [71] T. Iwasaki, T. Sawada, H. Kamada, A. Fujishima and K. Honda, *J. Phys. Chem.* **83**, 2142 (1979)
- [72] T. Iwasaki, S. Oda, T. Sawada and K. Honda, *Photogr. Sci. Eng.* **25**, 6 (1981)
- [73] J. G. Parker and D. N. Ritka, *J. Chem. Phys.* **59**, 3713 (1973)
- [74] M. B. Robin, N. A. Kuebler, K. Kaya and Diebold *J. Chem. Phys. Lett.* **70**, 93 (1980)
- [75] M. B. Robin, *J. Lumin* **13**, 131 (1976)
- [76] M. B. Robin and N. A. Kuebler, *J. Am. Chem. Soc.* **97**, 4822 (1975)
- [77] T. F. Hunter, D. Rumbles and M. G. Stock, *J. Chem. Soc. Faraday Trans. 2*, **70**, 1010 (1974)
- [78] M. Huetz-Aubert and R. Tripodi, *J. Chem. Phys.* **55**, 5724 (1971)
- [79] F. Lepoutre, G. Louis and J. Taine, *J. Chem. Phys.* **70**, 2225 (1979)
- [80] D. A. Hutchins, and T. A. Tam, *IEEE Trans. Ultrasonics, Ferroelectrics and Frequency Control* **34** 429 (1986)
- [81] A. Rosencwaig, *Adv. Electron. Electron Phys.* **46**, 207 (1978)
- [82] G. F. Kirkbright and S. L. Castleden, *Chem. Br.* **16**, 661 (1980)
- [83] A. C. Tam and Y. H. Wong, *Appl. Phys. Lett.* **36**, 471 (1980)

- [84] R. J. Von Gutfeld and R. L. Melcher, **Appl. Phys. Lett.** **30**, 257 (1977)
- [85] Y. H. Wong, R. L. Thomas and G. F. Hawkins, **Appl. Phys. Lett.** **32**, 538 (1978)
- [86] Y. H. Wong, R. L. Thomas and J. J. Pouch, **Appl. Phys. Lett.** **35**, 368 (1979)
- [87] E. A. Ash, E. Dieulesaint and H. Rakout, **Electron. Lett.** **16**, 470 (1980)
- [88] G. Buss and A. Rosencwaig, **Appl. Phys. Lett.** **36**, 815 (1980)
- [89] G. Buss and A. Ograbeck, **J. Appl. Phys.** **51**, 3576 (1980)
- [90] S. Perkowitz and G. Buss, **Opt. Lett.** **5**, 228 (1980)
- [91] J. F. McClelland, R. N. Kniseley and J. L. Schmit, **Scanned Image Microscopy**, edited by E. A. Ash (Academic Press, New York), p.533 (1980)
- [92] R. A. Macfarlane, L. D. Hess and G. L. Olson, **IEEE 1980 Ultrasonics Symposium Proceedings**, edited by B. R. McAvoy, 1, p. 628, (IEEE, Piscataway, New Jersey) (1980)
- [93] H. K. Wickramasinghe, R. C. Bray, V. Jipson, C. F. Quate and J. R. Salcedo, **Appl. Phys. Lett.** **33**, 923 (1978)
- [94] Y. S. Touloukian, **Thermophysical Properties of Matter**, (IFI/Plenum, New York, 1970)
- [95] M. J. Adams and G. F. Kirkbright, **Analyst** **102**, 281 (1977)
- [96] F. L. Lepoutre, P. Charpentier, A. C. Boccara, and D. Fournier, **Tech. Digest of 2nd Inter. Topical Meeting on PA Spectroscopy**, Berkley, MA3 (1981)
- [97] Y. Sugitani and M. Fujinami, **Bull. Chem. Soc. Jpn** **54**, 722 (1981)
- [98] J. Philip and K. N. Madhusoodanan, **Phys. Rev.** **B36**, 4127 (1988)

- [99] K. N. Madhusoodanan, J. Philip, S. Asokan and E. S. R. Gopal, **J. Material Sci. Lett.** **7**, 1333 (1988)
- [100] K. N. Madhusoodanan and J. Philip, **Pramana - J. Phys.** **32**, 821 (1989)
- [101] K. N. Madhusoodanan, K. Nandakumar, J. Philip, S. S. K. Titus, S. Asokan and E. S. R. Gopal, **Phys. Stat. Solidi (a)** **114**, 525 (1989)
- [102] K. N. Madhusoodanan and J. Philip, **Phys. Stat. Solidi (a)** **108**, 775 (1988)
- [103] K. Nandakumar, K. N. Madhusoodanan and J. Philip, **J. Acoust. Soc. Ind. XVII (3& 4)**, 351 (1989)
- [104] K. N. Madhusoodanan, M. R. Thomas and J. Philip, **J. Appl. Phys.** **62**, 1162 (1987)
- [105] J. Isaac, J. Philip and B. K. Chaudhuri, **Pramana - J. Phys.** **32**, L167 (1989)
- [106] R. T. Swimm, **Appl. Phys. Lett.** **42**, 955 (1983)
- [107] A. Lachaine and P. Poulet, **Appl. Phys. Lett.** **45**, 953 (1984)
- [108] A. Lachaine, **J. Appl. Phys.** **57 (ii)** , 5075 (1985)
- [109] S. Thomas, J. Isaac and J. Philip, **Rev. Sci. Instrum.** **66**, 3907 (1995)
- [110] J. Isaac, J. Philip and B. K. Chaudhuri, **Pramana - J. Phys.** **31**, L153 (1988)
- [111] K. N. Madhusoodanan, R. Sreekumar and J. Philip, **J. Acoust. Soc. Ind. XVII(3 & 4)**, 347 (1989)
- [112] J. Isaac and J. Philip, **J. Appl. Phys.** **69**, 7765 (1991)

CHAPTER 2

INSTRUMENTATION

For performing the work presented in this thesis, a photoacoustic (PA) imaging experimental setup has been fabricated. The essential parts of this experimental setup are a PA spectrometer and a microprocessor controlled scanning unit. The general aspects of PA spectrometer and the necessary instrumentation work done for setting up this experimental arrangement are outlined in this chapter.

2.1 General aspects of the PA spectrometer

A PA spectrometer is assembled with following units (i) a source of radiation with sufficient intensity, (ii) arrangement for intensity or frequency modulation of light, (iii) PA cell which contains a sample and a suitable acoustic transducer and (iv) signal processing unit. The block diagram of a basic PA spectrometer is shown in Fig.(2.1).

2.1.1 Source of radiation

Based on the nature of PA studies, different types of radiation sources are used for sample excitation. Incandescent or arc lamps and lasers are two popular types of light sources commonly used. The important parameters for the selection of a radiation source are (a) the power available with usable band width (b) the wavelength range (c) tunability of the source and (d) the ease of modulation of intensity and sometimes of wavelength as well.

High pressure Xe arc lamps, high pressure Hg lamps, tungsten lamps, Nernst glower etc are the commonly used incoherent sources. Any of these lamps and monochromator combination can provide continuous tunability over a wide wavelength

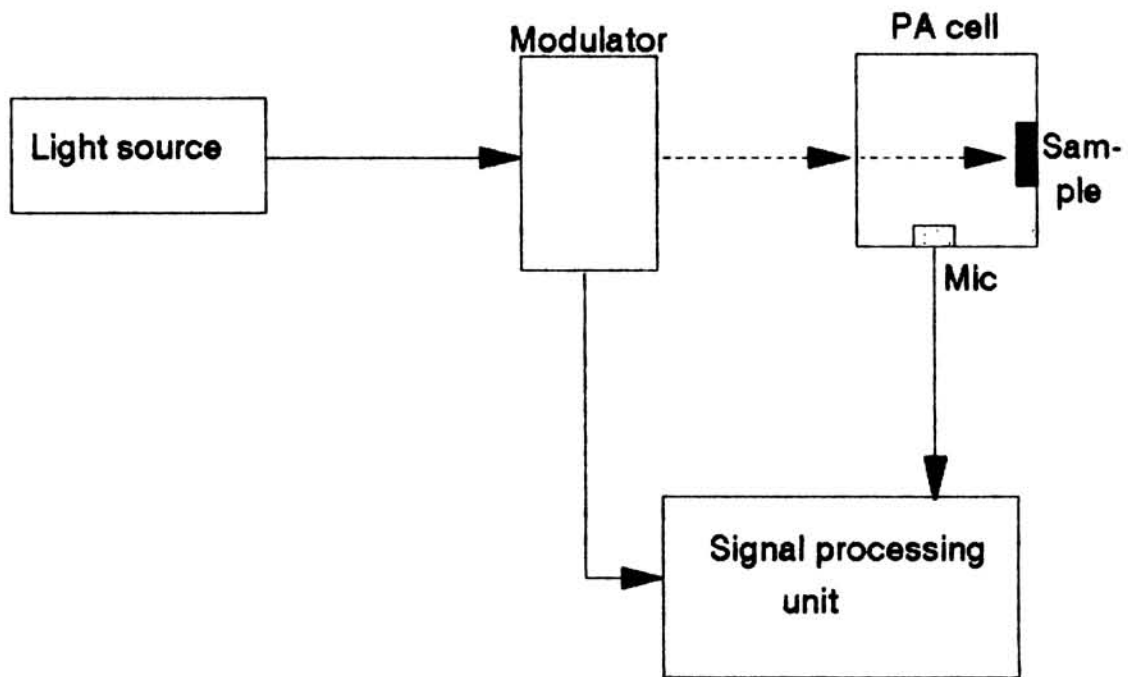


Fig 2.1 : Block diagram of a basic PA spectrometer

range from the infrared to the ultraviolet. Lasers are widely accepted radiation sources in PA experiments, especially for measuring weakly absorbing samples. This is mainly because of their high spectral radiance resulting from the extremely narrow line widths and high collimation. Because of spectral purity, lasers can be effectively used for high resolution PA spectroscopy experiments. The limited tunability is a main drawback of laser sources.

2.1.2 Modulation

The incident light beam has to be modulated for the generation of PA signals. Either amplitude or frequency of the incident radiation has to be modulated. Amplitude modulation is a more accepted and widely used method because it can be accomplished by relatively inexpensive mechanically chopping methods. The depth of modulation in this case is nearly 100%. While using mechanical choppers, precaution should be taken to minimize the vibration noise transmitting directly from the chopper to the microphone detector. Amplitude modulation can also be accomplished by electrical as well as electro - optic methods. In the case of CW lasers, modulation can be achieved by varying the discharge tube current. Electro - optic modulation involves changing the plane of polarization of an incoming polarized light beam in a nonlinear optical crystal (ADP or KDP) by the application of a modulated electric field across the crystal. Frequency modulation can be employed to eliminate the PA signals generated due to wavelength independent absorption at the cell windows. In dye lasers, rapid frequency changes can be obtained by using an electro - optic tuner instead of a birefringent filter. Frequency modulation is well suited for narrow line width absorbers such as atomic and diatomic species.

2.1.3 Photoacoustic cell

The PA cell is considered as the heart of a PA spectrometer. The PA cell contains the sample and microphone. The microphone is used to detect the PA signal generated inside the cell. Proper cell design is very important for the generation of PA signal of detectable amplitudes. Some of the important criteria governing the design of a PA cell are given below.

(i) The cell should be acoustically isolated from the surroundings. For this the cell should be designed with good acoustic seals and with walls of sufficient thickness to form a good acoustic barrier. The thermal mass of the cell walls should be large.

(ii) The PA signal arising due to light absorption in cell windows and walls should be as small as possible for the wavelength region of interest and the interior of the cell highly reflecting. Although the cell walls will absorb some of the incident and scattered light, the resulting PA signal will be quite feeble as long as the thermal mass of the walls is quite large. The cell geometry should be such that the scattered and reflected light towards the walls and microphone are as minimum as possible. Moreover, there should not be any contamination in the interior surfaces of the cell.

(iii) Since the PA signals vary inversely with the volume of the gas inside the cell[1], the cell dimensions should be so chosen that the volume of the cell is minimum. However, care must be taken to avoid dissipation of acoustic signal produced appreciably to the cell windows and walls before reaching the microphone. Also for all chopping frequencies of interest the length of the gas column, l_g , in the cell should be greater than the thermal diffusion length, μ_g , since it is this boundary layer of gas that acts as an acoustic piston generating the signal inside the cell. Tam[2] has suggested the optimum gas column length to be $l_g = 1.8 \mu_g$. Another important parameter that should be

considered in the design of a PA cell is the thermoviscous damping, because this could be a source of signal dissipation at the cell boundaries. Thermoviscous damping coefficient varies as $\omega^{1/2}$ and become important at high frequencies where as thermal diffusion length, which varies as $\omega^{-1/2}$ is predominant at low frequencies. Considering all these effects the distance between the sample and window can be chosen to be 1 - 3mm [3].

Depending upon the type of the experimental studies different types of cell design have appeared in literature[4,5]. The most common cell design adopts cylindrical geometry in which the light beam is centered along the axis. Such a cell can be operated either in the resonant mode or in the non-resonant mode. The pressure variations produced due to PA effect propagates radially towards and perpendicular to the exciting beam. The hydrodynamic equations describing the time variation of pressure at a given point in the cell have been solved for cylindrical[3,6-8] and other[9] cell geometries. The pressure distribution P within a cylinder of length L and radius R is given by[3]

$$P(r, \phi, z, t) = \cos(m\phi)\cos(k\pi z/L)J_m(\alpha_{m,n}\pi r/R)\exp(-i\omega t) \quad (2.1)$$

where J_m is the Bessel function of the first kind of order m and eigen values $k, m,$ and n relate to longitudinal ($k=1, m = n = 0$) and radial ($n= 1, k = m = 0$) acoustic modes respectively. It is found that the cell exhibits a number of acoustic resonances. The resonance frequencies are given by [3]

$$f_{res} = C_0/2[(k/L)^2 + (\alpha_{m,n}/R)^2]^{1/2} \quad (2.2)$$

where C_0 is the sound velocity in the gas and $\alpha_{m,n}$ is the n^{th} root equation $(dJ_m/dr)_{r=R} = 0$ The numerical values for the lowest order roots are $\alpha_{0,0} = 0, \alpha_{0,1} = 1.226$ and $\alpha_{1,0} = 0.589$. Cell resonances amplify the acoustic power at the resonance frequency. Geometries other than cylindrical have also been used in PA cell design. Ioli *et al.*[10]

directed the laser radiation transverse to a cylindrical sample cell and this configuration allowed excitations of a lower frequency longitudinal resonances with simultaneous placement of the microphone along the axis of the PA cell for more efficient coupling of the acoustic energy on to a small diaphragm microphone.

In addition to the radial and axial resonant cell design, there has been considerable interest in the use of cells that employ Helmholtz resonance[11- 13]. Here we have two volumes V_1 and V_2 which form respectively as sample and microphone chambers. These chambers are connected by a channel of length l_c and cross sectional area A . The resonance frequency is given by [3]

$$f_{res} = \frac{C_0}{2\pi} \sqrt{A/l_c V_r}$$

where $V_r = \frac{V_1 V_2}{V_1 + V_2}$. This configuration can avoid the generation of spurious acoustic signals due to the interaction of the scattered light from the sample, sample holder and window with the microphone surface. Another important advantage of this configuration is that one can keep the sample chamber away from the microphone chamber by using a sufficiently long connecting tube for performing temperature variation studies where the sample has to be kept at very low or very high temperatures[14,15].

The Brewster windows for minimum light scattering, multipassing for increased sensitivity, acoustic baffles for reduced effects due to window absorption etc, can be incorporated for improved performance of PA cells. The effects of window heating can be eliminated by using a differential cell design[16].

2.1.3 Acoustic detectors

The PA signal generated in the cell can be detected by any sensitive microphone. A condenser microphone produces electrical signal when a pressure wave impinges on the diaphragm. Such microphones generally have flat frequency response

up to $\approx 15\text{KHz}$, low distortion and are not sensitive to mechanical vibrations. Electret microphones[17] constructed using solid material of high dielectric constant, which are electrically polarized, can also be used for detecting PA signals. No bias voltage is required for electret microphone and due to the large capacitance/area possible from electret materials, they can be made into miniaturized microphones. Piezoelectric devices can also be used to sense the elastic waves generated in radiation absorbing solids and liquids[18,19,20]. These devices offer much better acoustic impedance matching to the condensed samples and can detect high frequency signals.

2.1.4 Signal processing

Since the PA signal is very weak, processing of the output signal from the microphone must be done with great care. In order to maximize the signal to noise ratio, the signal from the microphone preamplifier should be processed by an amplifier tuned to the chopping frequency. Generally a phase sensitive lock - in amplifier is used for this purpose. Using a phase sensitive lock - in amplifier[21] one can measure the phase as well as the amplitude of the PA signal. A lock - in amplifier can also eliminate noise from other sources. Using a dual phase lock - in amplifier the measurements can be taken very easily, particularly when both amplitude and phase vary simultaneously.

2.2 The present experimental setup

A photoacoustic imaging setup has been arranged by incorporating a single beam PA spectrometer with a microprocessor controlled scanning unit. All the investigations described in this thesis except depth profiling experiment has been performed with this experimental setup. A block diagram of the experimental setup is shown in figure 2.2. The main parts of the system are (1) a 10 mW He-Ne laser, (2) an electro mechanical chopper, (3) a PA cell, (4) a scanning unit and (5) a lock-in amplifier.

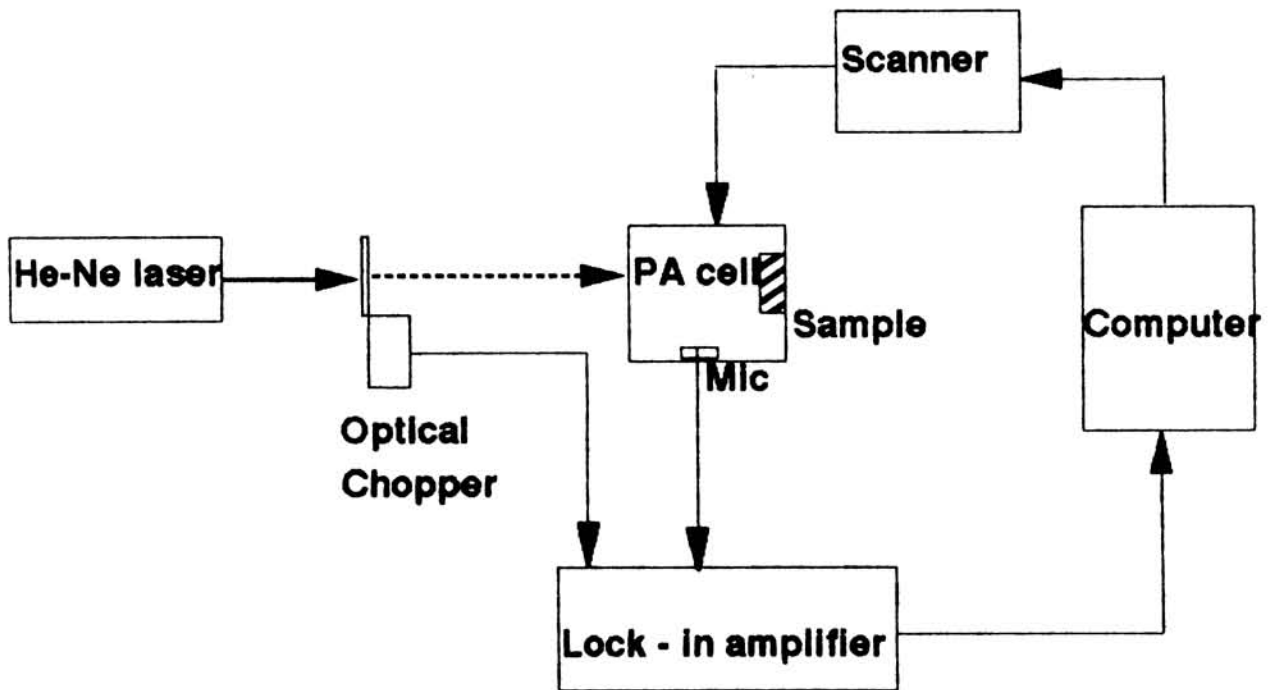


Fig 2.2 : Block diagram of the experimental setup used in this work

A 10 mW He-Ne laser (M/s Spectra Physic Inc.) has been used as the radiation source in most of the work reported in this thesis. It gives out continuous laser radiation of wave length 632.8nm. For the intensity modulation of the incident laser beam a mechanical chopper (Photon Technology International, Model OC 4000) is used. Using the two discs supplied with the chopper, one can vary the chopping frequency continuously from 4 to 4000 Hz. The chopper also provides the reference signal for triggering the lock-in amplifier.

A single phase lock-in amplifier (Stanford Research Systems, Model SR 510) is used for processing the PA signal detected by the microphone kept in the PA cell. The lock-in amplifier has a full scale sensitivity of 1nV to 500mV and an operating frequency range 0.5Hz to 100KHz. Phase can be adjusted in large steps of 90° and fine steps of 0.025°. Phase shift as well as frequency can be read on a four digit LCD display. The signal amplitude can be read either on the analogue meter or on the auto ranging LCD display.

2.2.1 Construction and standardization of the PA cell

The PA cell is considered as the heart of any PA spectrometer. A small volume room temperature PA cell which is suitable to be attached to the mechanical scanning unit has been fabricated for the present investigations. The design aspects of this PA cell is outlined below.

The small volume non-resonant PA cell is made of aluminum. Fig. 2.3 gives a sketch of the cell with its various parts. An axial bore of diameter 2.2cm is made in a solid aluminium cylinder of diameter 6cm and length 6cm which constitute the cell body. The sample holder, which is also made of aluminium, can be just fitted into this bore. The sample holder is designed in such a way that samples of different thicknesses

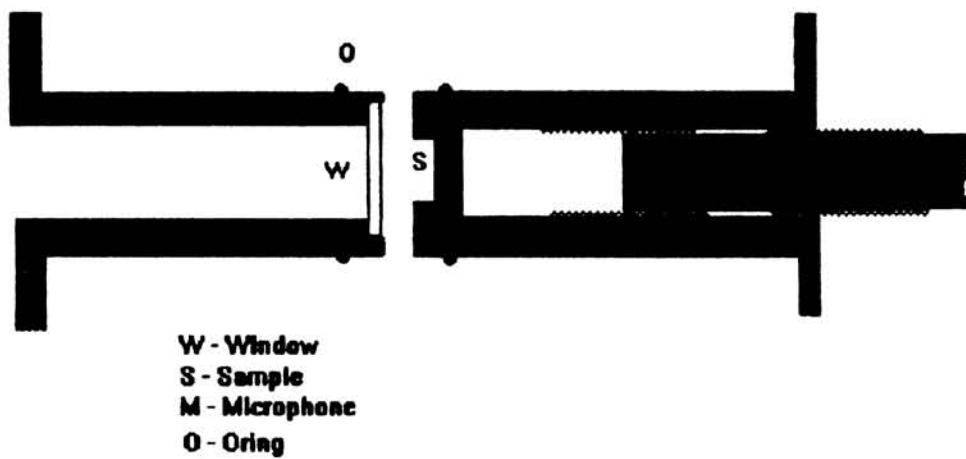
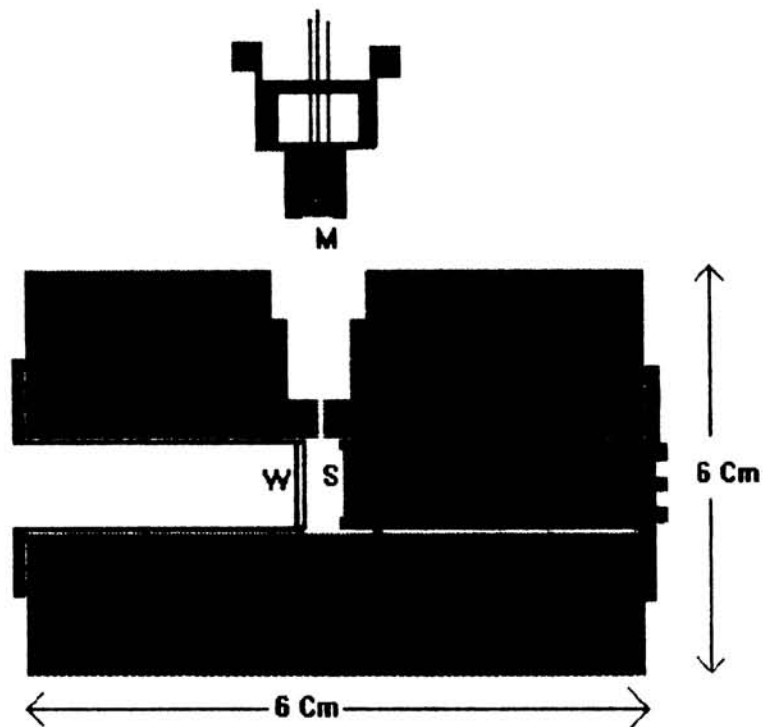


Fig 2.3 : A cross sectional view of the room temperature PA cell

can be accommodated in the cell. A glass window is provided to illuminate the front surface of the sample. 'O' rings on the window and sample holder are used to isolate the cell volume acoustically from outside.

The PA signal is detected using a microphone kept very close to the sample compartment through a side port in the cell body. A small size high sensitive electret microphone (Knowels, Model BT 1759) having a built in FET preamplifier has been used for the detection of the acoustic signals. It has got a flat frequency response in the frequency range 10 Hz to 5000 Hz. Power source to the microphone and its preamplifier are enclosed in a metallic case. A BNC connector is attached to the case for taking the microphone signal to the lock-in amplifier. The minimum distance between the sample and window is 2 mm. This is very much greater than the thermal diffusion length of air which is 0.06 mm at a chopping frequency of 10 Hz. The minimum volume of the enclosed air in the cell is ≈ 1 cc. The distance between the window and sample can be adjusted by moving the window holder.

The frequency response of this PA cell has been measured using carbon black as the standard sample. Carbon black sample is irradiated with the chopped beam of He-Ne laser at various chopping frequencies. The amplitude as well as the phase of the PA signal generated in the cell have been measured. The variation of PA signal amplitude with chopping frequency for the carbon black sample is shown in Fig. 2.4. This plot clearly shows the ω^{-1} dependence of the PA signal as predicted by the R-G theory at chopping frequencies above 40 Hz . This means that the cell response will be best for a chopping frequency around 40 Hz. The corresponding variation in the phase of the PA signal is shown in Fig. 2.5. For a saturated PA signal, R-G theory predicts that the phase shift at the sample surface should be constant.

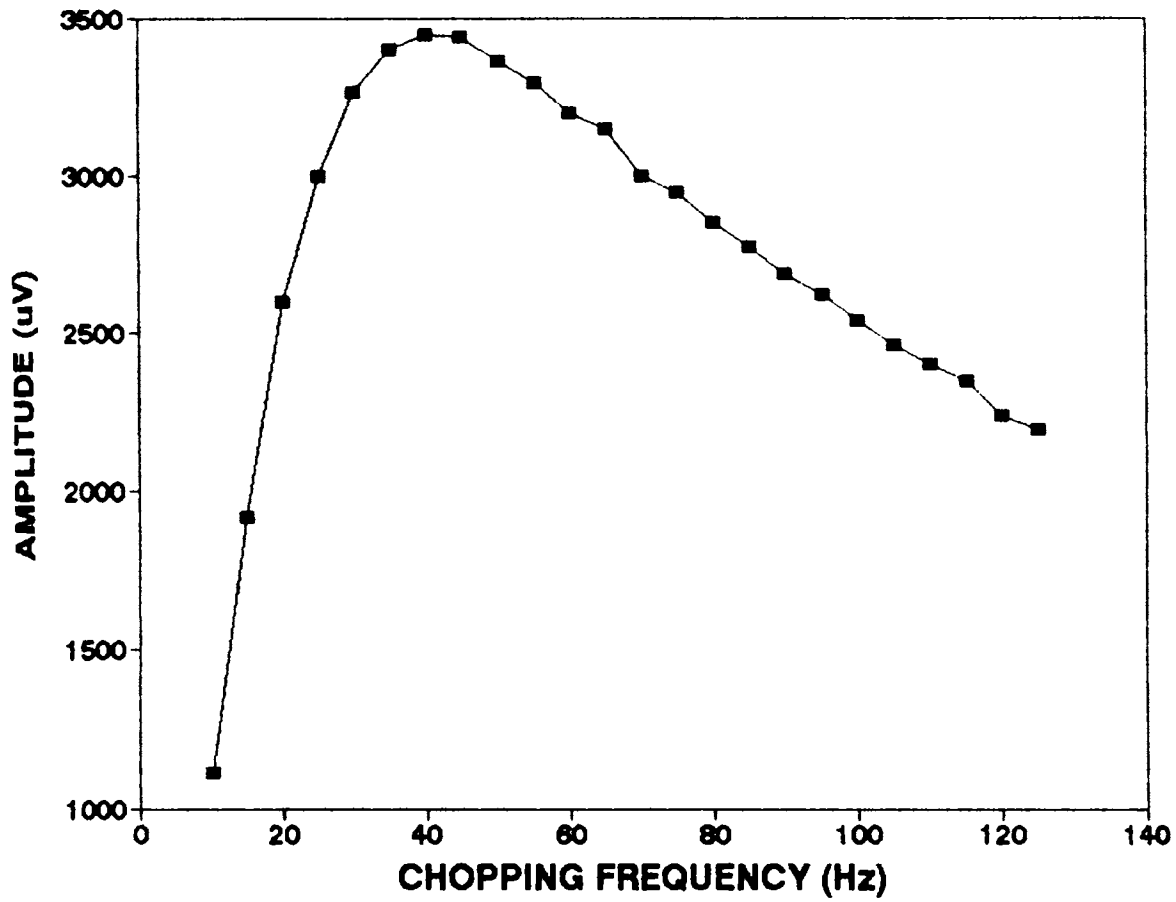


Fig 2.4 : Variation of the PA amplitude with chopping frequency for carbon black sample

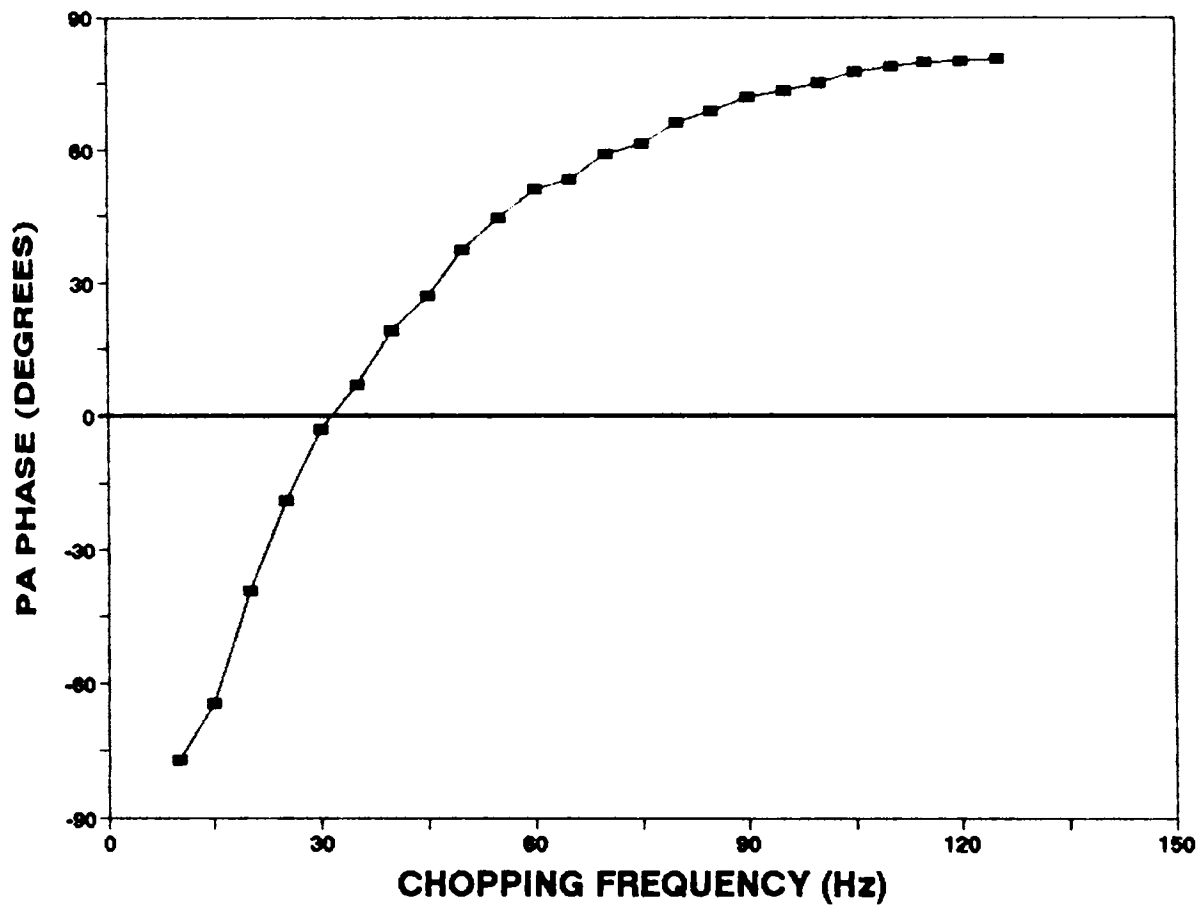


Fig 2.5 : Variation of the PA phase with chopping frequency for carbon black sample

2.2.2 Microprocessor controlled scanning unit

In order to obtain the surface or subsurface images of a sample by the photoacoustic or photothermal imaging technique, it must be subjected to a surface scan with an intensity modulated beam of light after placing it inside a PA cell. Because of the electrical neutrality of light, surface scanning with a light beam has ~~be~~ accomplished by nonelectrical methods. For achieving the surface scan, a mechanical scanning unit which is controlled by a microcomputer system, has been designed and fabricated. The unit enables one to scan the surface of a sample point by point with an optical beam and produce a photoacoustic image of the surface and interior of the sample. The technical details of the system, including mechanical parts, controlling hardware and software are given in the following sections.

2.2.2.a Mechanical assembly of the scanning unit

The scanning unit which we have fabricated is a platform which is capable of moving in both X and Y directions. The main parts of this platform are made of cast iron. The different parts of the mechanical assembly of this platform are shown in Fig. 2.6. The platform P which is provided with the facility for fitting the PA cell on it, can be moved along the tracks provided on the beam H. The nut N_1 which is able to move along the shaft S_1 is attached firmly to the platform P. The shaft is fixed on the horizontal beam by means of two ball bearings B_1, B_1 . Thread on the shaft is made with a pitch of 1 mm. This shaft is attached to the shaft of a stepper motor of torque 3 Kg-cm by means of gear and wheel arrangement. When the stepper motor I begins to rotate, the platform moves along the beam H in either direction depending on the direction of rotation of the stepper motor. The beam H and the components on it all together are attached to the vertical pillar R using shaft S_2 , nut N_2 and ball bearings (B_2, B_2) as in the same way the platform is attached on the beam H using the shaft S_1 ,

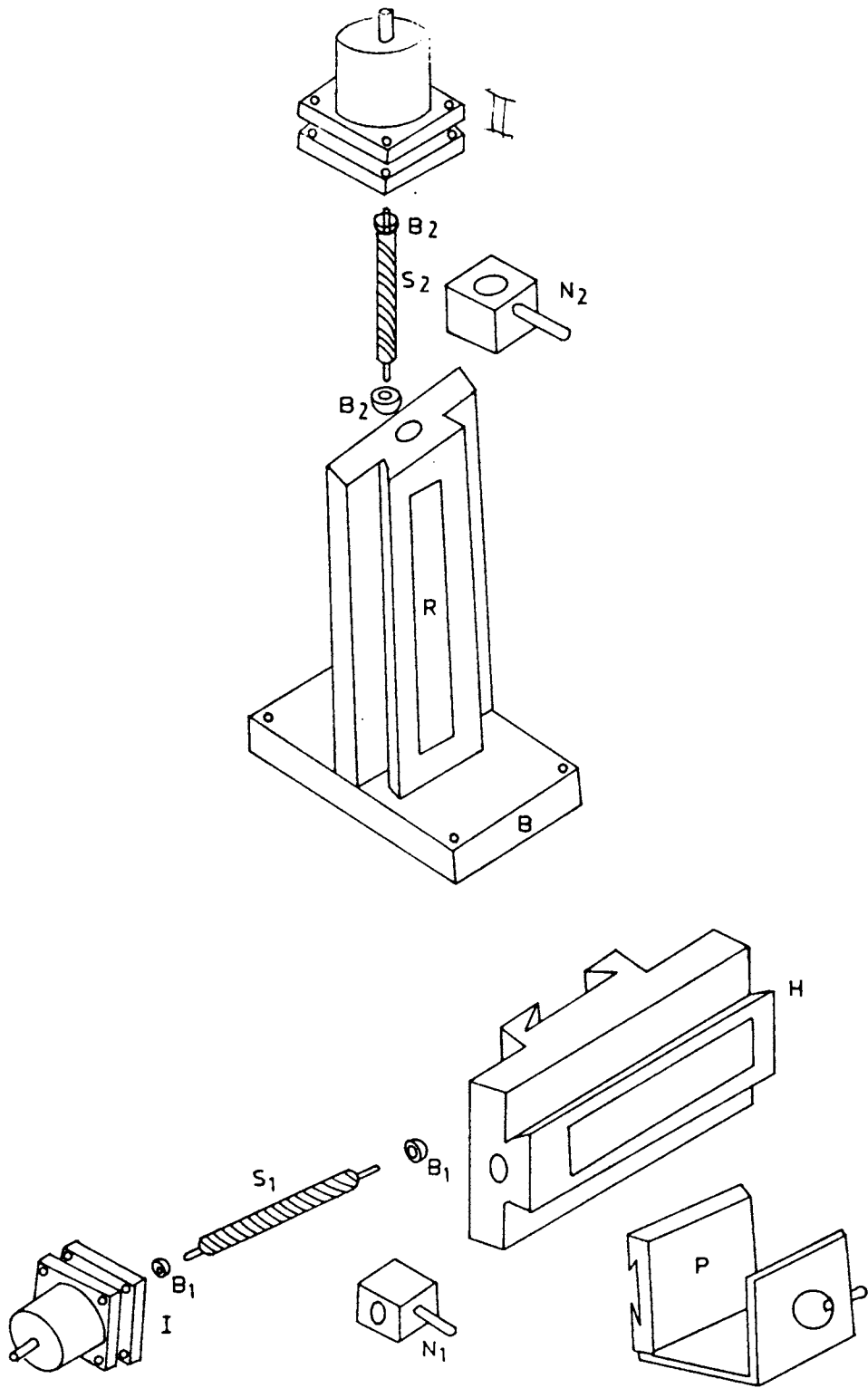


Fig 2.6 : Mechanical assembly of the PA scanning unit

the nut N_1 and the ball bearings (B_1, B_1). The pillar R is fixed rigidly on a base B. The vertical movement of the platform is performed with a 10 Kg-cm torque stepper motor. The beam H and the platform on it together can move either in the upward or downward direction depending upon the direction of rotation of the stepper motor II.

2.2.2.b Description of the stepper motors and driving circuit

Stepper motors are more convenient to be interface to a computer system, because they are themselves digital electromechanical devices[22, 23]. Stepper motor rotates only through steps, unlike ordinary d.c motors, upon delivering current to some set of coils in a particular manner repeatedly. We have employed two stepper motors, one of torque 3 Kg- cm and the other of torque 10 Kg- cm (type DSC 20, DSC 31, Unique systems and controls Pvt. Ltd.), for driving the platform. Both are 4 phase stepper motors. They operate at a d.c voltage of 12 volt and consume approximately 8 watts power. The phase configuration of a typical 4 phase stepper motor is exhibited in Fig. 2.7. All the primed end of the coils i.e. A' , B' , C' and D' are taken as common and are connected to the negative of the supply. A combination of two phases out of four selected in a particular order are switched to the positive supply simultaneously for a single step motion.

In order to use the stepper motor continuously, one has to energise repeatedly the four combinations of phases following the sequence shown in Tables 2.1 or 2.2.

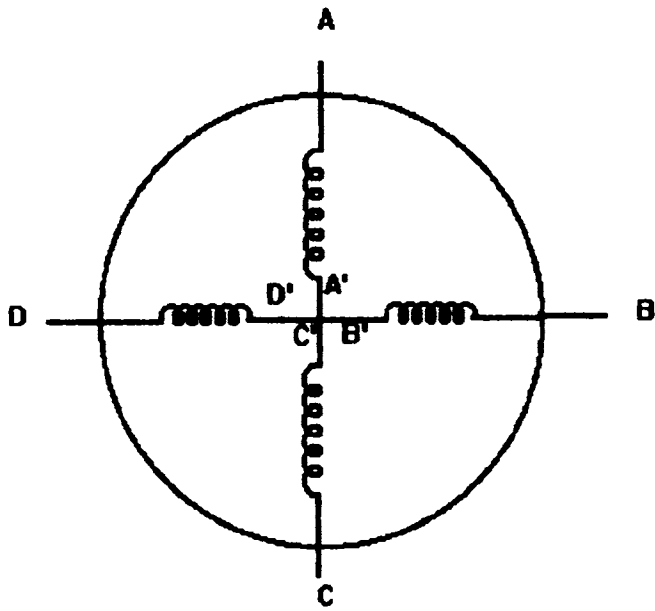


Fig 2.7 : Phase configuration of a typical four phase stepper motor

Table 2.1

Forward Rotation

Step	A	B	C	D
1	1	0	0	1
2	1	0	1	0
3	0	1	1	0
4	0	1	0	1

Table 2.2

Reverse Rotation

Step	A	B	C	D
1	0	1	0	1
2	0	1	1	0
3	1	0	1	0
4	1	0	0	1

The sequence of the Table 2.1 is for forward motion whereas the sequence of Table 2.2 is for reverse motion of the stepper motor. the speed of the motor can be controlled by varying the intervals in between each pulse sequence applied to the motor. Both motors used in our scanning unit can rotate 1.8° for each step. This means that, the motors require 200 steps motion for a complete rotation. Since the pitch of the shafts of the platform which are coupled to the stepper motors is 1 mm, the spatial shift of the platform is $1/200$ mm for every step.

The driving circuit of the two stepper motors is shown in Fig. 2.8 [24]. This circuit is composed of two channels, such that one channel is for driving one stepper motor. There are four sets of darlington pair transistors in each channel in the switching mode which are connected serially with each coil of the stepper motor and power supply. Each of the four coils of the motor can be energized separately by applying a small positive voltage (≈ 5 V) at the free end of the base resistor of each darlington pair. The distribution of the base voltage to each channel as in the sequence given in the Tables 2.1 and 2.2 is managed by a microcomputer built around an Intel 8085 processor.

The circuit diagram of the transistorised regulated power supply of 12 Volt, which can deliver a maximum load current of 2A is used to drive the two stepper motors in the scanning unit, is shown in Fig. 2.9.

2.2.2c Description of microprocessor interfacing

2.2.2c.1 Hardware

We have interfaced the scanning unit which is discussed in the above section 2.2.2 with an Intel 8085 [25,26,27] processor in a microprocessor kit (Dynalog Microfrind I, Dynalog Microsystem) through a programmable peripheral interface 8255 provided in the kit.

The system consists of the 8085A CPU, keyboard display controller 8279, two programmable peripheral interfaces 8155 and 8255, 4K ROM 2732, 2K RAM 6116 and other TTL devices essential for decoding and control signal generation. The address data and control bus are brought to the edge connector for expansion. The parallel I/O lines provided by 8155 and 8255 are separately brought out on two 26 pin flat cable connectors. The basic memory map and I/O map of the system are given in Tables 2.3

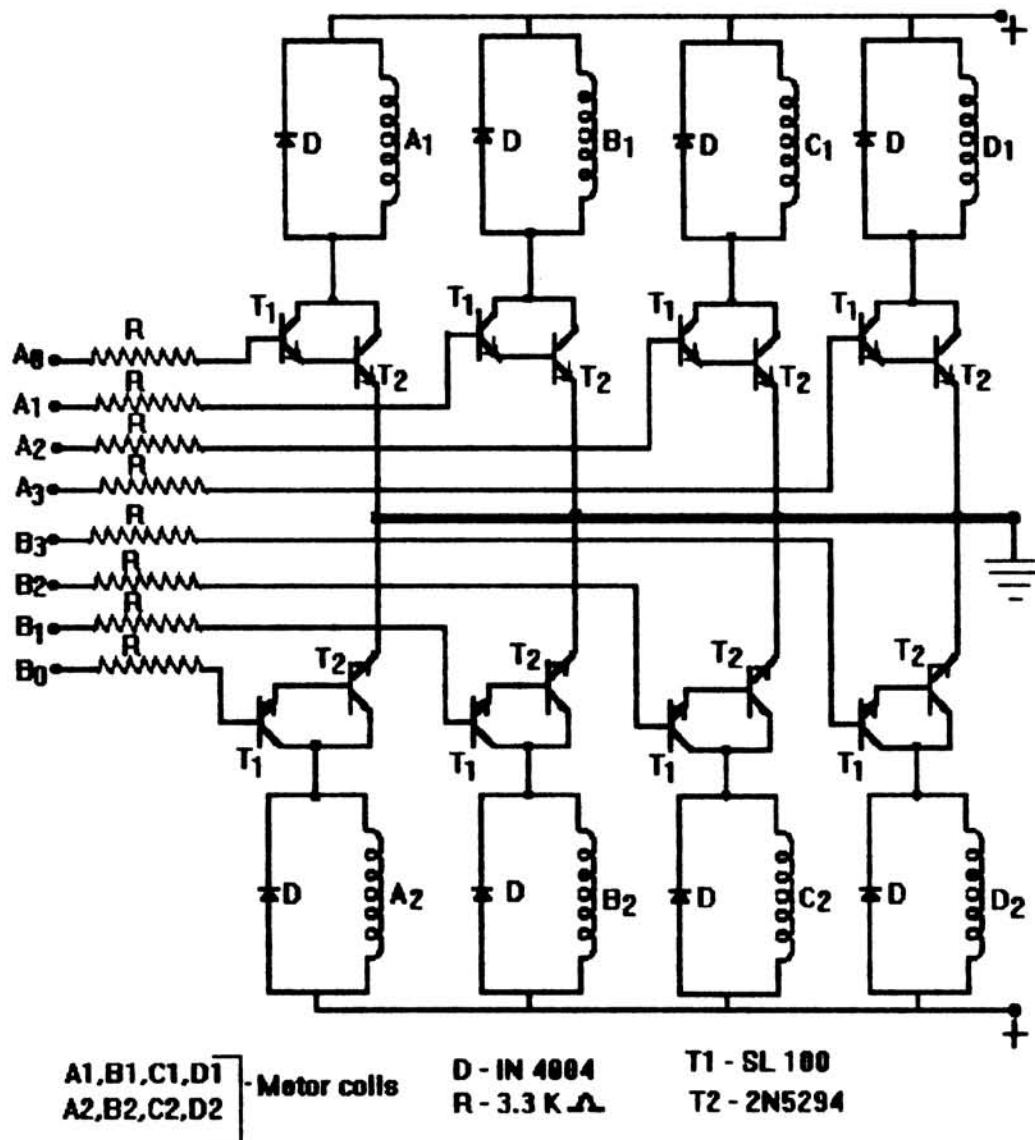


Fig 2.8 : Driving circuit of the PA scanning unit

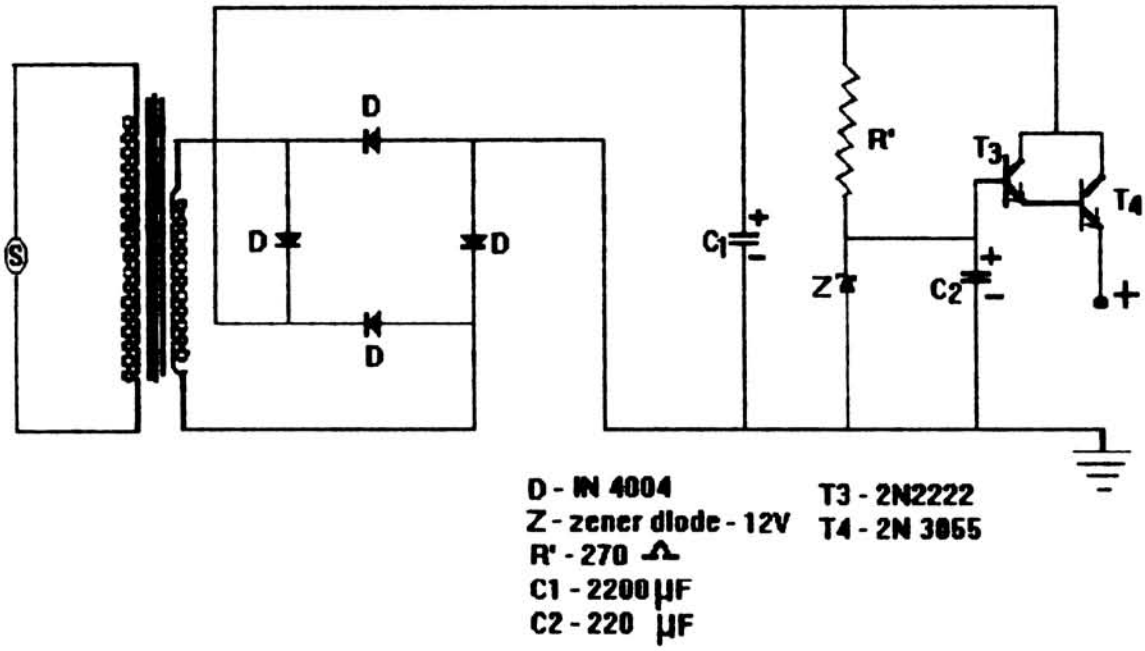


Fig 2.9 : Circuit diagram of power supply

and 2.4 respectively [28].

Table 2.3 Memory Map

0000 - 0FFF	- 4K system monitor 2732
1000 - 17FF	- 2K user RAM 6116
1800 - 1FFF	- 2K user RAM 6116
2000 - 27FF	- Not available to user
2800 - 2FFF	- user RAM 2K
3000 - 37FF	- user RAM 2K
4000 - 4FFF	- user EPROM 4K
5000 - 5FFF	- user EPROM 4K
6000 - 6FFF	- user EPROM 4K

Table 2.4 I/O Map (8255, 8279 & 8155)

I/o Address		
00 - 03	00 to 03 for 8255A - 5 PIO	
04	- Read - Write	Read key board FIFO Write data to display
05	Read Write	read status word Write command word
06 & 07	Not used	not available
08	command/ Status Register (CSR) of 8155	
09	PA register	
0A	PB register	
0C	PC register	
0D	Timer High byte	
0E & 0F	Not used, not available	

The 8255A PPI provides three 8 bit ports for transferring data between the peripheral devices and the microprocessor [25].

The address of three I/O ports available in the 8255A PPI is given below.

<u>Address</u>	<u>Port</u>
00	A
01	B
02	C
03	control register

The signal configuration of 8255A [25] PPI is depicted in Fig. 2.10. Data is

transferred between the microprocessor and the 8255A on the $D_0 - D_7$ bus. The three ports of the 8255A can operate in any one of the following three modes.

Mode 0 : Basic input / output

Mode 1 : Strobed input / output

Mode 2 : Bidirectional data bus

The mode definition and control word format of the PPI[25] is shown in Fi.2.11.

The two stepper motors in the scanning unit are interfaced with the microprocessor through port A (motor I) and port B (motor II). For this purpose we have made a control word 80H which is selected when the three ports A, B and C are in 0 mode and output configuration. The block diagram of interfacing of the scanning unit is shown in Fig 2.12. Since, 4 bit control signal is enough for the operation of each stepper motor the least significant 4 bits of each of ports A and B are connected to the driving circuit using flat cable connectors.

2.2.2c.2 Software

We have also developed a software package for operating the scanning unit. Using this software package one can operate the scanning unit in step by step fashion with the desired speed. The area to be scanned can also be controlled with the software. The flowchart of the program is given in Fig. 2.13. The software package is fused in a 4K EPROM 2732 and installed in User EPROM field. The complete program in assembly language along with Op codes is given in Appendix 1.

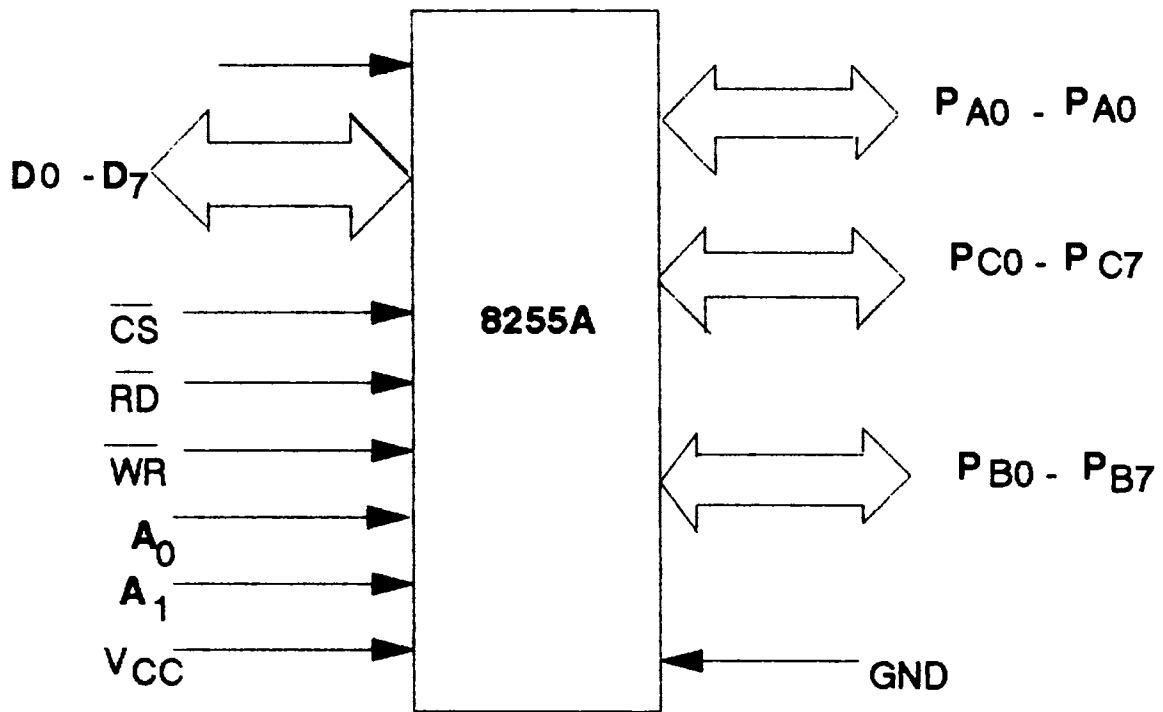


Fig 2.10 : Signal configuration of 8255A PPI

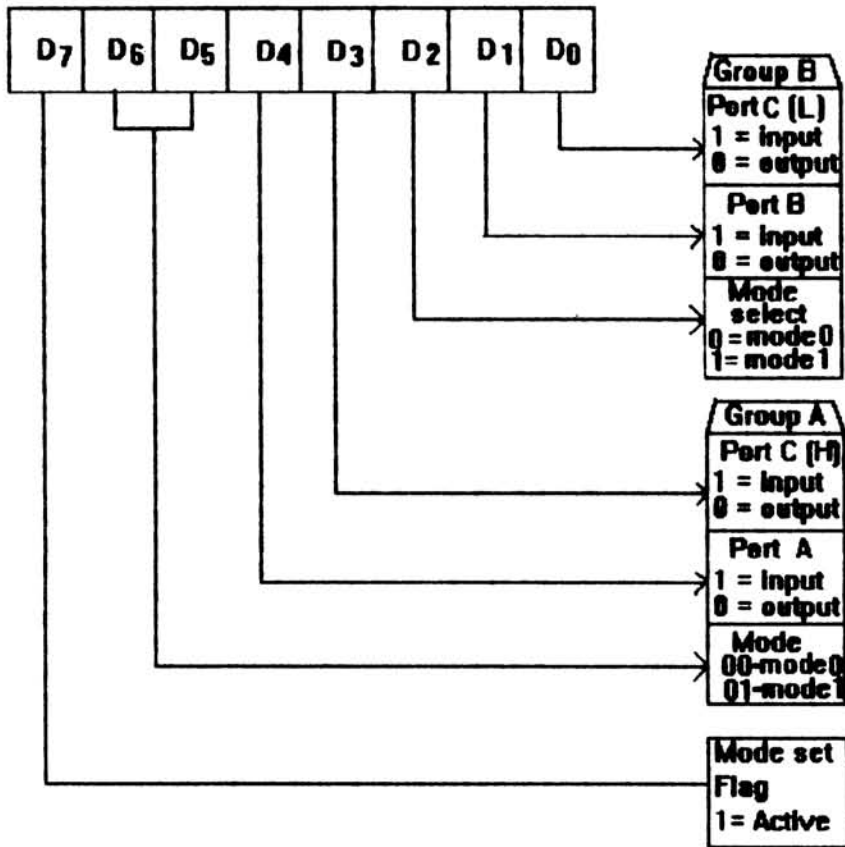


Fig 2.11 : Mode definition and control word

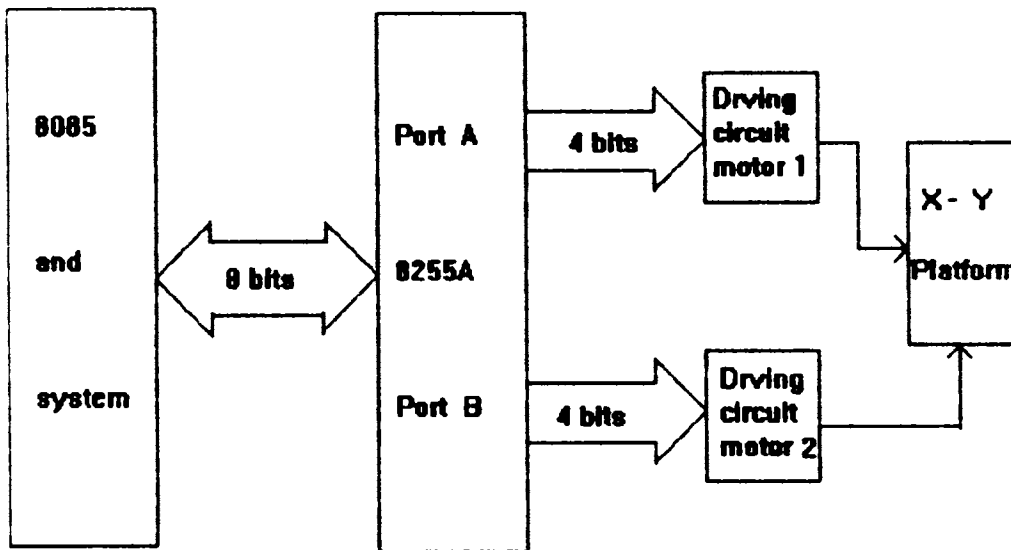


Fig 2.12 : Block diagram of interfaced scanning unit

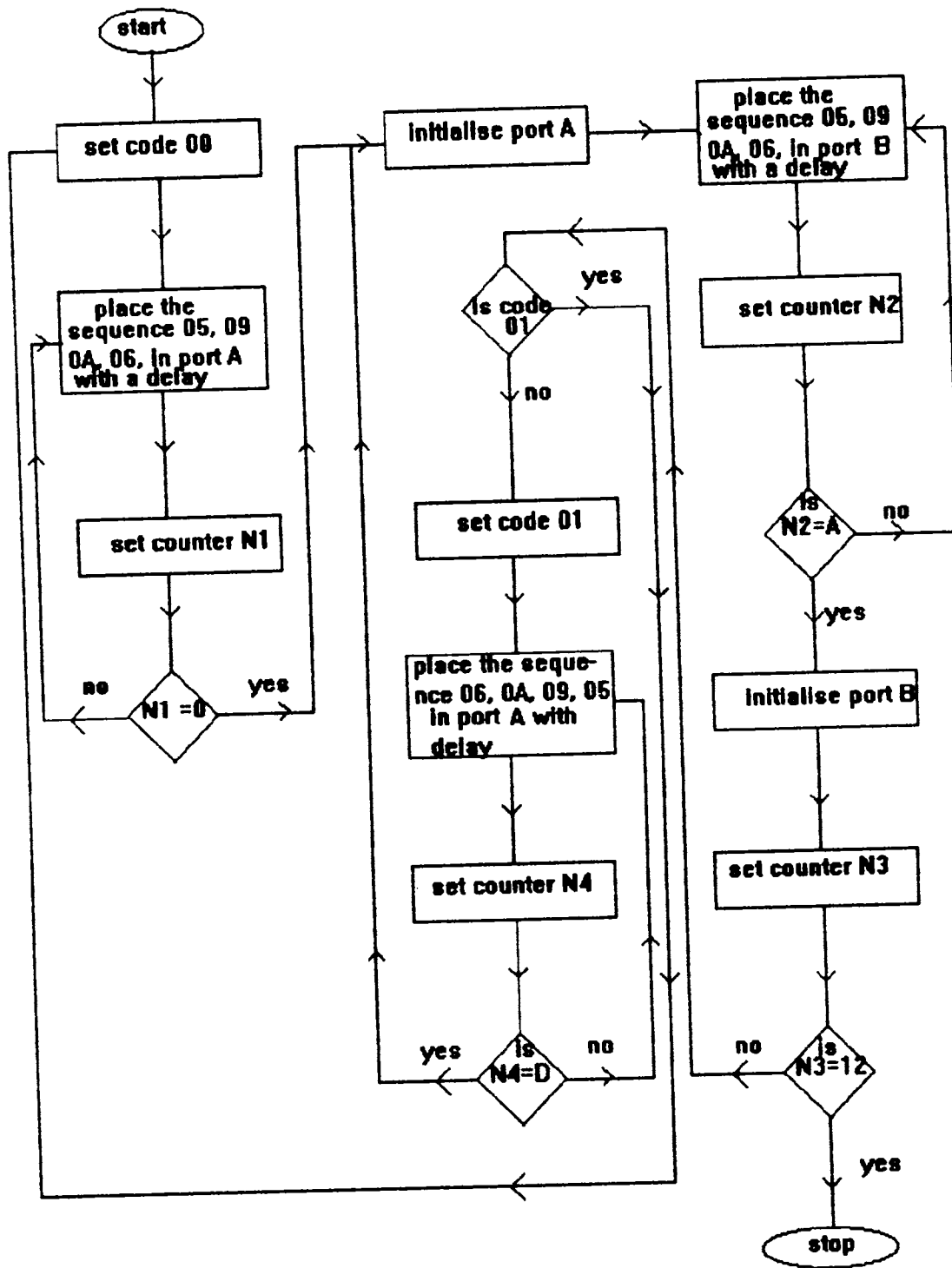


Fig 2.13 : Flowchart of software package of the PA scanning system

2.3 Automated photoacoustic imaging unit

A photograph of the automated imaging set is displayed in Fig. 2.14. Functioning of the setup has been tested several times before the actual experiments were carried out. Using this setup one can scan a surface of area of 7 cm x 7 cm in a step by step fashion. But our usual requirement of scanning area is very small, about 3 cm² which is the cross sectional area of the PA cell. This setup provides very good lateral resolution of the order of 5 micron per step. Although the stepwise motion of the PA cell in the setup contribute some noise to the PA signal, it can be eliminated by increasing the time delay between each step during motion. The overall performance of this imaging setup is found to be good and reliable.

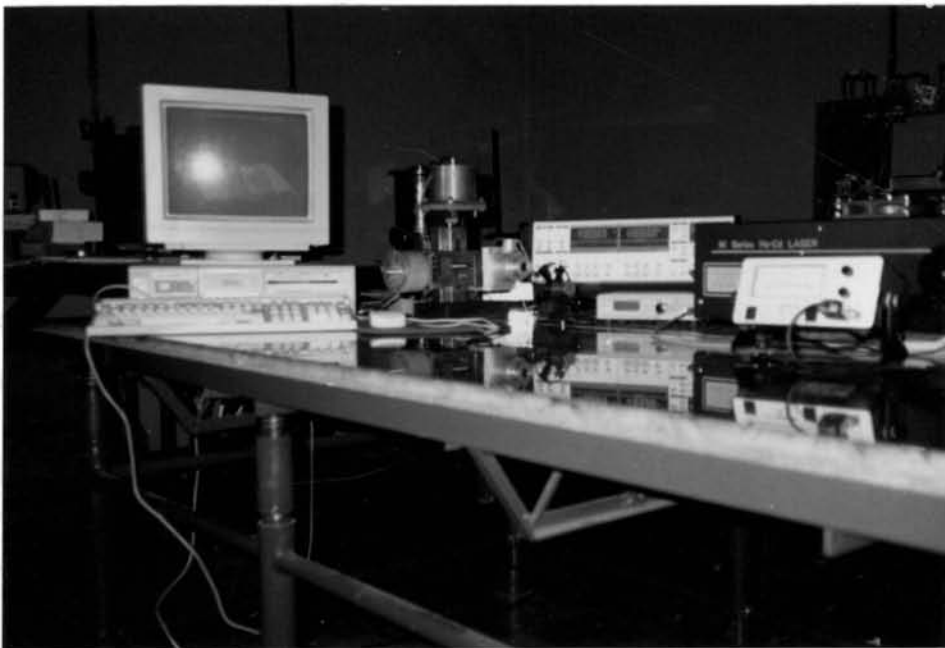
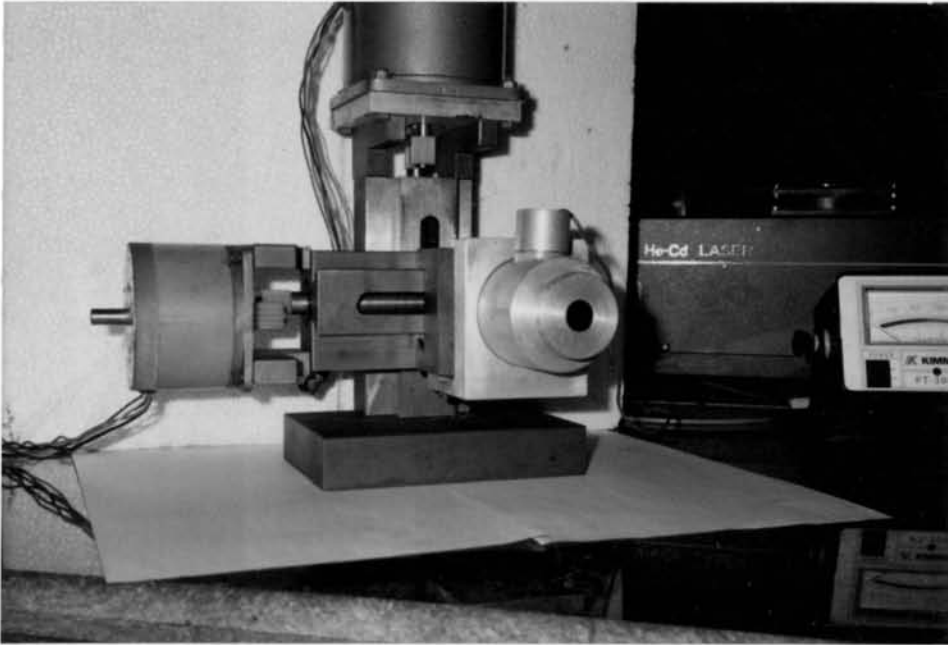


Fig 2.14 : Photograph of the PA scanning system

References

- [1] A. Rosencwaig and A. Gersho, *J. Appl. Phys* **47**, 64 (1976)
- [2] A. C. Tam, *Ultrasensitive Laser spectroscopy*, P-1 ed: Klinger, (Academic Press, New York, 1983)
- [3] A. Rosencwaig, *Photoacoustics and Photoacoustic spectroscopy* (Wiley New York, 1980)
- [4] C. F. Dewey, *Optoacoustic spectroscopy and Detection*, P-47, ed: Y. H. Pao, (Academic press, New York, 1977)
- [5] L. G. Rosengren, *Appl. Opt.* **14**, 1960 (1975)
- [6] P. M. Morse, *Vibration and Sound* (Mc Graw - Hill, New York, 1948)
- [7] L. A. Farrow and R. F. Richton, *J. Appl. Phys.* **48**, 4962 (1977)
- [8] C. F. Dewey Jr., R. D. Kamm and C. E. Hackett, *Appl. Phys. Lett.* **23**, 633 (1978)
- [9] E. Kritchman, S. S. Shtrikman and M. Statkine, *J. Opt. Soc. Amer.* **68**, 1257 (1978)
- [10] N. Ioli, P. Violino and M. Meucci, *J. Phys. E* **12**, 168 (1979)
- [11] N. C. Fernelius and T. W. Hass, *Appl. Opt.* **17**, 3348 (1978)
- [12] N. C. Fernelius, *Appl. Opt.* **18** 1784 (1979)
- [13] R. S. Quimby, P. M. Selzer and W. M. Yen, *Appl. Opt.* **16**, 2630 (1977)
- [14] J. C. Murphy and L. C. Aamodt, *J. Appl. Phys.* **48**, 3502 (1977)

- [15] P. A. Bechthold, M. Campagna and J. Chatzipetros, **Opt. Commun.** **36**, 369 (1981)
- [16] T. F. Deaton, D. A. Dapatie and T. W. Walker, **Appl. Phys. Lett.** **26**, 300 (1975)
- [17] G. M. Sessler and J. E. West, **J. Acoust. Soc. Amer.** **53**, 1589 (1973)
- [18] A. Hordvik and H. Schlossberg, **Appl. Opt.** **16**, 101 (1979)
- [19] C. K. N. Patel and A. C. Tam, **Appl. Phys. Lett.** **34**, 467 (1979)
- [20] C. L. Sam and M. L. Shand, **Opt. Commun.** **31**, 174 (1979)
- [21] M. L. Meade, **Lock - in amplifier: Principles and Applications** (Peter Peregrinus Ltd., London, 1983)
- [22] S. Boada, M. P. Srinivasan and A. Pittet **Stepping motors**, (Center for Electronic design and Technology, IISc, Bangalore)
- [23] S. W. Fardo and D. R. Patrick, **Electrical Power Systems Technology**, (Prentice Hall, Inc. Englewood)
- [24] B. S. Sonde, 'Power supplies' **Monographs on solid state Electronic Instrumentation: 5** (Tata Mc Graw - Hill, New Delhi 1981)
- [25] R. S. Gaonkar, **Microprocessor Architecture, Programming and Application with the 8085 / 8080A** (Wiley Eastern Ltd., New Delhi 1993)
- [26] A. P. Mathur, **Introduction to Microprocessors**, (Tata Mc Graw Hill, New Delhi)
- [27] A. P. Malvino and D. P. Leach, **Digital Principles and Applications**, 4th Ed. (Mc Graw Hill , New Delhi 1986)
- [28] **Operation Manual of Microfrind I** (dynalog Microsystems)

CHAPTER 3

PHOTOACOUSTIC IMAGING OF SOLID SAMPLES

3.1 Introduction

Photoacoustic (PA) imaging is an emerging technology having very important applications for material characterization and nondestructive evaluation[1] of opaque solid materials. PA imaging of a solid can provide information about surface as well as subsurface features[2,3] of the sample. Photoacoustic imaging can be realised with different intensity modulated heat sources, such as lasers[3,4] or particle beams[5,6] and with various detectors such as microphones[3], ultrasonic transducers[4] or infrared detectors[7,8,9]. A number of review papers have appeared in literature covering various aspects of the technique[10-14]. These include articles by Busse[10], Rosencwaig[11] and Birnbaum and White[12]. Photoacoustic (PA) imaging can be easily accomplished by scanning the sample with an intensity modulated beam of focused laser light[15]. PA images with high spatial resolution can bring out microscopic level information from surface as well as subsurface of a solid sample. The spatial resolution depends on two factors (i) the spot size of the excitation light beam and (ii) modulation frequency of the light beam[3].

The work presented in this chapter is mainly aimed at evaluating the PA imaging technique in unveiling the surface and the subsurface informations of solid samples. This technique has been applied in different samples prepared from selected materials having widely different thermal properties. All the samples are prepared in such a way that artificial defects with known features have been introduced at the surface or interior of the samples. The experimental details, results obtained and a discussion of the results are described below separately for each sample.

3.2 Experimental details

The PA imaging setup, which has already been discussed in Chapter 2, is used for the present work. Depending upon the requirement, the He-Ne laser in the PA imaging experimental setup can be replaced by a He-Cd laser (120mW) of wavelength 442nm. The samples preferred for PA imaging are either in the form of a wafer or solid disc of nearly 2cm diameter. Samples subjected to PA imaging in the present work are silicon wafers, brass discs, nylon discs and teflon discs. The samples are chosen to have widely varying thermal properties.

3.2a PA imaging of silicon wafer samples

A silicon wafer of diameter nearly 2cm and thickness 0.5mm is used as a sample for surface PA imaging by making few scratches of nearly 1mm width on one side. Both surfaces of the sample, that is the surface having the scratches and the opposite surface without scratches, are scanned with a chopped He-Ne laser beam in a step by step fashion by keeping it in the PA cell of the imaging setup. The stepwise movement of the scanning system is in accordance with the software embedded in the system. Because of the finite spot size of the laser beam, the system is programmed so as to make a finite shift for each step in the X and Y directions. The lateral shift per step in the X and Y directions are respectively selected as 0.25mm and 0.5mm. Amplitude of the PA signals from each point on the surface of the sample is measured directly on the lock-in amplifier. The software of the system also provide few seconds of delay between each step, for stabilizing the output of the lock-in amplifier.

The surface of the silicon sample is scanned from top to bottom (Y - direction) in twenty lines. In each horizontal line (X- direction) scanning is completed in twenty steps. The sample is mounted in the PA cell in such a way that the scratches on the

sample come in the vertical plane of the surface area which is subjected to surface scanning. The other side of the silicon sample has also been scanned with chopped beam of He-Ne laser in a similar manner to bring out the difference.

The backlash error of the scanning unit due to reverse motion of the motors is determined to be nearly 10%. The PA signals obtained from the surface of the silicon wafer are manipulated by accommodating the backlash error in horizontal scanning and plotted to obtain a pseudo-3D view with the help of a computer.

3.2a.1 Results and discussion

PA imaging of front as well as rear surfaces of silicon wafer have been repeated a number of times by varying the modulation frequency of the excitation beam. The data obtained in each cases has been analysed and plotted separately. A typical pseudo-3D plot of the PA image obtained from the surface of the silicon wafer having surface scratches is shown in Fig. 3.1(a). This plot very clearly depicts the position of the scratches on the surface of the silicon sample. The nonuniformity of PA signals appearing at certain regions in the plot may be due to the presence of step like discontinuities present on the surface of the silicon wafer. Before conducting the experiments the surface of the silicon wafer has been examined very closely and ensured that the surface doesn't posses any discontinuity other than the scratches as far as possible. Therefore it can be concluded that the variations of PA signals in a particular region in the plot shown in Fig.3.1(a) is due to the presence of the scratch only.

From the theory of PA effect it is obvious that the amplitude of the PA signal generated from a point in the sample is primarily dependent upon the amount of light energy absorbed at that point. Naturally, the scratched or rough portion of the surface absorbs more energy. This is the cause of the increase in amplitude of PA signals

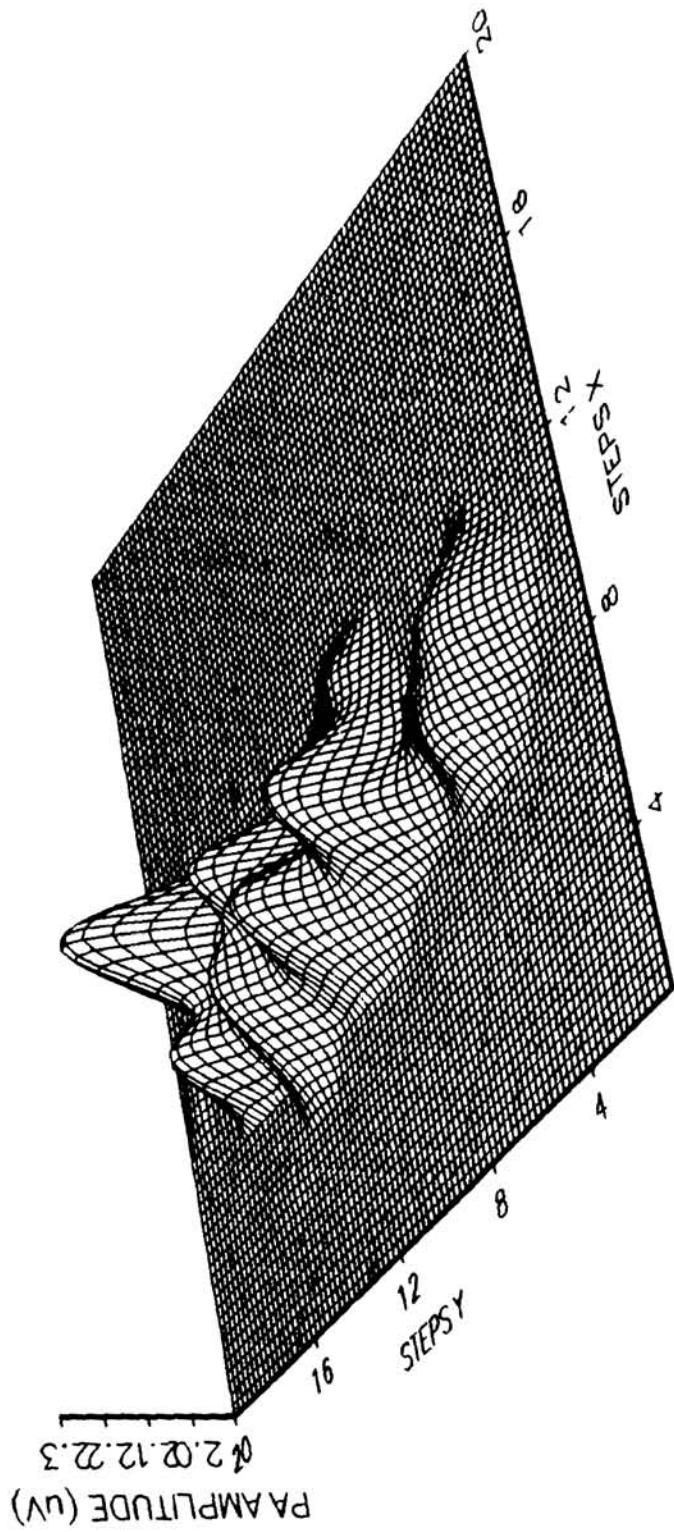


Fig 3.1a : Pseudo-3D, PA surface image of silicon wafer

at the scratched portions of the sample. Moreover, the thermal conductivity of the scratched region could be different from that of the background which also contribute to an enhancement in PA amplitude.

The plot shown in Fig. 3.1(b) is a hand plot of amplitude of PA signals obtained from a selected line on the surface of the same sample.

The data obtained during the rear surface scanning are also plotted in a similar manner. Fig. 3.2(a) and 3.2(b) are respectively the pseudo-3D computer plot and hand plot of a typical set of PA data obtained from the rear surface. In rear surface or subsurface PA imaging, chopping frequency of the excitation beam has an important role. PA imaging can unveil the rear surface or subsurface features only if it is within the thermal diffusion length the of PA signal. Therefore chopping frequency of the excitation beam in the rear surface imaging is selected in such a way that the silicon wafer is thermally thin at that frequency.

Figures 3.2(a) and 3.2(b) are the PA images of the rear surface of the silicon wafer having no scratches, at chopping frequencies 40Hz and 57Hz respectively. At these frequencies the silicon wafer is thermally thin. In these figures one can observe some nonuniformities of PA amplitude at certain region. It has been ensured that surface of the silicon wafer which is scanned with the laser beam does not posses any discontinuity. Since a glass plate is used as the backing of the sample, there is no chance of any discontinuity on the backing surface except due to the scratches made. Under these circumstances one can conclude that the variation of PA amplitude at a particular region in the sample is due to the presence of the scratch in the rear surface. f.c

3.2b PA imaging of nylon sample

Nylon disc is another sample which has been subjected to front and rear surface

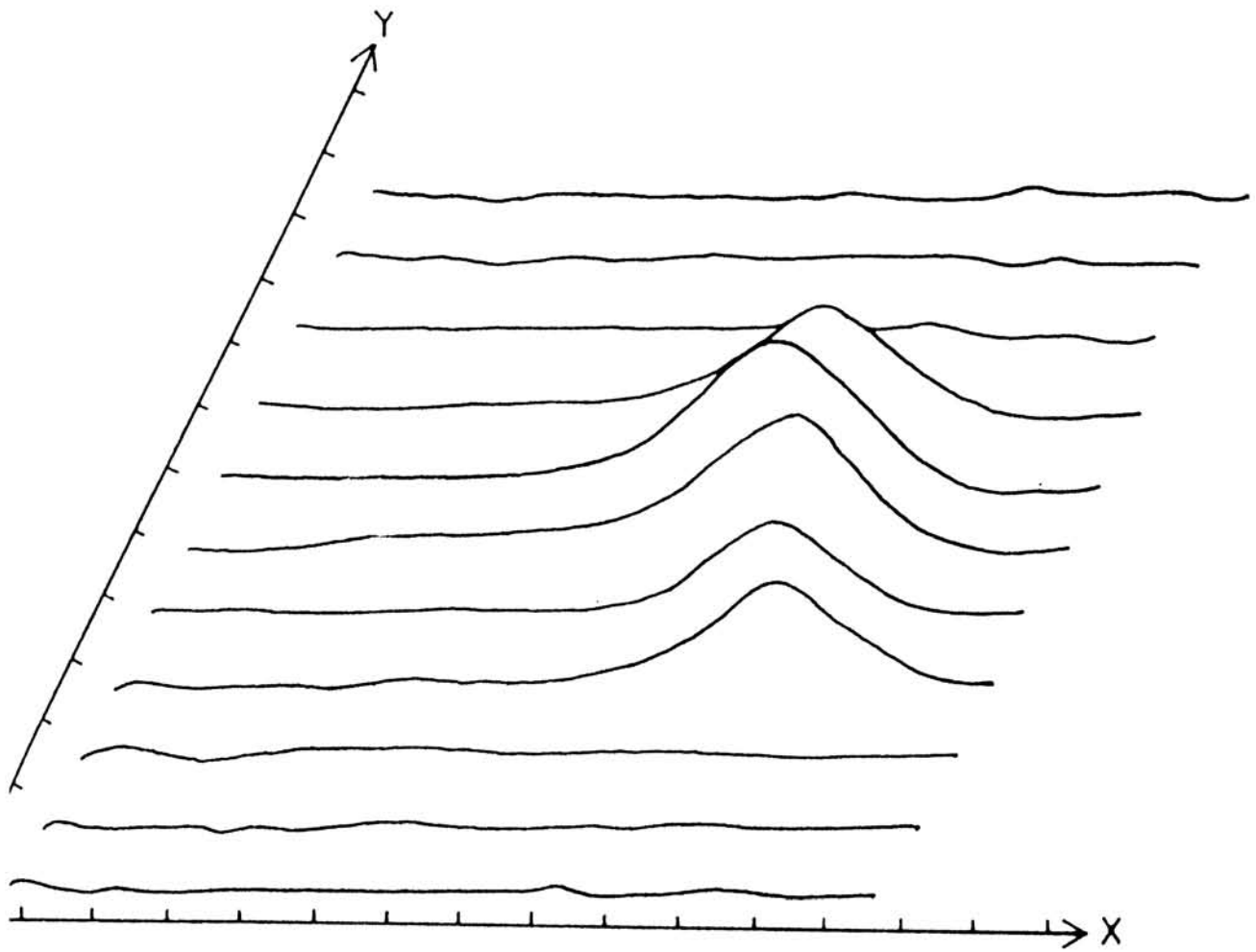


Fig 3.1b : Variations of PA signal amplitude with scanning distance from the surface of silicon wafer

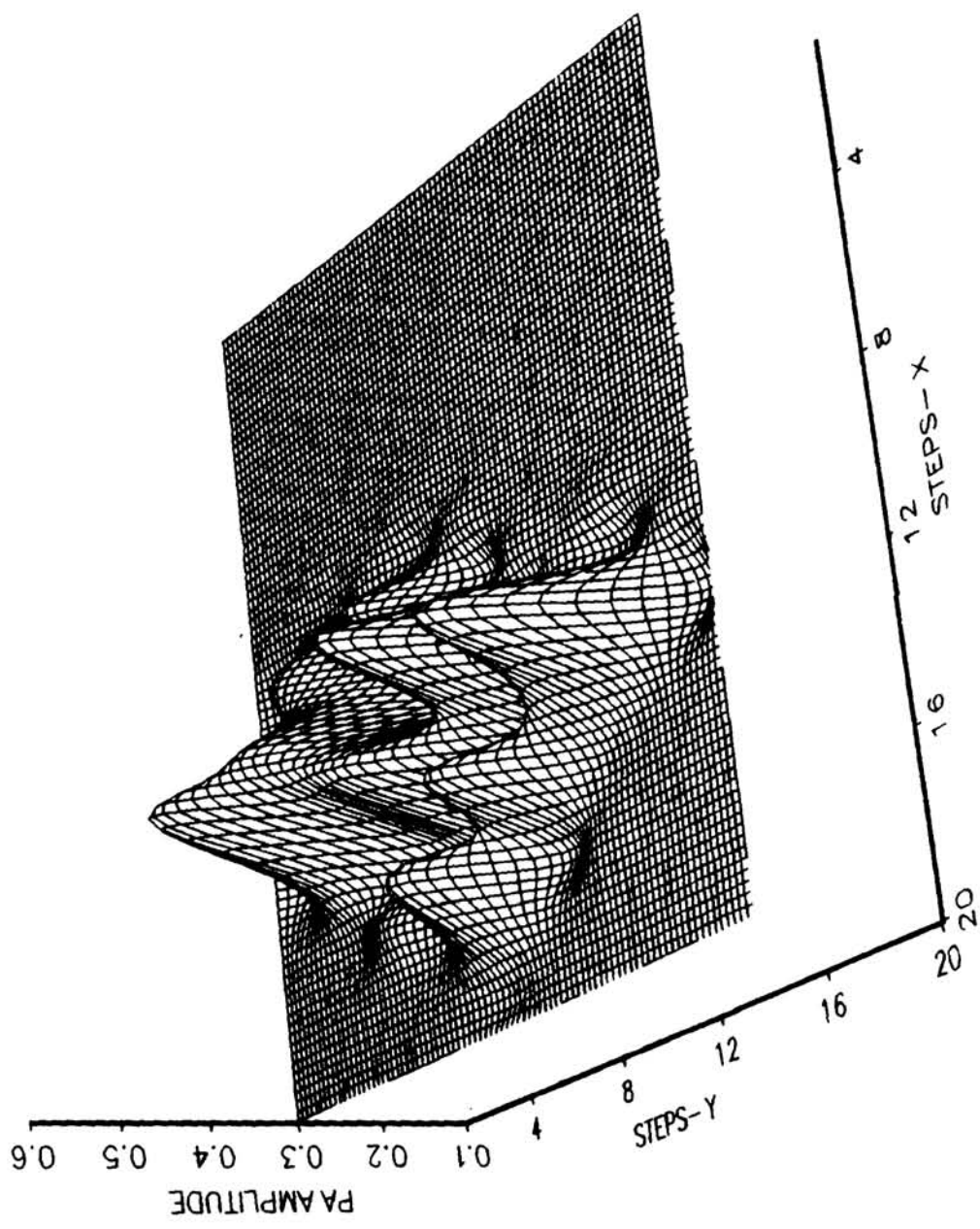


Fig 3.2a : Pseudo-3D, PA image of rear surface of silicon wafer

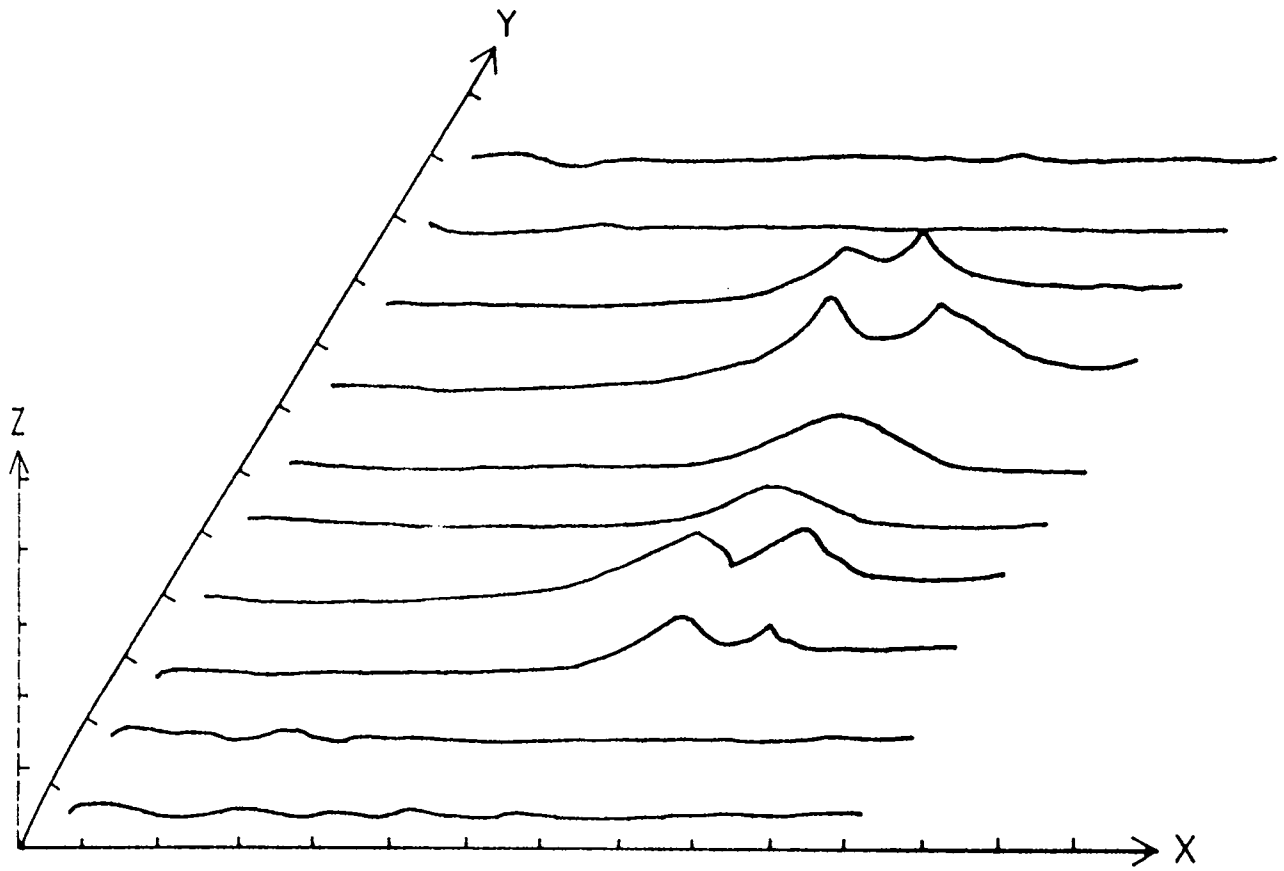


Fig 3.2b : Variations of PA signal amplitude with scanning distance from rear surface of silicon wafer

imaging. A circular nylon disc of diameter 2cm and thickness 2.5mm is prepared and its surface made as smooth as possible by hand lapping with fine emery paper. Three pin size pits are made on one surface in such a manner that two of them are in the same line, while the third pit is slightly inclined to this line. The diameter of these pits are equal and approximately 0.5mm, but their depths are different.

This sample has been subjected to surface as well as rear surface imaging. The experiments have been performed using a He-Cd laser (120mw, 442nm wavelength) as excitation source. The sample is placed in the PA cell in such a way that the pits on the sample surface are in the horizontal plane perpendicular to the light beam. The surface of nylon disc having pits is scanned with the chopped He-Cd laser beam by operating the scanner in X and Y directions in a step by step fashion. The linear shift for each step of the scanner is set to 0.5mm either in both X and Y directions. The frequency of the chopper is selected at 40Hz. The area containing the pits on the surface of the nylon disc is scanned in eight lines. Each line consists of twenty six steps. PA signals from all the points are collected and plotted as a pseudo-3D plot, and is shown in Fig. 3.3(a). As is evident from this figure, the three pits can be seen in the photoacoustic image of the sample.

The same sample has also been subjected to rear surface imaging. One of the three pits is filled with little amount of lamp black. The surface of the nylon disc without pits is scanned with chopped beam of He-Cd laser in the same manner as was done in surface imaging. Here also the sample is arranged in the cell in such a way that the pits are in the horizontal plane perpendicular to the light beam. The amplitude of the PA signals from the surface of nylon disc having no discontinuities are as shown in Fig. 3.3(b). In this figure the presence of the pits on the reverse side is evident in the image.

Chopping
freq?

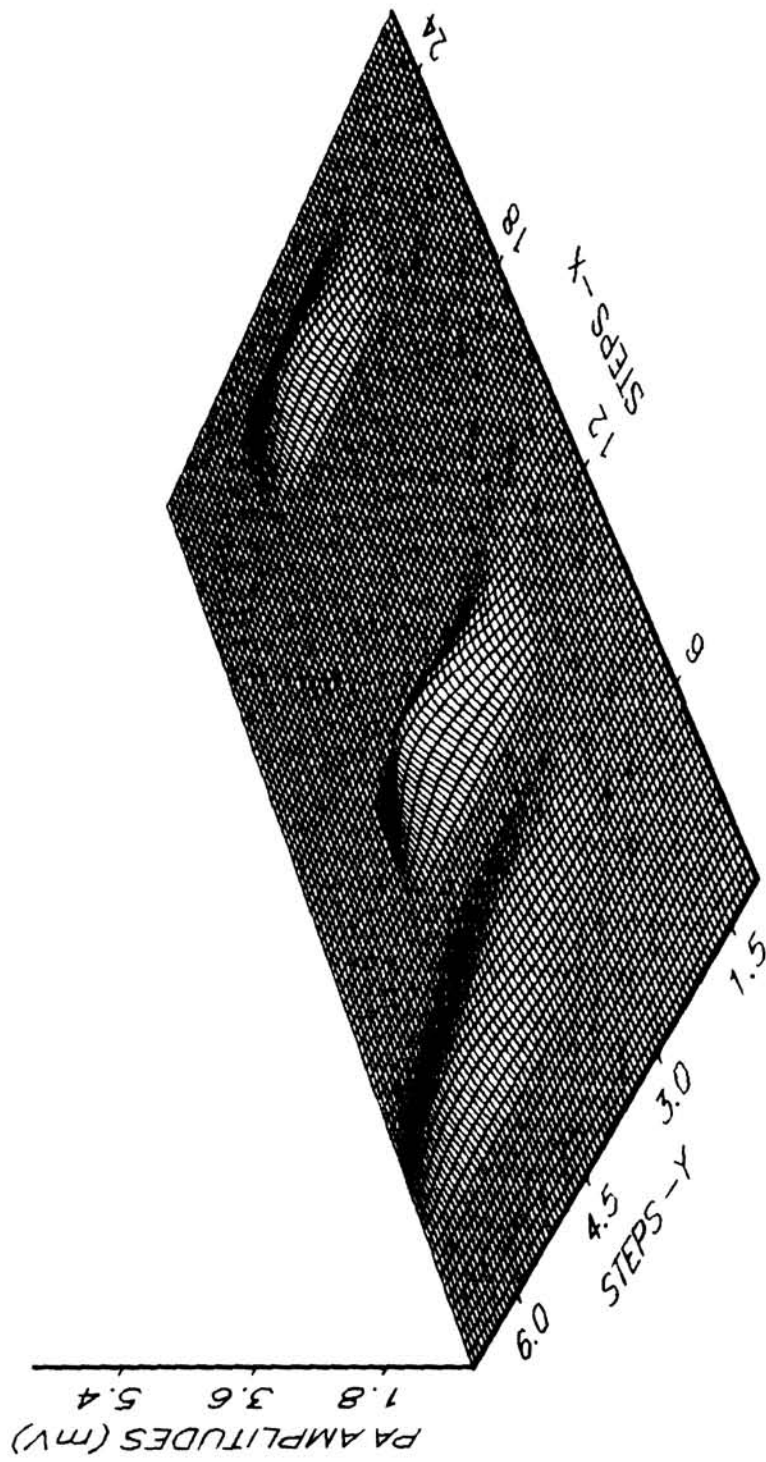


Fig 3.3a : Pseudo-3D, PA surface image of nylon disc

3.2b.1 Results and discussion

The surface PA image of nylon disc having three pits on the same surface, shown in Fig 3.3(a), very clearly shows the positions of the three pits on the surface of the disc. The amplitude of the PA signals are enhanced at the positions of the pits. Increase in PA signal at the positions of pits means that excess of light energy is absorbed at these regions. Relatively higher roughness and larger area of absorbing regions at the position of the pits are the reasons for the increase in the PA signal amplitude. Distance between the distorted regions in the figures can be measured as nearly 3mm and 5mm from left to the right direction respectively. The distance between the pits have been measured respectively as 2.78mm and 4.8mm respectively using a travelling microscope. An error of the order of 8% found in this measurement can be attributed to the finite spatial resolution of the technique.

In Fig. 3.3(b) there are two regions where the PA amplitude is different from the background. It can be concluded without any doubt that these two regions correspond to the positions of the two pits on the back side of the nylon disc. Although there are three pits on the sample, the rear surface image could bring out information about two only. This is due to the difference in the depths of the pits. According to the theory of PA effect PA imaging can reveal the subsurface features only within the thermal diffusion length of the sample. Amplitude of PA signals is increased at one position, while decreased in the other position. It is confirmed that the PA signals are increased in the position of the pit containing lamp black in the rear surface. Lamp black is a good light absorber and also is a good emitter of photothermal waves. In the second pit lamp black is absent. Therefore amplitude of PA signals is low there. Through this experiment it has been possible to establish the power of PA imaging as a probe for testing the presence of impurities as well as defect in the subsurfaces of a

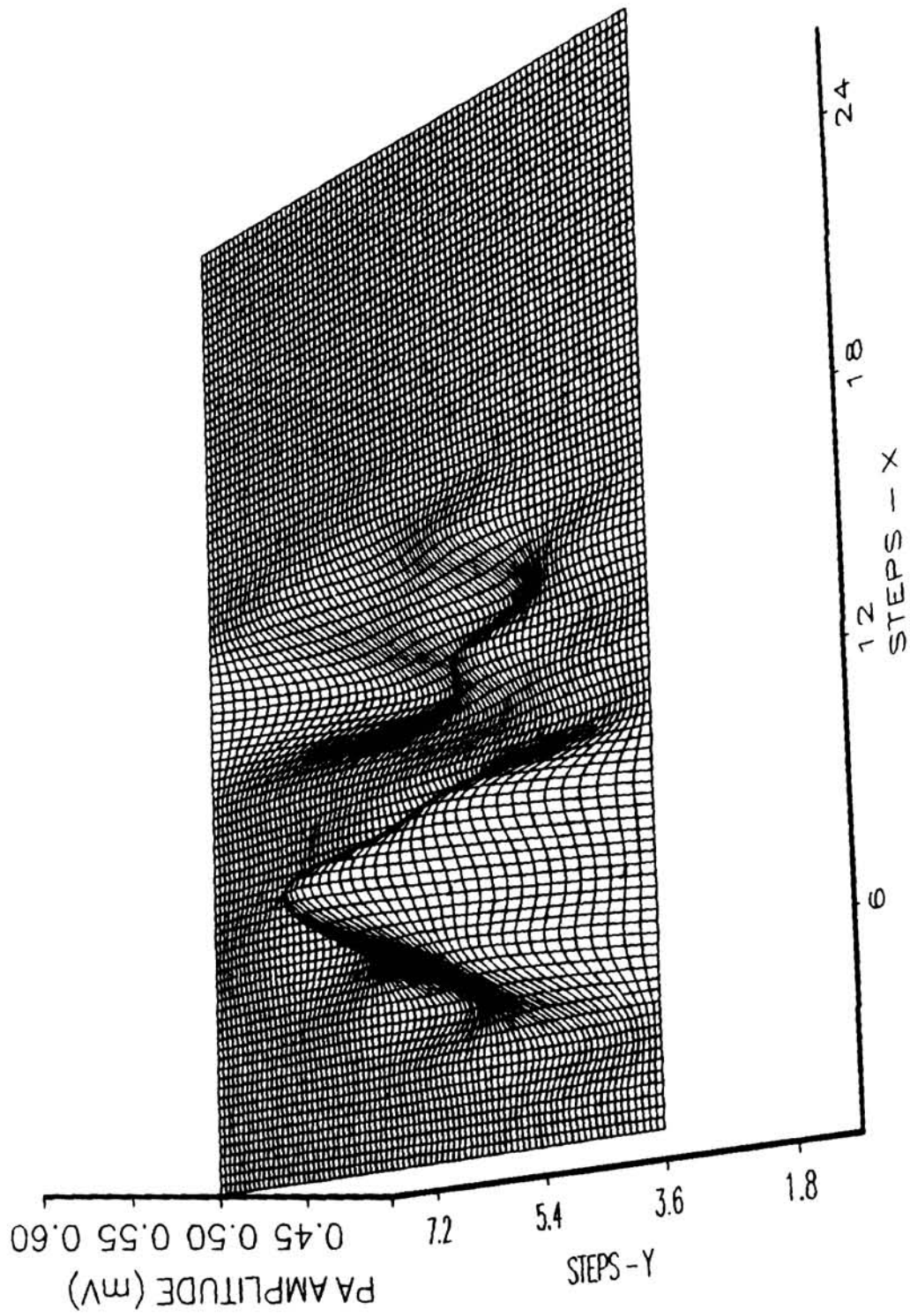


Fig 3.3b : Pseudo-3D, PA image of rear surface of nylon disc

solid sample in a nondestructive manner.

3.2c PA imaging of brass disc

A brass disc of diameter 1.75cm containing two pits of diameter 1.15mm separated by a distance of 2.7mm on one surface has also been used as a sample for surface as well as rear surface imaging. Thickness of the sample is 4.54mm. Each pit has a depth nearly of 4.4mm. Both surfaces of this sample are subjected to PA scanning with the He-Cd laser chopped at 40 Hz. A rectangular area of 40 x 8 steps (X - step = 0.25mm ; Y - step = 0.5mm) on the surface of the sample is scanned with intensity modulated beam of laser in a step by step fashion as described earlier. Amplitudes of the PA signals obtained from front surface and rear surface are plotted separately and are shown in Fig. 3.4(a) and 3.4(b) respectively.

The surface image shown in Fig. 3.4(a) and rear surface image shown in Fig. 3.4(b) indicate very clearly the positions of the pits. In the surface image the amplitude of the PA signals is enhanced to a large magnitude because the surface image has been recorded after filling the pits with little amount of lamp black. But rear surface imaging is performed without any lamp black in the pits. The amplitude of the PA signals are smaller from the back surface above the pits. Even though the amplitude variations are not so distinct as in the previous case, the positions of the pits are easily identifiable from the recorded PA image.

3.2d Subsurface PA imaging in teflon sample

An actual subsurface PA imaging has been attempted on a teflon sample using our setup. For this a teflon disc is prepared with 1.8cm diameter and nearly 4mm thickness. A thin copper wire of diameter 0.3mm is inserted into the disc diametrically slant to its surface as shown in Fig. 3.5. The position of the copper wire is deeper from

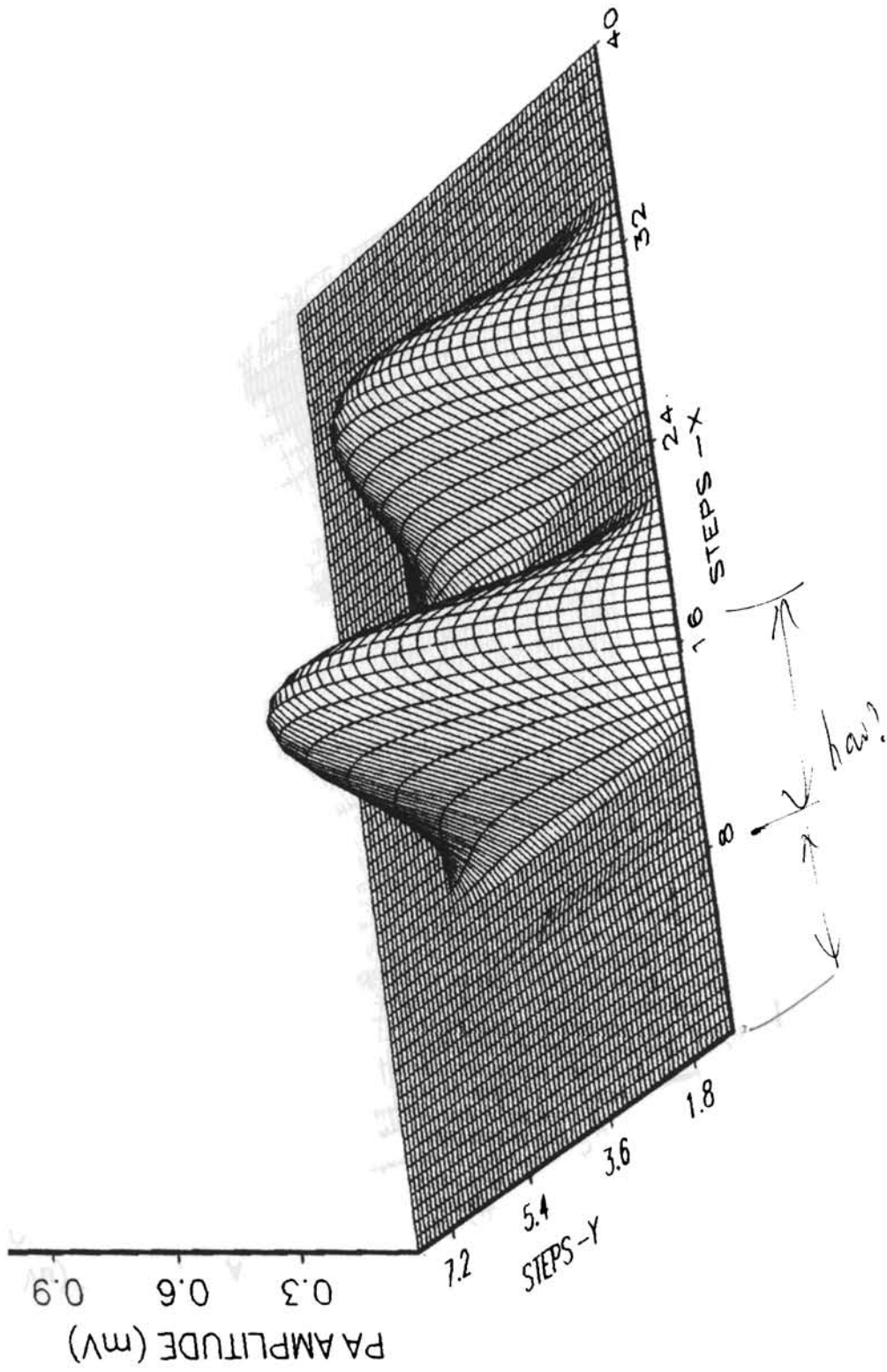


Fig 3.4a : Pseudo-3D, PA surface image of brass disc

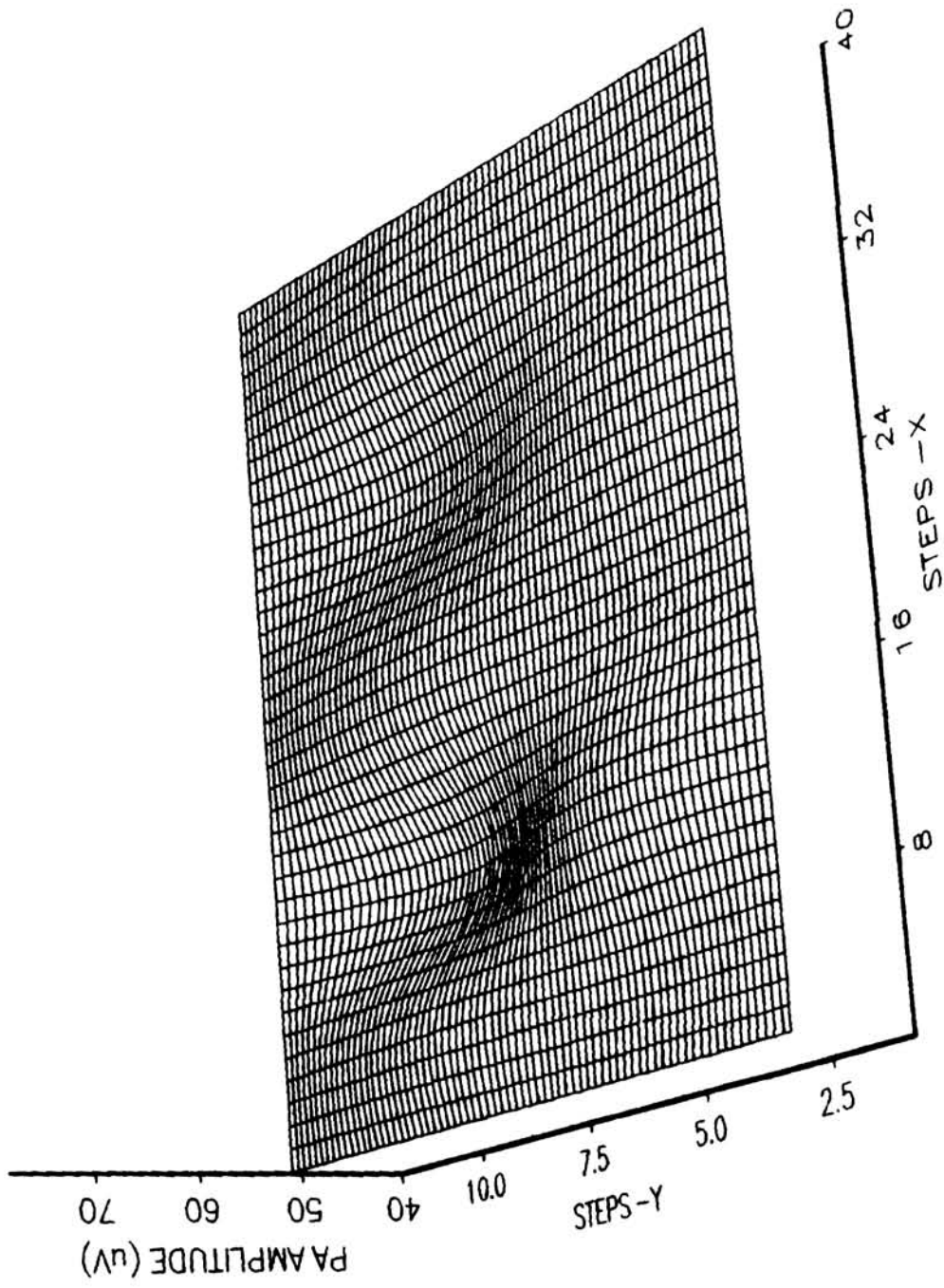


Fig 3.4b : Pseudo-3D, PA image of rear surface of brass disc

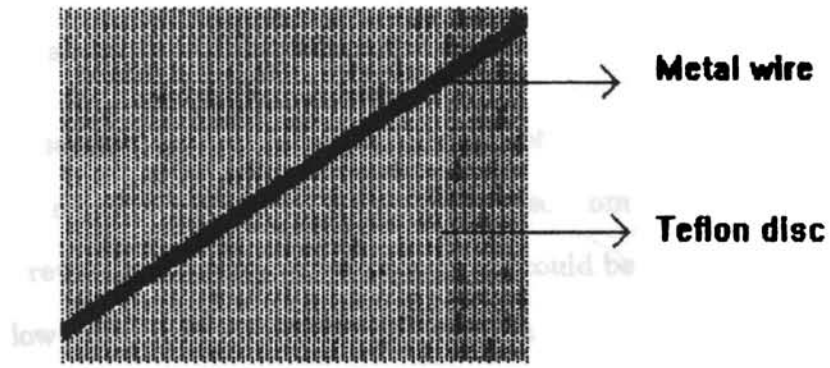


Fig 3.5 : Cross sectional view of teflon disc inserted with metal wire

the surface of disc as it is inserted more into the disc. The sample has been preferred like this to demonstrate depth profiling ability of the PA imaging technique. The opposite surfaces of the sample have been made perfectly flat and smooth.

The sample has been subjected to PA scanning by intensity modulated beam of the He-Cd laser modulated at a frequency of 20Hz. The scanning is performed vertically by keeping the sample in the cell such that the copper wire in the sample is aligned horizontally and is perpendicular to the light beam. The central region of the sample is scanned vertically in 12 lines, 1mm apart. Each line has been scanned in ten steps at 0.5mm apart. Amplitude of the PA signals obtained during scanning the surface of the sample are plotted in pseudo three dimensions and is shown in Fig.3.6.

Obviously Fig. 3.6 shows the presence of the metal wire in the central region. Although the metal wire is present inside the disc from one end to the other, the PA image could reveal it only at a certain length. It could be fetched neither at great depth nor at very low depth from the surface of the teflon disc. This can be explained as follows. (1) At high depths the metal wire passes through region beyond the thermal diffusion length of the PA signal for the selected chopping frequency. Therefore PA imaging of the metal wire could not be possible in that region, because PA signal cannot penetrate so deep into that region to detect it. (2) At the low depth region both the teflon surface layer and the metal wire in the subsurface can be considered as thermally thin, hence the PA signal comes mainly from the surface below the metal wire, that is from the teflon itself. So the thermal wave do not see the metal wire.

3.3 Conclusions

The experimental results presented in this chapter confirm the capability of PA technique for surface as well as subsurface imaging of solids. In all cases it is

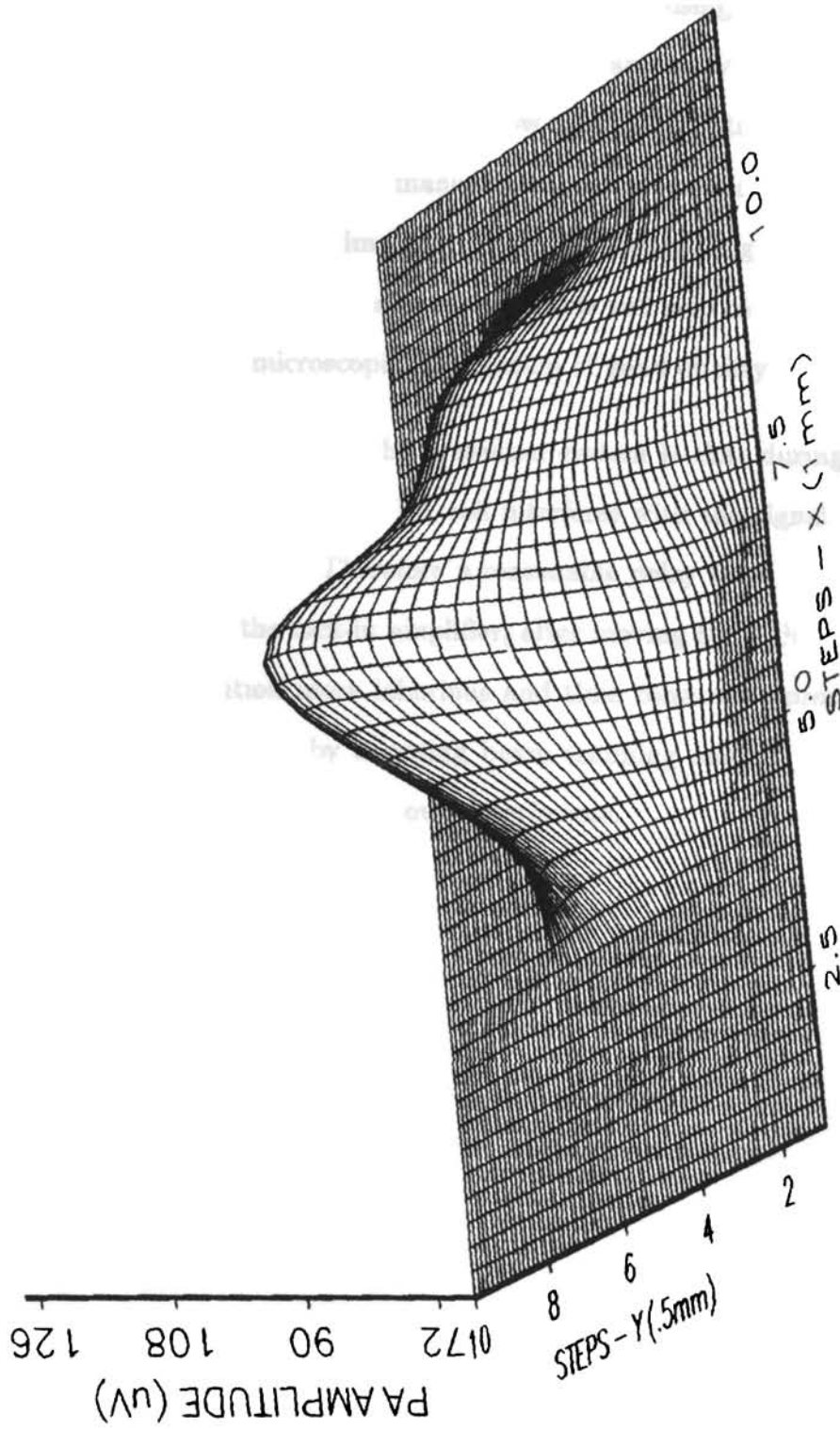


Fig 3.6 : Pseudo-3D, PA surface image of teflon disc inserted with a metal wire

found that the image of defects and voids are spatially spread more than the actual size of the defect. This can be eliminated to certain extent by increasing the spatial resolution. Even though there is some theoretical limitations, the PA imaging system can be operated with few ten times higher resolution by using highly focused laser beam modulated at higher frequency and operating the scanning system with finer steps. But the present experiments are conducted at low spatial resolution because it is found to be more convenient to take data manually. One can exploit the maximum possible resolution of the existing PA imaging system by automating the scanning and data acquisition part by interfacing to a computer. This will help to produce the surface and subsurface images with microscopic information of good quality.

Another draw back of the presented system is that during data acquisition noise due to the movement of the PA cell interferes with the signal. This noise takes few seconds to settle down. Therefore a reasonable delay time has to be provided to stabilize the output of the lock-in amplifier, after moving through each step. This has made the data acquisition more laborious and time consuming process. This can be overcome to a large extent by adopting beam scanning method rather than PA cell scanning which we have adopted in our experiments.

References

- [1] R. L. Thomas, L. D. Favro and P. K. Kuo, **Can. J. Phys.** **64**, 1234 (1986)
- [2] F. A. McDonald, G. C. Wetsel, Jr. and G. E. Jamieson, **Can. J. Phys.** **64**, 1265 (1986)
- [3] Shu - Yi Zhang and Li Chen, **Can. J. Phys.** **64** 1316 (1986)
- [4] A. Rosencwaig and G. Busse, **Appl. Phys. Lett.** **36**, 725 (1980)
- [5] C. S. Cargill, **Nature** **286**, 691 (1980)
- [6] E. Brandis and A. Rosencwaig, **Appl. Phys. Lett.** **37**, 98 (1980)
- [7] H. Ermet, F. H. Dacol, R. L. Melcher and T. Baumann, **Appl. Phys. Lett.** **44**, 1136 (1984)
- [8] K. R. Grice, L. J. Inghart, L. D. Favro, P. K. Kuo and R. L. Thomas, **J. Appl. Phys.** **54** 6245, (1983)
- [9] A. Rosencwaig and J. Opsal, **IEEE Trans. on Ultrasonic, Ferroelectrics and Frequency Control Vol. UFFC-33 (5)**, 516 (1986)
- [10] G. Busse, **IEEE Trans. Sonics & Ultrasonics**, **SU-32 (2)**, 355 (1985)
- [11] A. Rosencwaig, **Anu. Rev. Matter. Sci.** **15**, 103 (1985)
- [12] G. Birnbaum and G. S. White, **Research Techniques in nondestructive testing Vol.7 (Academ. Press Inc. London England)**, 259 (1984)
- [13] J. C. Murphy, J. W. MacLachlan and L. C. Aamodt, **IEEE Trans. UFFC - 33 (5)** , 529 (1986)
- [14] A. C. Tam, **Rev. of Mod. Phys.** **58**, 381 (1986)

- [15] A. Rosencwaig, **Photoacoustics and photoacoustic spectroscopy** (Wiely, NewYork 1980)

CHAPTER 4

PHOTOACOUSTIC DEPTH PROFILING IN MULTILAYER SOLID STRUCTURE

4.1 Introduction

The technique of PA depth profiling can provide information on the thickness of a surface layer, depth of a sublayer, thermal diffusivity of a layer, thermal barriers or other irregularities below the surface and depth dependent optical absorption features in a sample[1-7]. Such techniques should be quite useful for the semiconductor industry, thin-film technologies and different areas of surface science[6,7,8]. Furthermore, depth profiling techniques are uniquely suitable for certain *in vivo* studies in medicine and biology, where normal optical reflection or extinction measurements cannot be performed without elaborate sample preparations[9-11]. Although there are different strong theoretical models for PA depth profiling in layered transparent and opaque solid samples[12-15], this technique is still not adopted as a commercial technique in thin-film or semiconductor industries. Therefore it is interesting to undertake systematic investigations to evaluate the feasibility of PA depth profiling technique for measuring thickness and to determine thermal diffusivities of different material layers in a multilayered sample.

In this chapter we present our experimental work and results of our attempts to do depth profiling in a multilayer sample prepared with different materials. The basic principle, experimental method, sample configuration and results obtained are described in detail in the following sections.

4.2 Principle of the technique

The basic principle of the PA depth profiling technique is that, the depth of the point of origin of the PA signal in a sample can be varied by changing the chopping frequency of the irradiating light beam. The amplitude and phase of the PA signal depends on the thermal properties of the material from which the PA signal originates. The other parameters involved in the generation of the PA signal are l_j , μ_j , α_j and K_j which are the thickness, thermal diffusion length, thermal diffusivity and thermal conductivity of the sample respectively. The suffix j is used to indicate that the parameters correspond to the j^{th} region of a multilayer sample as shown in Fig. 4.1.

According to the Rosenzweig - Gersho theory of the photoacoustic effect[14], the photoacoustic signal intensity Q for an optically opaque solid ($\beta \ll l_1$), as long as $\mu > \beta$, is given by

$$Q \propto \frac{(\alpha_{j+1})^{1/2}}{(2\pi f K_{j+1})}, \quad \text{for thermally thin case of } \mu_j > l_j \quad (4.1)$$

$$Q \propto \frac{(\alpha_j)^{1/2}}{(2\pi f K_j)}, \quad \text{for thermally thick case of } \mu < l_j \quad (4.2)$$

In the above expression, β is the optical absorption length of region (1) and f is the chopping frequency of incident light beam shown in Fig. 4.1.

From equation (4.1) it is clear that, for $\mu_j > l_j$, the thermal property of the $(j+1)^{\text{th}}$ region of the sample comes in the expression for PA signal amplitude. Whereas, in equation (4.2), for $\mu_j < l_j$, the PA signal depends on the thermal property of j^{th} region of the sample. The thermal diffusion length of the j^{th} layer of the sample material is given by

$$\mu_j = \left(\frac{\alpha_j}{\pi f}\right)^{1/2} \quad (4.3)$$

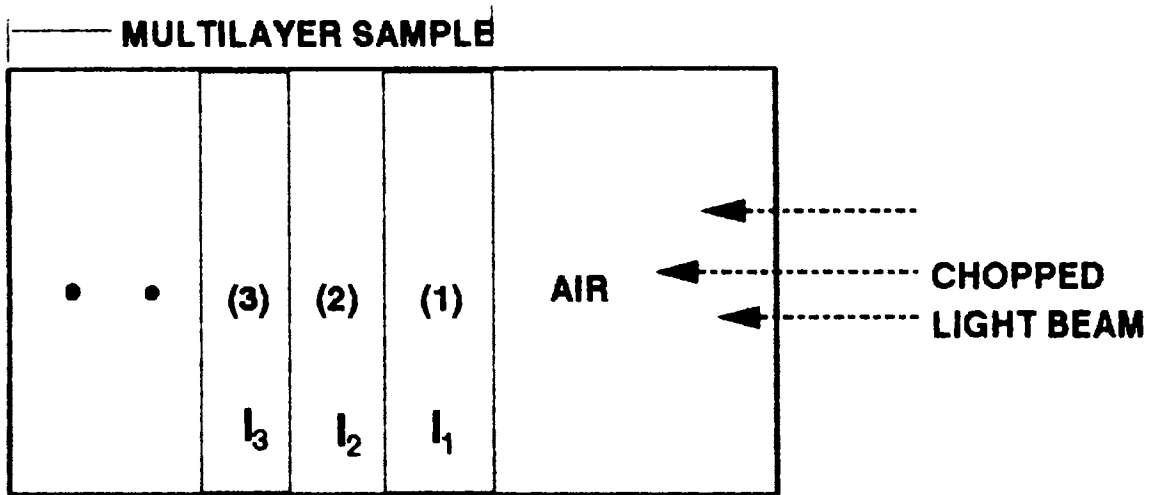


Fig 4.1 : Simple PA cell geometry with a multilayer solid sample inside.

Therefore the thermal diffusion length μ can be changed by changing the chopping frequency of the excitation light beam. Thus we can expect to get noticeable changes in PA signal amplitude and phase as the sample subjected to depth profiling by varying the chopping frequency. Therefore one can determine the depth dependent thermal characteristics of a sample by subjecting it to a chopping frequency analysis of the PA signal amplitude or phase. Whenever the thermal diffusion length in one layer of the sample reaches the boundary of another material with different thermal diffusion length, a discontinuity in the PA signal amplitude or phase can be observed. Therefore it is possible to obtain the thermal diffusivity of any material in the j^{th} layer of known thickness l_j by finding the chopping frequency f_{cj} at which the PA signal amplitude or phase undergoes noticeable changes. This chopping frequency f_{cj} is the characteristic frequency of the j^{th} layer.

On the other hand, we can determine the thickness l_j of each individual layer of a multi-layered solid sample if the thermal diffusivity α_j of the material of the layer is known and by measuring the corresponding characteristic frequency f_{cj} .

4.3 Experimental method

A photoacoustic spectrometer consisting of a radiation source (He-Ne laser, $\lambda = 632.6\text{nm}$, 10mW), a room temperature PA cell, optical chopper (Photon Technology International, Model OC4000) and a lock-in amplifier (Stanford Research system SR510) as shown in Fig. 4.2 is used for performing the depth profiling experiments on multilayer samples

In order to carry out error free frequency analysis of the PA signal amplitude and phase, the PA cell in the experimental setup must be free from resonance at least in the frequency range of interest in the experiment. Since the PA cell which is already

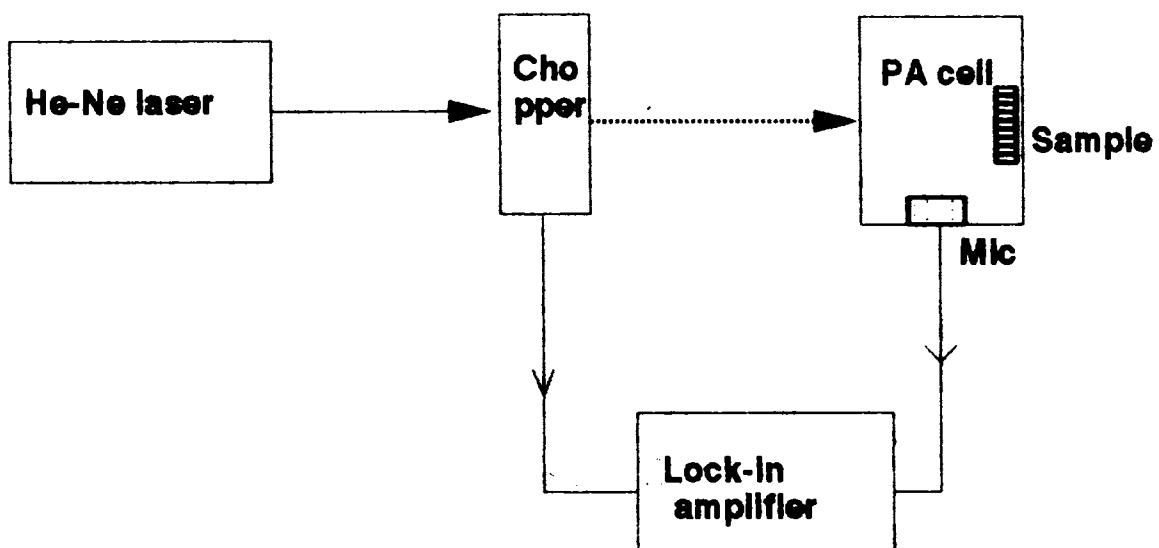
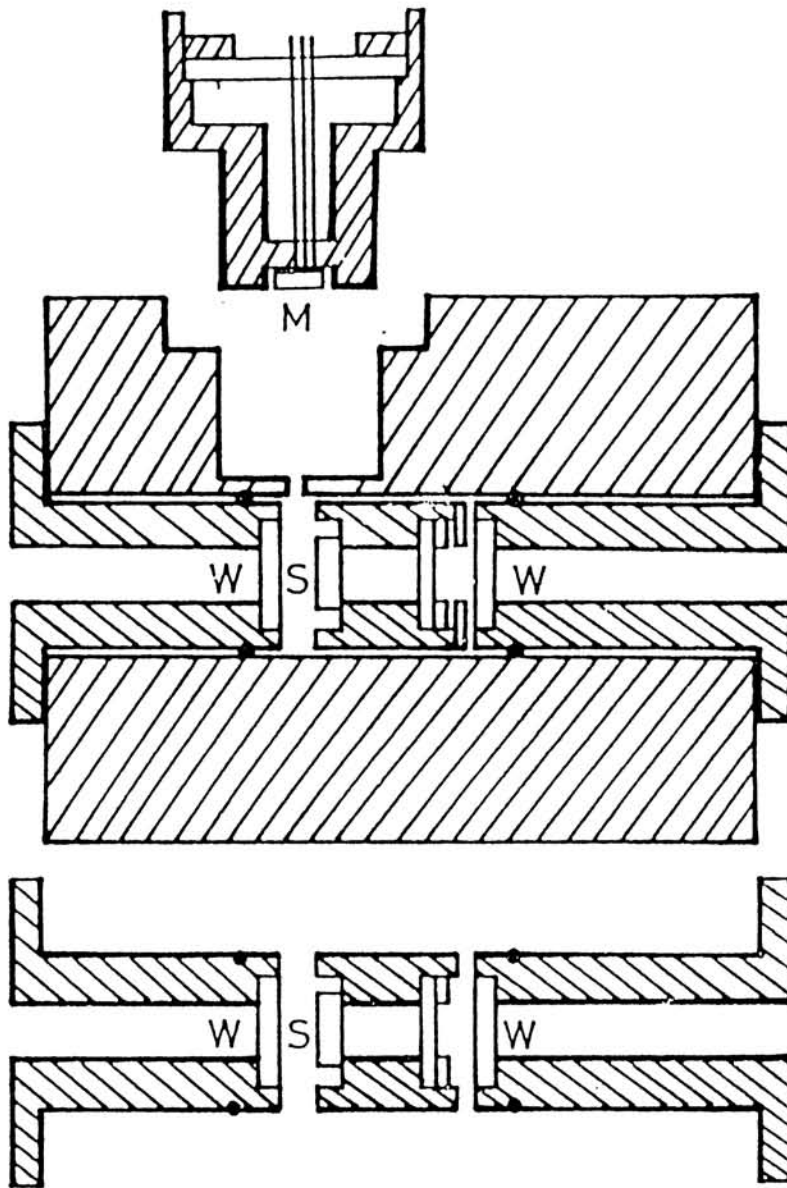


Fig 4.2 : Block diagram of PA spectrometer.

discussed in the Chapter 2 has a resonance at near 40Hz and this frequency is within the frequency range of our interest, we have used another room temperature PA cell for performing these depth profiling experiments. A cross sectional view and dimensions of various parts of this PA cell fabricated in aluminium are shown in Fig. 4.3. Frequency response of the cell using a standard absorber (lamp black) as a sample are given in figures 4.4 and 4.5. Note that these figures follow the predictions of the R-G theory for an optically opaque and thermally thin sample.

4.4 Sample Structure

A multilayered sample structure is prepared with a silicon wafer and a brass disc kept one over other and placed on a glass substrate as shown in Fig. 4.6. A glass disc of diameter 2cm and thickness 2mm is used as the backing and it also acts as the bottom layer of the sample structure. A brass disc of thickness $450\mu\text{m}$ and diameter 1cm is attached to the glass disc with a fine layer of silver paint. Thickness of the bonding layer of silver paint has been measured as nearly $120\mu\text{m}$. The top layer of the sample configuration is formed with a rectangular piece (1cm X 0.5cm) of silicon wafer of thickness $370\mu\text{m}$ fixed over the brass disc again with silver paint. Silver paint is selected as the binding material, because it can provide good thermal contact between the different layers. This sample configuration gets bound together firmly in a day or so if kept undisturbed at room temperature. This five layered sample (including glass backing and two silver paint layers) is subjected to a photoacoustic frequency analysis after keeping it inside the PA cell shown in Fig. 4.3 and undertaking the experiment with the setup already discussed. For enhancing the signal, a very thin coating of lamp black is applied over the top surface of the sample. The thickness of this layer is of the order of $10\mu\text{m}$ which makes it thermally thin at all the chopping frequencies used in these experiments.



W - WINDOW
S - SAMPLE
M - MICROPHONE

Fig 4.3 : Configuration of the PA cell used in these studies.

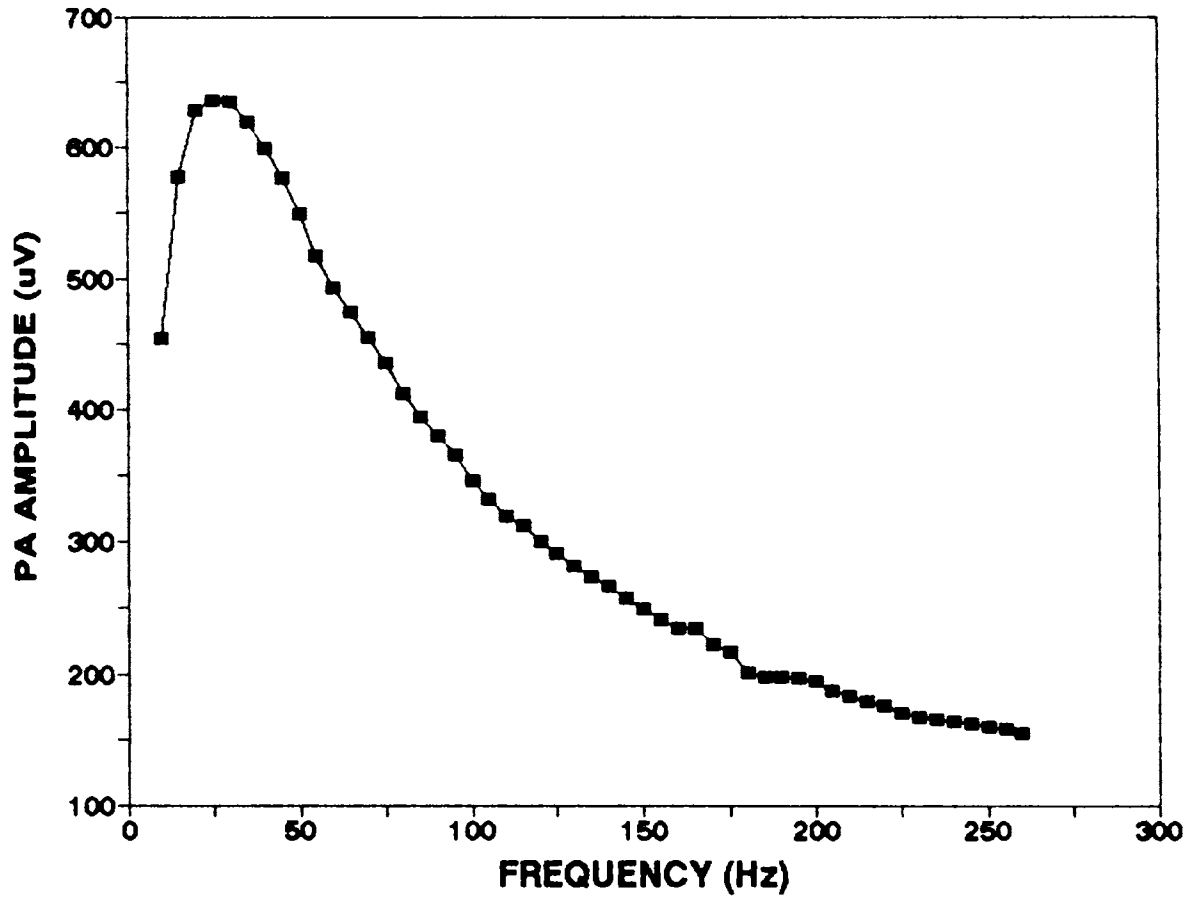


Fig 4.4 : Variation of PA amplitude with frequency for carbon black sample for cell shown in Fig 4.3.

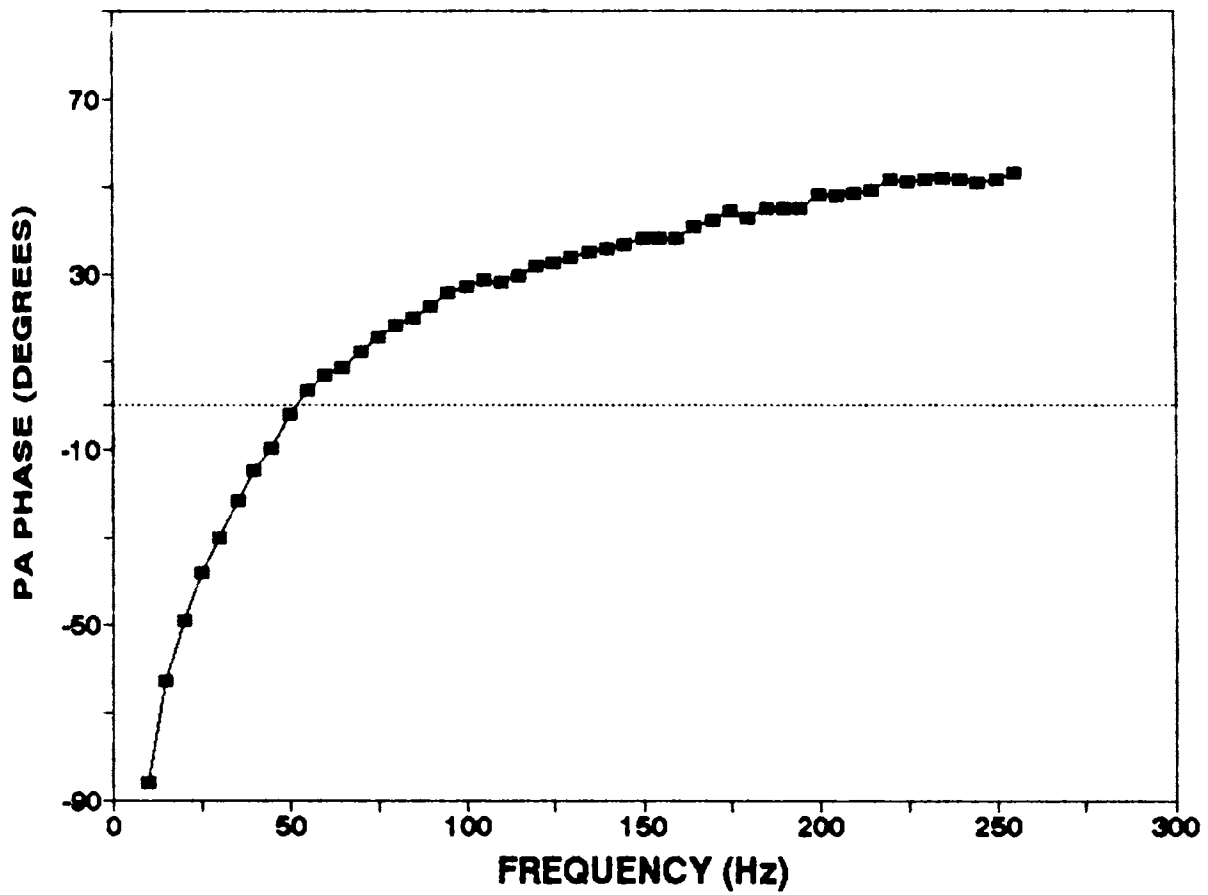


Fig 4.5 : Variation of PA phase with frequency for carbon black sample for cell shown in Fig 4.3.

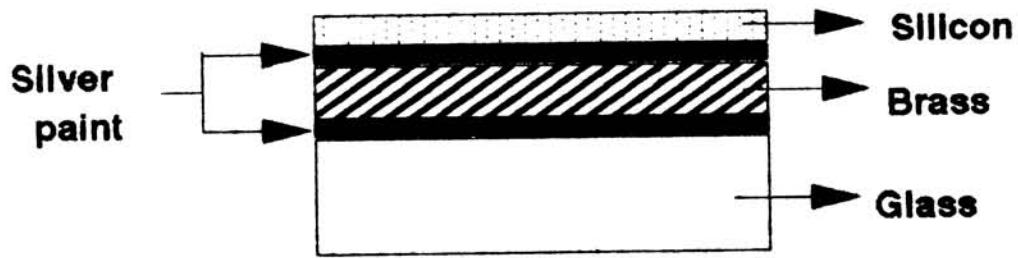


Fig 4.6 : Sample configuration of the multilayer solid structure.

4.5 Results and discussion

Amplitude and phase of the PA signals obtained from the sample have been recorded by varying chopping frequency from 20Hz to 300Hz in steps of 5Hz. Amplitudes of the PA signals at various chopping frequencies from the sample have been normalised with those obtained from thermally thin lamp black at the corresponding frequencies. Normalisation is a standard method to nullify the frequency dependent cell characteristics from the PA amplitudes. The normalised PA amplitude versus chopping frequency is plotted in Fig. 4.7. In the phase measurement, we have determined the difference in phase of PA signals from the sample and the lamp black for each chopping frequency to eliminate the cell characteristics. The phase differences ($\Delta\phi$) at various chopping frequencies of the sample are shown in the Fig. 4.8.

In the figures showing the frequency dependence of PA amplitude and phase difference, one can observe some discontinuities or sharp changes at certain points. Certainly, these discontinuities are due to the shift of point of origin of the PA signal from one layer to the adjacent layer. These discontinuities are observed in the figures at approximately 40Hz, 60Hz, 160Hz and 220Hz. Using equation (4.3), we have calculated the characteristic frequencies of brass disc of thickness 450 μm and silicon layer of thickness 370 μm as 54Hz and 223Hz respectively. By comparing the calculated characteristic frequencies of the brass layer and silicon layer, one can infer that the discontinuities in the graphs at 60Hz and 220Hz are due to the change of brass layer and silicon layer from thermally thin to thermally thick regimes.

The above agreement has led us to infer the discontinuities at 40Hz and 160Hz as due to the characteristic frequencies of silver paint layers between glass and brass and brass and silicon layers respectively of the multilayered sample. Thickness of the silver paint layer between glass and brass layers has been determined as 120 μm . By

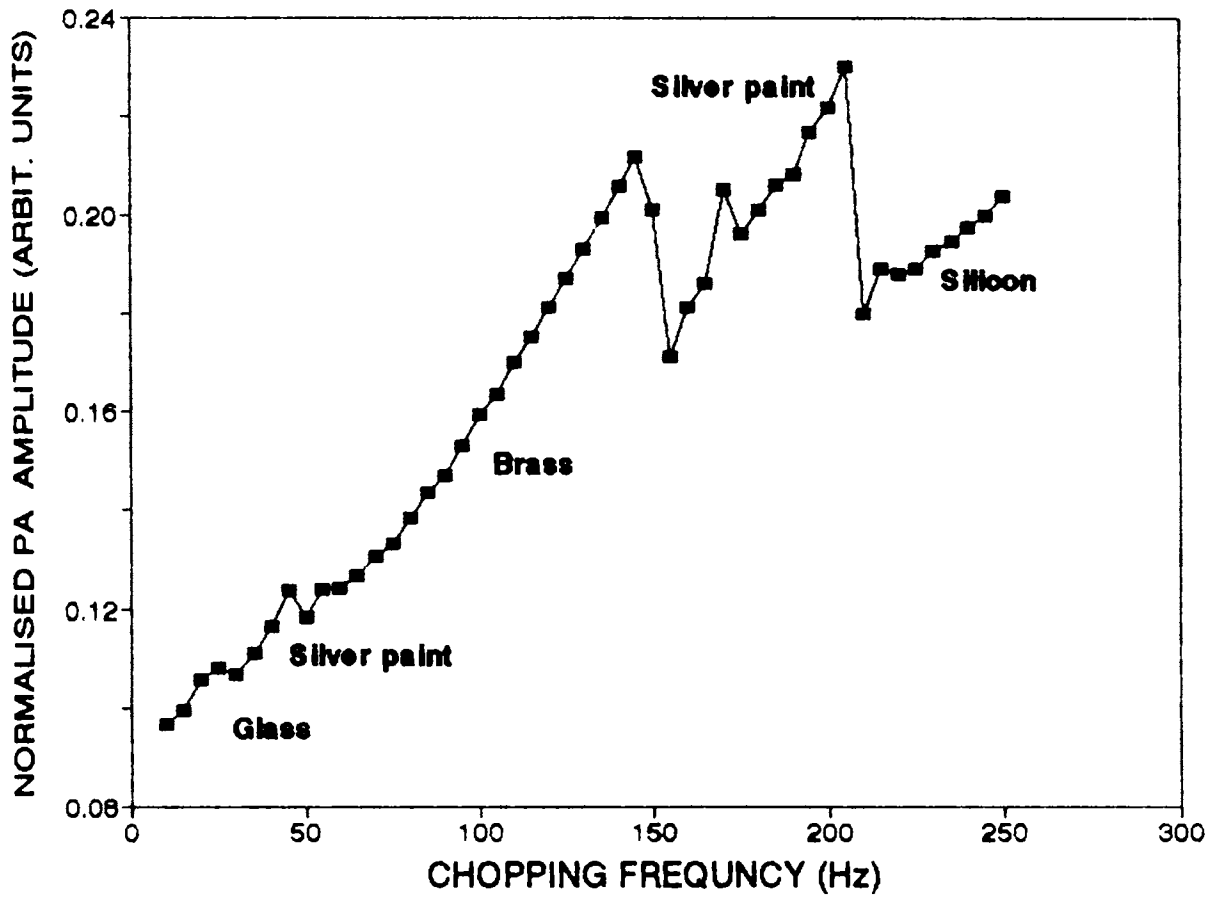


Fig 4.7 : Variation of normalised PA amplitude with frequency for the multilayer sample shown in Fig 4.6.

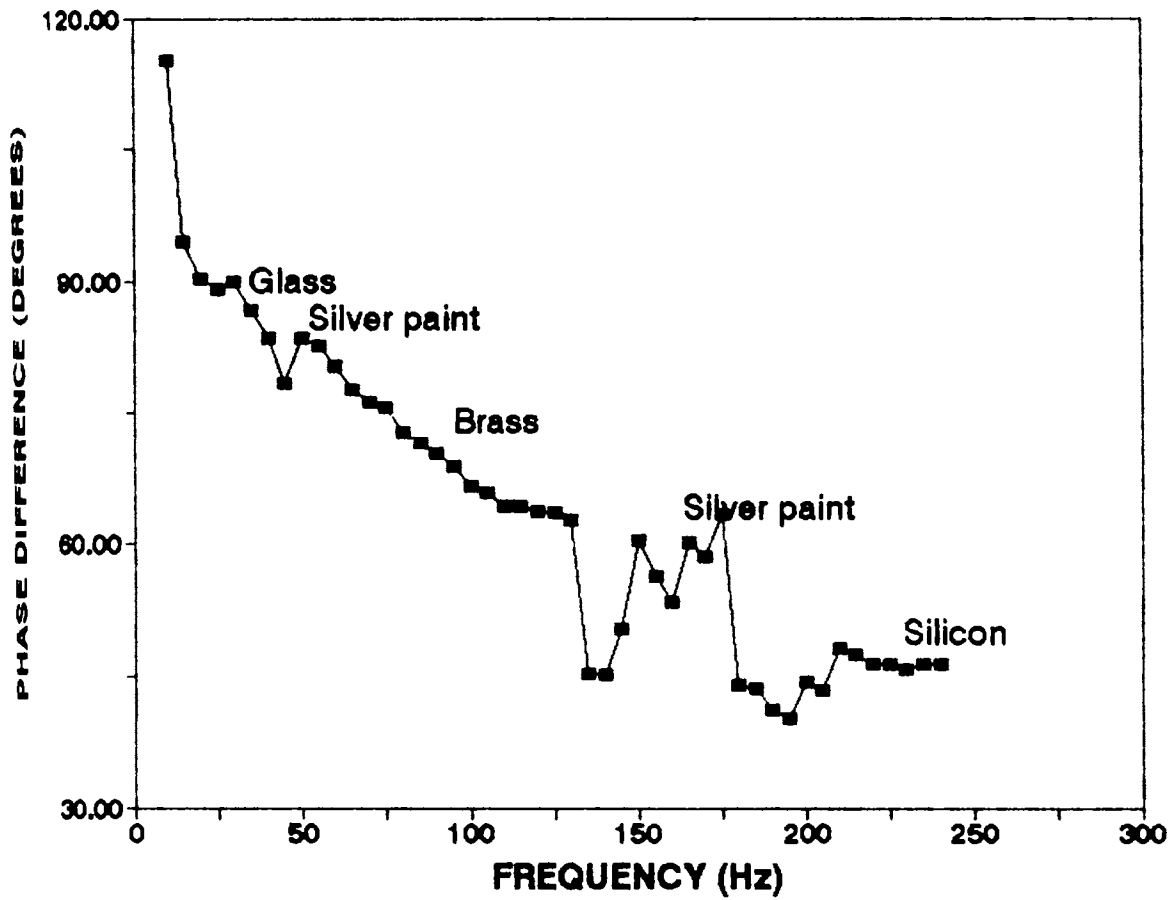


Fig 4.8 : Variation of PA phase difference with chopping frequency for the sample configuration shown in Fig 4.6.

assuming 40Hz as the characteristic frequency of the silver paint layer of thickness $120\mu\text{m}$, we have estimated the thermal diffusivity (α) of the silver paint as $0.018\text{cm}^2\text{sec}^{-1}$. This value could not be cross checked, because thermal parameters of the silver paint could not be found in hand books.

We have also determined the thickness of the second layer of silver paint between brass disc and silicon wafer by assuming 160Hz as the characteristic frequency of that layer and thermal diffusivity of the silver paint as $\alpha = 0.018\text{cm}^2\text{sec}^{-1}$. It is determined as $60\mu\text{m}$. There is a reasonable agreement between photoacoustically measured thickness and that measured with a micrometer of least count $10\mu\text{m}$.

Thickness of different layers of the sample determined by depth profiling technique are tabulated in the Table 4.1. This table also provides the thicknesses of various layers measured with the micrometer for comparison. Similarly, experimentally determined thermal diffusivities of different materials in the sample configuration and those taken from hand books are tabulated as Table 4.2 for comparison. The data presented in Tables 4.1 and 4.2 demonstrates that the thickness values and thermal diffusivity values determined in our experiment is in good agreement with the corresponding values available within experimental limits. Our results demonstrate the power of the PA technique in determining the properties of multilayer structures.

T
543-531522
201

Table 4.1

Thickness of each layer of the sample configuration shown in Fig. 4.6 determined by the PA depth profiling method.

Materials in different layers	Characteristic frequency obtained in PA experiments (Hz)	Thickness of each layer μm	
		Determined by PA technique	Measured with micrometer
Silicon	220	373 ± 7	370 ± 5
silver paint (Second layer)	160	59.8 ± 2	50 ± 5
Brass	60	427 ± 10	450 ± 5

Why different axes?

Table 4.2

Thermal diffusivities of materials in the various layers of the sample configuration shown in Fig. 4.6.

Material in different layers	Thickness of the layer ($\mu\text{ m}$)	Experimentally obtained characteristic frequency (Hz)	Thermal diffusivity $\alpha\text{ cm}^2\text{ sec}^{-1}$	
			Determined experimentally	Calculated <i>how?</i>
Silicon	370	220 ± 5	0.95 ± 0.02	0.96
Silver paint (I - layer)	120	40 ± 1	$0.018 \pm 9 \times 10^{-4}$	not verified
Brass	450	60 ± 1.5	$0.38 \pm 9.5 \times 10^{-3}$	0.34 ?

4.6 Conclusions

The experimental results obtained by us are in accordance with the predictions of the R -G theory. The experimental results demonstrate that the frequency scanning technique can be used not only for depth profiling of a multilayer samples but also to determine the thermal diffusivities of the constituent layers of a layered sample. This method is also found to provide a convenient method to determine or to compare the thermal diffusivities of different materials of a multilayered sample. The accuracy of the technique can be enhanced by carefully controlling the rate of frequency scanning. Through these experiments we have substantiated that PA phase and amplitude variation measurements give results which are in agreement with each other. Moreover, experimental results from amplitude as well as phase measurements in multilayered samples are in good agreement with the predictions of the R - G theory.

References

- [1] A. Lachine, **J. Appl. Phys.** **57**, 5075 (1986)
- [2] R. Tilgner, J. Baumann and M. Beyfuss, **Can. J. Phys.** **64**, 1287 (1986)
- [3] J. Baumann and R. Tilgner, **Can. J. Phys.** **64**, 1291 (1986)
- [4] R. S. Linebarger, B. R. Tittmann, J. M. Richardson and K. A. Marsh, **Can. J. Phys.** **64**, 1311 (1986)
- [5] M. Egee, R. Dartois, J. Mar and C. Bissieux, **Can. J. Phys.** **64**, 1297 (1986)
- [6] H. Coufal and P. Hefferle, **Can. J. Phys.** **64**, 1200 (1986)
- [7] S. I. Yun and H. J. Seo, **J. de Physique** **c6** 459 (1981)
- [8] C. A. Bennet, R. R. Patty, **Appl. Opt.** **20** 911 (1981)
- [9] S. D. Campbell, S. S. Yee and M. A. Afromowitz, **IEEE Trans. Biomed. Eng. BME - 26**, 220 (1979)
- [10] Qing Pan, Shu-ye Qiu, Shu-yi zhang, Ji-bin Zhang and Si-ming zhu, **Photoacoustic and photothermal phenomena** **58**, 542 (Springer-Verlag 1988)
- [11] R. M. Leblance and C. N. N'soukpoe - Kossi, **Photoacoustic and photothermal phenomena** **58**, 514 (Springer - Verlag 1988)
- [12] J. Opsal and A . Rosencwaig, **J. Appl. Phys.** **53**, 4240 (1982)
- [13] J. Baumann and R. Tilgner, **J. Appl. Phys.** **58**, 1982 (1985)
- [14] A. Rosencwaig, A. Gersho, **J. Appl. Phys.** **47**, 64 (1976)
- [15] L. C. Aamodt and J. C. Murphy, **Can. J. Phys.** **64** 1221 (1986)

CHAPTER 5

TERMAL CHARACTERISATION OF SOLIDS BY A PHOTOACOUSTIC SCANNING TECHNIQUE : PRINCIPLE AND THEORY

5.1 Introduction

Thermal characterisation of materials is one of the most important applications of the photoacoustic effect[1]. In photoacoustics, thermal characterisation of a sample is usually accomplished by determining either the thermal diffusivity $\alpha = k/\rho C$ or the thermal effusivity $e = \sqrt{k\rho C}$ of the material of the sample[2,3]. The PA technique enables one to measure both these parameters. Simultaneous determination of thermal diffusivity and effusivity leads to the evaluation of the thermal conductivity k and specific heat C of the material of the sample. The commonly used photoacoustic methods to determine thermal diffusivity of a sample have already been outlined in the first chapter of this thesis.

The most popular method to determine thermal diffusivity by PA method involves a chopping frequency analysis of the photoacoustic signal amplitude or phase and determination of the critical frequency, f_c , at which the sample changes from a thermally thin regime to a thermally thick regime[4,5,6]. An alternative to this method is to vary the distance between the point where the heat is generated and the point at which the thermal oscillations are detected. Coesar *et al.*[7] have adopted this method by varying the position of a laterally incident laser beam on a transparent sample. A plot of the photoacoustic amplitude and phase versus the distance x provides the thermal diffusivity α by a data fit to expression with an exponential and linear dependence on $(-a, x)$. Here a_s is the thermal diffusion coefficient defined by $a_s = \sqrt{\omega/2\alpha}$. A

related technique has been adopted to determine the thermal conductivity and specific heat of an opaque sample by measuring the variations in photoacoustic phase with frequency for different sample thicknesses[3]. By adopting the R-G theory to specialised experimental conditions and analysing the generated PA signal amplitude and phase, different authors have determined the thermal diffusivity[8] or thermal conductivity and specific heat simultaneously[9] of a variety of samples.

Another technique to measure the thermal diffusivity of a solid sample involves determination of the amplitude ratio or phase lag of the photoacoustic signal between the front and rear surface illuminations at a single chopping frequency[10,11]. This method is attractive in the sense that the measurement is independent of the sample thickness and chopping frequency. Phase lag measurements are found to give better results than the amplitude ratio method[10]. Pessoa *et al.*[12] have measured the phase lag by illuminating the front and rear surfaces of the sample simultaneously using two beams of light derived from the same source.

All the methods described above suffer from the limitation that the measurement accuracy is dependent on PA cell calibration. Measurements involving variations in sample thickness or chopping frequency can cause errors in the measurements. Measurements of amplitude ratio or phase lag between front and rear surfaces also do depend on the experimental conditions.

We have developed a photoacoustic scanning technique to measure thermal diffusivity of solid samples. This technique has the advantage that the measurement is free of PA cell parameters and experimental conditions. The principle and theory behind this technique are outlined in this chapter. The following chapter gives details of the experimental technique and the results obtained.

In this chapter we put forward the necessary theoretical background of the photoacoustic scanning technique which is more or less free from the drawbacks of the existing PA techniques to measure the thermal parameters of a solid sample. This photoacoustic scanning technique enables one to determine the thermal effusivity of a sample directly. The method employs a sample configuration in which the backing for a good light absorber layer is changed from one backing sample (reference) to another backing sample (experimental) as the absorber surface is scanned with an intensity modulated light beam. The amplitude and phase of the PA signals do undergo sharp variation as the backing is changed from one to the other as will be demonstrated in the next chapter. By measuring the amplitude ratio of the PA signals from the two regions or by measuring the PA phase differences as the backing is changed from one to the other one can determine thermal effusivity of one of the backing sample, provided effusivities of other backing sample and absorber sample are known. The principle of the technique and necessary theory to arrive at the required expressions are described in the following sections.

The one dimensional R-G theory[13] of PA effect is assumed as the fundamental one which forms the starting point to derive the necessary expressions for the amplitude ratio and phase difference involved in the PA scanning technique. The expressions do not involve the PA cell parameter or the experimental conditions at which the PA scanning experiment is carried out. Principle of the method and adaptation of the R-G theory to this experimental situation are outlined below.

5.2 Principle of the technique

Consider the experimental configuration shown in Fig. 5.1. Here the experimental sample b_1 whose thermal effusivity is to be determined is inserted in the reference sample b_2 whose thermal effusivity is known. The experimental sample is inserted into

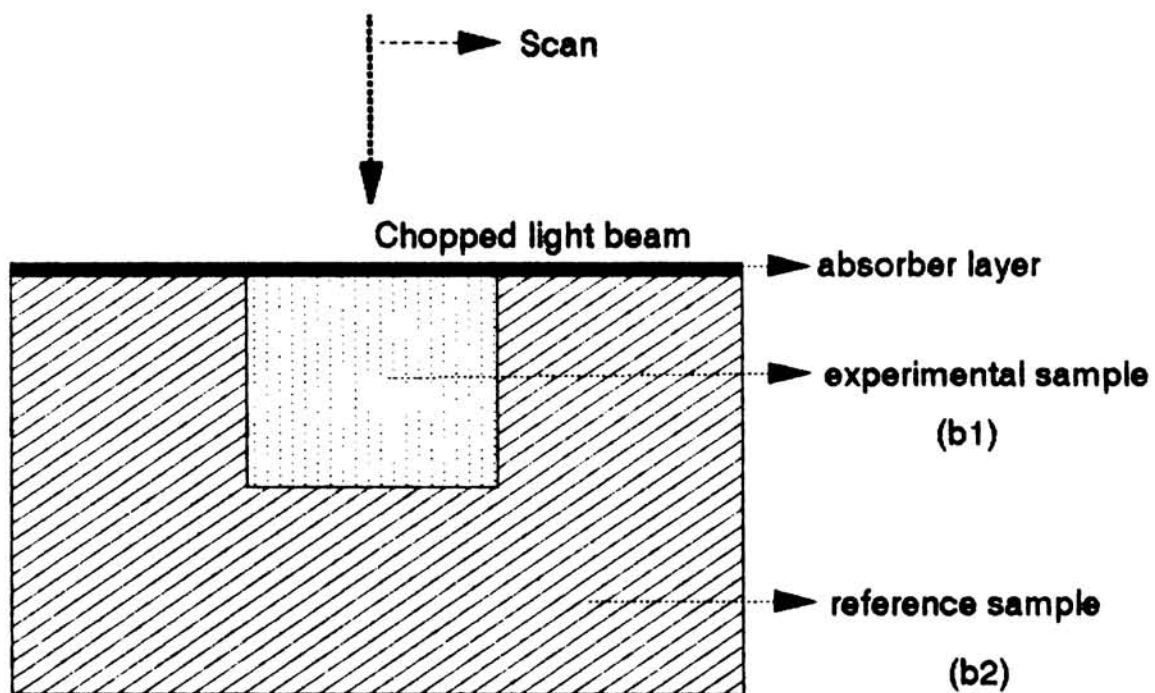


Fig. 5.1 : Experimental configuration

the reference sample in such a way that the top of both the samples are flat and are at the same level. A thin layer of a highly light absorbing material such as carbon black is coated over the entire top surface of the sample configuration. This layer of the light absorbing material is considered as the actual sample of negligible thickness from which the PA signal is generated. This sample can be considered as a thin sample with two different backings b_1 and b_2 in the same horizontal level. Assume that the top surface of the sample can be irradiated with a chopped beam of light and the light beam can scan the surface of the sample in a step by step fashion. The details of the experimental set up will be discussed in the next chapter. The above sample configuration can be kept in a photoacoustic cell and the PA amplitude as well as phase can be measured as the sample surface is scanned with the light beam in a one dimensional fashion changing the backing from b_2 to b_1 and back to b_2 . In this configuration the absorber layer acts as the thermally thin photoacoustic sample with two thermally thick backing media. The backing medium is changed from the reference sample b_2 to the experimental sample b_1 and again to reference sample as the absorber layer is scanned with the chopped beam of light.

Since the sample is made in such a way that both reference sample and experimental sample are of thickness larger than the thermal diffusion length at the chopping frequency used, one can apply the one dimensional R-G theory to this configuration. Thus one can derive an expression for amplitude ratio of PA signals from the two regions of the sample with different backing media. Similarly it is possible to derive an expression for the difference in phase of the PA signal from the two regions of the sample. We show that by measuring either the amplitudes ratio or phase difference of the PA signals, thermal effusivity of the experimental backing sample can be determined. Since we take the ratio of amplitudes or difference of phases, no cell parameters and experimental conditions are involved in the analysis.

The necessary expressions are derived in the following section starting from the original R-G expression for the complex PA signal.

5.3 Application of R-G theory to the present sample configuration

Consider the sample geometry shown in Fig. 5.2, where a good light absorber such as carbon black coated over a backing medium enclosed in a cylindrical PA cell is exhibited. The backing material has thermal conductivity, k_b , density, ρ_b and specific heat C_b and the corresponding parameters for carbon black are k_c , ρ_c and C_c respectively. These parameters for air medium in front of the absorber layer are k_a , ρ_a and C_a respectively. For the three media, the thermal diffusivity is $\alpha = k/\rho C$, the thermal diffusion coefficient is $a = \sqrt{\omega/2\alpha}$ and thermal diffusion length is $\mu = 1/a$ with the corresponding subscripts for the three media as before. Here ω is the modulation frequency (angular) of the light beam. Since this sample geometry and the PA cell configuration are very similar to that adopted by Rosencwaig and Gersho[13] to derive the complex envelope of the sinusoidal pressure variation generated in the PA cell, we can take equation (1.23) from Chapter 1 as the expression for the complex PA signal in the present situation without any loss of generality. Hence, the equation (1.23) can be rewritten as

$$Q = \frac{\beta I_0 \gamma P_0}{2\sqrt{2}T_0 k_a a_a (\beta^2 - \sigma^2)} \left[\frac{(r-1)(b+1)e^{\alpha b} - (r+1)(b-1)e^{-\alpha b} + 2(b-r)e^{-\beta c}}{(g+1)(b+1)e^{\alpha c} - (g-1)(b-1)e^{-\alpha c}} \right] \quad (5.1)$$

The parameters appearing in this equation have already been defined in chapter 1. The subscripts b , c and a refer to parameters for the backing medium, sample (carbon black) and air respectively. l_b , l_c and l_a are the thicknesses of the backing sample, carbon black sample and air medium in front of the carbon black sample respectively. In the present case thickness of absorber layer is negligibly small. That is $l_c \ll l_a$, $l_c \ll l_b$ and $\mu_b \gg l_c$.

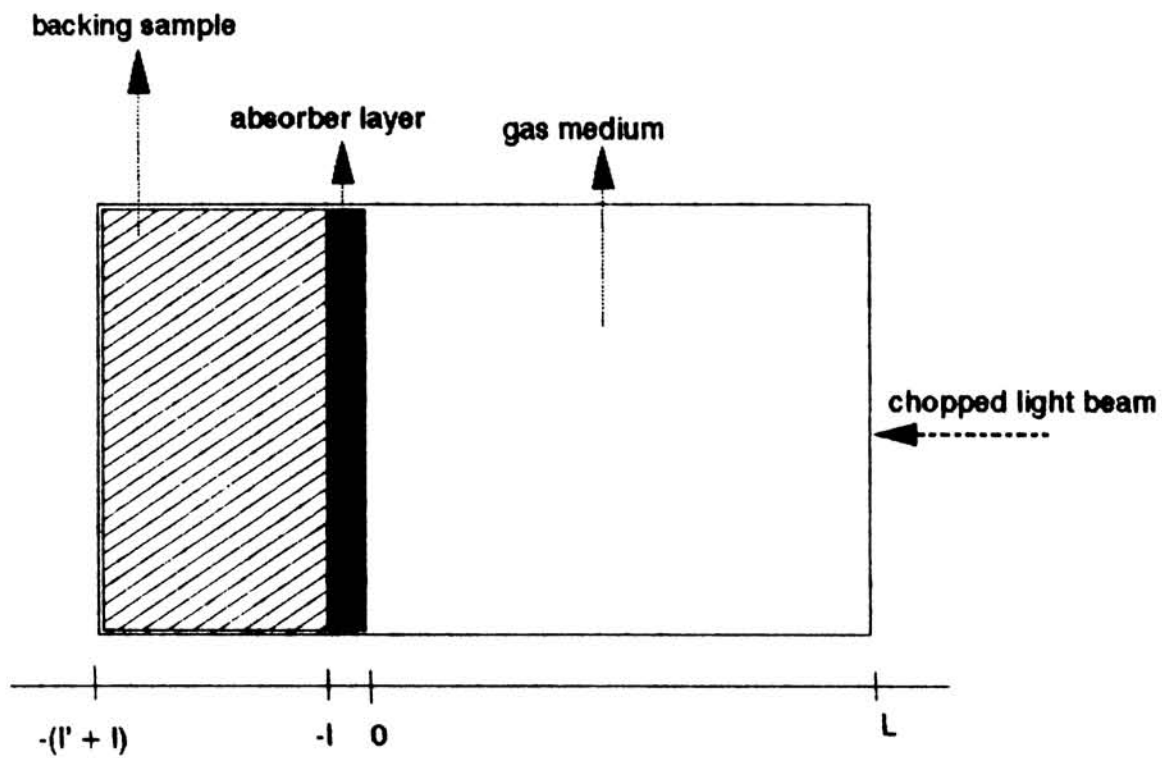


Fig. 5.2 : Geometry of a cylindrical PA cell with a sample

As has been defined in R-G theory[13] as well as in Chapter I, parameters b and g are defined as

$$b = \frac{k_b a_b}{k_c a_c}$$

and

$$g = \frac{k_a a_a}{k_c a_c} \quad (5.2)$$

In our experiments we have used a very thin (1 - 10 μm thickness) layer of carbon black as the sample, the medium in front of the sample is air and the backing samples are different. The thermal parameters of the various media, taken and calculated from literature[13,14] are tabulated in Table 5.1. In equations (5.2), if we substitute for a as

$$\begin{aligned} a &= \frac{1}{\mu} \\ &= \left(\frac{\omega}{2\alpha}\right)^{1/2} \end{aligned}$$

we find that, at the same modulation frequency ω , b and g give the thermal effusivity ratios of the corresponding media, or

$$b = \frac{e_b}{e_c} \quad (5a)$$

and

$$g = \frac{e_a}{e_c} \quad (5.3b)$$

where $e = (k\rho C)^{1/2}$ is the thermal effusivity of the corresponding media.

Due to the fact that the thickness of our carbon black layer is very small, the phase lag caused by it to a thermal wave propagating across it, given by $\psi = \frac{L}{\mu}$, is very small.

Table 5.1

Thermal parameters of various media involved in the experiments

Thermal conductivity k (cal/cm-sec °C)	Thermal diffusivity α (cm ² /sec)	Thermal diffusion length at 40 Hz μ (cm)	Thermal diffusion coefficient a (cm ⁻¹)	ka (cal/ sec °C)	Thermal effusivity e cal cm ⁻² K ⁻¹ s ^{-1/2}
5.7×10^{-5}	0.19	3.9×10^{-2}	25.64	1.46×10^{-3}	1.31×10^{-4}
7.86×10^{-5}	0.002	3.99×10^{-3}	250.63	1.97×10^{-2}	1.76×10^{-2}
2.6×10^{-1}	0.34	5.2×10^{-2}	18.95	5	0.443
9.16×10^{-1}	1.12	9.4×10^{-2}	10.59	9.7	0.87
6×10^{-4}	1.28×10^{-3}	3.2×10^{-3}	3.14×10^2	0.19	0.017
3.57×10^{-1}	0.37	5.4×10^{-2}	18.37	6.6	0.585

At the same time it acts as the source of heat at the surface of the backing medium. So there is a direct thermal coupling between the backing medium and air and the effusivity ratio b given in equation(5.3A) can very well be written as

$$b = \frac{e_b}{e_a} = \frac{k_b a_b}{k_a a_a} \quad (5.4A)$$

Again, due to the fact that the thickness of the carbon black layer is very small compared to the wavelength of the thermal wave, the thermal wave doesn't actually see the carbon black layer; but at the same time thermal effusion is there from it to the backing medium as well as into air. Since $k_a a_a$ is smaller than $k_c a_c$ and both these are much smaller than $k_b a_b$, the backing sample sees just one source of heat externally and it doesn't distinguish between the carbon black layer and air medium. Under this assumption, from the point of view of PA generation at the surface of the backing medium, we can write g as

$$g = \frac{e_c}{e_a} = \frac{k_c a_c}{k_a a_a} \quad (5.4B)$$

The purpose of redefining b and g as in equations (5.4) is to eliminate the thermal parameters of air from subsequent derivations. In the next chapter it can be seen that there is good agreement between calculated and experimental values which justifies this assumption. The relative change in thermal effusivity values between different backing samples is accounted for by defining the thermal wave reflection coefficients at the boundary between the carbon black layer and the backing media later in this chapter.

The other terms in equation (5.1) are defined as before in the following way

$$r = (1 - i)\beta/2a_c$$

$$\sigma = (1 + i)a_c$$

$$a_c = \sqrt{\omega/2\alpha_c} \quad (5.5)$$

$l_\beta = 1/\beta$ is the optical absorption length, where β is the absorption coefficient.

For optically thick solids, such as carbon black, β is very high and l_β is very small. Therefore, $l_\beta < l_c$. Since carbon black sample is thermally thin, $l_c \ll \mu$ and $l_\beta \ll \mu$, where μ is the thermal diffusion length of the absorber layer defined by $\mu = k_c/\rho_c C_c$. Therefore we can very well assume that $e^{\beta a_c} \rightarrow 0$, and $e^{\pm\sigma l_c} = e^{\pm(1+i)a_c l_c} \rightarrow 1$. Since β is very high and l_c very small, a_c is small. Under these realistic assumptions, equation (5.1) can be simplified to

$$Q = \frac{\beta I_0 \gamma P_0}{2\sqrt{2}T_0 k_c l_c a_c (\beta^2 - \sigma^2)} \left[\frac{(r-1)(b+1) - (r+1)(b-1)}{(g+1)(b+1) - (g-1)(b-1)} \right]$$

which can be rewritten as

$$Q = \frac{Y(r-b)}{(\beta^2 - \sigma^2)(g+b)} \quad (5.6)$$

where

$$Y = \frac{\beta I_0 \gamma P_0}{2\sqrt{2}T_0 k_c l_c a_c} \quad (5.7)$$

Substituting for r and σ from (5.5) in equation (5.6) we get

$$Q = Y \frac{(1-i)p - b}{(\beta^2 - i2a_c^2)(g+b)} \quad (5.8)$$

where $p = \beta/2a_c$. Therefore

$$Q = Y \frac{[p - b - ip]}{\beta^2(g+b) - i2a_c^2(g+b)} \quad (5.9)$$

Put

$$p - b = x$$

$$\beta^2(g+b) = y$$

$$2a_c^2(g+b) = z \quad (5.10)$$

then we get

$$Q = Y \left[\frac{x - ip}{y - iz} \right]$$

This can be rewritten as

$$Q = Y \left[\frac{(x - ip)(y + iz)}{y^2 + z^2} \right],$$

or,

$$Q = Y \left[\frac{(xy + pz)}{(y^2 + z^2)} + i \frac{(zx - py)}{(y^2 + z^2)} \right] \quad (5.11)$$

Put

$$H = \frac{xy + pz}{y^2 + z^2}$$

and

$$J = \frac{zx - py}{y^2 + z^2} \quad (5.12)$$

Then

$$Q = Y[H + iJ] \quad (5.13)$$

Therefore the amplitude and phase of the PA signal are given by

$$A = Y\sqrt{H^2 + J^2} \quad (5.14)$$

$$\Phi = \tan^{-1}(J/H) \quad (5.15)$$

5.3a Amplitude of PA signal

Substituting for H and J in equation (5.14), we get

$$\begin{aligned} A &= Y \left[\left(\frac{xy + pz}{y^2 + z^2} \right)^2 + \left(\frac{zx - py}{y^2 + z^2} \right)^2 \right]^{1/2} \\ &= Y \left[\frac{x^2y^2 + p^2z^2 + x^2z^2 + p^2y^2}{y^4 + z^4 + 2y^2z^2} \right]^{1/2} \end{aligned} \quad (5.16)$$

Substituting for x , y and z , one gets

$$x^2y^2 = \beta^4 [p^2g^2 + p^2b^2 + 2gbp^2 + g^2b^2 + b^4 + 2gb^3 - 2g^2pb - 2pb^3 - 4pb^2g] \quad (5.17)$$

$$p^2 z^2 = 4a_c^4 p^2 g^2 + 4a_c^4 p^2 b^2 + 8a_c^4 p^2 gb \quad (5.18)$$

$$\begin{aligned} x^2 z^2 = & 4a_c^4 p^2 g^2 + 4a_c^4 p^2 b^2 + 8a_c^4 p^2 gb + 4a_c^4 b^2 g^2 + 4a_c^4 b^4 \\ & + 8a_c^4 gb^3 - 8a_c^4 g^2 pb - 8a_c^4 pb^3 - 16a_c^4 gpb^2 \end{aligned} \quad (5.19)$$

$$p^2 y^2 = p^2 \beta^4 g^2 + p^2 \beta^4 b^2 + 2p^2 \beta^4 gb \quad (5.20)$$

Adding equations (5.17), (5.18), (5.19) and (5.20), we get the numerator of (5.16) as

$$\begin{aligned} x^2 y^2 + p^2 z^2 + x^2 z^2 + p^2 y^2 = & 2\beta^4 p^2 g^2 + 2\beta^4 p^2 b^2 + 4\beta^4 p^2 gb + \beta^4 g^2 b^2 + \beta^4 b^4 \\ & + 2\beta^4 gb^3 - 2\beta^4 pbg^2 - 2\beta^4 pb^3 - 4\beta^4 gpb^2 + 8a_c^4 p^2 g^2 \\ & + 8a_c^4 p^2 b^2 + 16a_c^4 p^2 gb + 4a_c^4 b^2 g^2 + 4a_c^4 b^4 \\ & + 8a_c^4 gb^3 - 8a_c^4 g^2 pb - 8a_c^4 pb^3 - 16a_c^4 gpb^2 \end{aligned} \quad (5.21)$$

Similarly the denominator of the equation(5.16) works out to be

$$\begin{aligned} y^4 + z^2 + 2y^2 z^2 = & \beta^8 g^4 + 6\beta^8 g^2 b^2 + 4\beta^8 g^3 b + \beta^8 b^4 + 4\beta^8 gb^3 + 16a_c^8 g^4 + 96a_c^8 g^2 b^2 \\ & + 64a_c^8 g^3 b + 64a_c^8 gb^3 + 16a_c^8 b^4 + 8a_c^4 \beta^4 g^4 + 16a_c^4 \beta^4 g^2 b^2 \\ & + 32a_c^4 \beta^4 g^3 b + 8a_c^4 \beta^4 b^4 + 32a_c^4 \beta^4 gb^3 + 32a_c^4 \beta^4 g^2 b^2 \end{aligned} \quad (5.22)$$

For a good absorber layer, such as carbon black, β is very high. So all the powers of β are assumed to tend to infinity. Since $p = \beta/2a_c$, all powers of p are also assumed to tend to infinity. Under these conditions, equations (5.21) and (5.22) further get simplified into

$$x^2 y^2 + p^2 z^2 + x^2 z^2 + p^2 y^2 = 4a_c^4 b^2 g^2 + 4a_c^4 b^4 + 8a_c^4 gb^3 \quad (5.23)$$

$$y^4 + z^2 + 2y^2 z^2 = 16a_c^8 g^4 + 96a_c^8 g^2 b^2 + 64a_c^8 g^3 b + 64a_c^8 gb^3 + 16a_c^8 b^4 \quad (5.24)$$

Therefore the ratio between equations (5.21) and (5.22) turn out to be

$$\frac{b^2(g+b)^2}{4a_c^4[(g^2+b^2)^2+4gb[(g+b)^2-gb]} \quad (5.25)$$

Hence the magnitude of the PA signal amplitude, given by eqn. (5.14) works out to be

$$A = Y \left[\frac{b^2(g+b)^2}{4a_c^4[(g^2+b^2)^2+4gb[(g+b)^2-gb]} \right]^{1/2} \quad (5.26)$$

where

$$\begin{aligned} b &= \frac{k_b a_b}{k_a a_a} = \frac{k_b(\omega/2\alpha_b)^{1/2}}{k_a(\omega/2\alpha_a)^{1/2}} \\ &= \frac{\sqrt{k_b \rho_b C_b}}{\sqrt{k_a \rho_a C_a}} = \frac{e_b}{e_a} \end{aligned} \quad (5.27)$$

is the ratio between thermal effusivities of the backing medium and air. Similarly

$$g = \frac{k_c a_c}{k_a a_a} = \frac{e_c}{e_a} \quad (5.28)$$

is the ratio between the thermal effusivities of carbon black and air.

Substituting for b and g , expressed in terms of thermal effusivities given by (5.27) and (5.28), we can express the PA amplitude given by (5.26) as

$$A = Y \left[\frac{e_b^2(e_c + e_b)^2}{4a_c^4[(e_c^2 + e_b^2)^2 + 4e_c e_b[(e_c + e_b)^2 - e_c e_b]} \right]^{1/2} \quad (5.29)$$

Since the sample consists of two different backing materials with different thermal effusivities e_{b1} and e_{b2} , the amplitudes of PA signals from the two regions of the sample can be expressed by

$$A_1 = Y \left[\frac{e_{b1}^2(e_c + e_{b1})^2}{4a_c^4[(e_c^2 + e_{b1}^2)^2 + 4e_c e_{b1}[(e_c + e_{b1})^2 - e_c e_{b1}]} \right]^{1/2} \quad (5.30)$$

and

$$A_2 = Y \left[\frac{e_{b2}^2(e_c + e_{b2})^2}{4a_c^4[(e_c^2 + e_{b2}^2)^2 + 4e_c e_{b2}[(e_c + e_{b2})^2 - e_c e_{b2}]} \right]^{1/2} \quad (5.31)$$

Therefore, the ratio of the amplitudes from the two regions of the sample with the two different backings works out to be

$$\frac{A_1}{A_2} = \left[\frac{e_{b1}^2 (e_c + e_{b1})^2 [(e_c^2 + e_{b2}^2)^2 + 4e_c e_{b2} [(e_c + e_{b2})^2 - e_c e_{b2}]]}{e_{b2}^2 (e_c + e_{b2})^2 [(e_c^2 + e_{b1}^2)^2 + 4e_c e_{b1} [(e_c + e_{b1})^2 - e_c e_{b1}]]} \right]^{1/2} \quad (5.32)$$

5.3b Phase of the PA signal

Starting with equation (5.15) one can deduce the expression for the phase of PA signal generated in the cell, which can be rewritten as

$$\Phi = \text{Tan}^{-1} \left[\frac{(p-b)(g+b)}{g(p+b)} \right] \quad (5.33)$$

Since p is much larger than b , $(p-b) \approx (p+b)$. Therefore

$$\Phi = \text{Tan}^{-1} \left[\frac{(g+b)}{g} \right]$$

which when expressed in terms of thermal effusivities works out to be

$$\Phi = \text{Tan}^{-1} \left[1 + \frac{e_b}{e_c} \right] \quad (5.34)$$

From this equation the phase of the PA signals from the two regions with different backing samples with effusivities e_{b1} and e_{b2} can be written as

$$\Phi_1 = \text{Tan}^{-1} \left[1 + \frac{e_{b1}}{e_c} \right] \quad (5.35)$$

$$\Phi_2 = \text{Tan}^{-1} \left[1 + \frac{e_{b2}}{e_c} \right] \quad (5.36)$$

Therefore, the difference in phase between the signals from the two regions of the sample is given by

$$\Phi_1 - \Phi_2 = \text{Tan}^{-1}\left[1 + \frac{e_{b1}}{e_c}\right] - \text{Tan}^{-1}\left[1 + \frac{e_{b2}}{e_c}\right] \quad (5.37)$$

5.3c Special cases

Equations (5.32) and (5.37) give the expressions for amplitude ratio and phase difference of PA signals generated from the two regions of the sample configuration shown in Fig. 5.1 as it is scanned with a chopped beam of light in a photoacoustics experiment. The expression for phase difference is comparatively simpler than the corresponding expression for amplitude ratio. But the values of Φ_1 and Φ_2 cannot be separated and treated independently in an experiment because one doesn't know the initial phase of PA signal in an experiment.

Rather complicated expressions for PA amplitude ratio can be simplified considerably by taking the thermal wave reflection coefficient, $R = \frac{(1 - e_b/e_c)}{(1 + e_b/e_c)}$ at the interface of the absorber layer and backing of the sample into account. Thermal wave reflection coefficient R determines the influence the of absorber layer in the PA signals generated from a sample of multilayer configuration[15,16].

If R_1 and R_2 are the thermal wave reflection coefficients at the absorber - backing boundaries defined by

$$R_1 = (1 - e_{b1})/e_c / (1 + e_{b1})/e_c$$

$$R_2 = (1 - e_{b2})/e_c / (1 + e_{b2})/e_c,$$

one can consider three special cases depending upon whether both R_1 and R_2 are negative or both are positive or one of them positive and the other negative.

Case I : R_1 and R_2 both are negative, ($e_c \ll e_{b1}$; $e_c \ll e_{b2}$)

This means that the thermal effusivity of the absorber layer is much smaller than the thermal effusivities of the two backing samples. Therefore, we can rewrite equation(5.32) as

$$\frac{A_1}{A_2} = \left[\frac{e_{b1}^4 [e_{b2}^4 + 4e_c e_{b2} [e_{b2}^2 - e_c e_{b2}]]}{e_{b2}^4 [e_{b1}^4 + 4e_c e_{b1} [e_{b1}^2 - e_c e_{b1}]]} \right]^{1/2}$$

which further gets simplified to

$$\frac{A_1}{A_2} = \left[\frac{e_{b1} [e_{b2} + 4e_c (1 - e_c/e_{b2})]}{e_{b2} [e_{b1} + 4e_c (1 - e_c/e_{b1})]} \right]^{1/2} \quad (5.38)$$

This is the situation when the two backing media have high thermal conductivity such as metallic samples.

Case II : R_1 and R_2 both are positive ($e_c \approx e_{b1} \approx e_{b2}$)

In this case thermal effusivity of the absorber layer and that of both backing samples are comparable. Therefore the equation (5.32) as such has to be used. For convenience we have rewritten the equation as follows.

$$\frac{A_1}{A_2} = \left[\left(\frac{e_{b1}}{e_{b2}} \right) r_1 \left[\frac{m_2 + 4e_c (P_2 - e_c e_{b2})}{m_1 + 4e_c (P_1 - e_c e_{b1})} \right] \right]^{1/2} \quad (5.39)$$

where

$$m_1 = \frac{(e_c^2 + e_{b1}^2)^2}{e_{b1}}$$

$$m_2 = \frac{(e_c^2 + e_{b2}^2)^2}{e_{b2}}$$

$$P_1 = (e_c + e_{b1})^2,$$

$$P_2 = (e_c + e_{b2})^2,$$

and

$$r_1 = (e_c + e_{b1})^2 / (e_c + e_{b2})^2.$$

Case III : One reflection coefficient negative and other positive

In this case either R_1 is negative and R_2 positive or vice versa. Therefore this case can be further separated as follows.

Case IIIa: R_1 negative and R_2 positive ($e_c \ll e_{b1}$; $e_c \approx e_{b2}$)

Here thermal effusivity of the absorber layer is much less than that of the backing sample b_1 , but comparable to the effusivity of the other backing sample b_2 . Therefore, equation(5.32) gets modified as

$$\frac{A_1}{A_2} = \left[\frac{e_{b1}^4 [(e_c^2 + e_{b2}^2)^2 + 4e_c e_{b2} [(e_c + e_{b2})^2 - e_c e_{b2}]]}{e_{b2}^2 (e_c + e_{b2})^2 [e_{b1}^4 + 4e_c e_{b1} [e_{b1}^2 - e_c e_{b1}]]} \right]^{1/2}$$

or,

$$\frac{A_1}{A_2} = \left[\left(\frac{e_{b1}}{e_{b2}} \right) \left[\frac{m_2/P_2 + 4e_c(1 - e_c e_{b2}/P_2)}{e_{b1} + 4e_c(1 - e_c/e_{b1})} \right] \right]^{1/2} \quad (5.40)$$

where m_2 and P_2 are as defined in case II above.

Case IIIb : R_1 positive and R_2 negative, ($e_c \approx e_{b1}$; $e_c \ll e_{b2}$)

In this case thermal effusivity of the absorber layer is comparable to the thermal effusivity of the backing sample b_1 , but much less than that of the backing sample b_2 . Then equation (5.32) can be rewritten as

$$\frac{A_1}{A_2} = \left[\frac{e_{b1}^2 (e_c + e_{b1})^2 [e_{b2}^4 + 4e_c e_{b2} (e_{b2}^2 - e_c e_{b2})]}{e_{b2}^4 [(e_c^2 + e_{b1}^2)^2 + 4e_c e_{b1} [(e_c + e_{b1})^2 - e_c e_{b1}]]} \right]^{1/2}$$

or,

$$\frac{A_1}{A_2} = \left[\left(\frac{e_{b1}}{e_{b2}} \right) \left[\frac{e_{b2} + 4e_c(1 - e_c/e_{b2})}{m_1/P_1 + 4e_c(1 - e_c e_{b1}/P_1)} \right] \right]^{1/2} \quad (5.41)$$

where m_1 and P_1 are defined as in case II above.

The amplitude ratio or the phase deference of PA signals from the sample configuration can be measured by scanning the sample surface in a one dimensional fashion with a light beam chopped at a constant frequency. The chopping frequency of

the light beam should be so chosen that the absorber layer of the sample is thermally very thin at that frequency. The physical thickness of the absorber layer is very critical in this method. The thickness of the layer must be uniform and should be very light. Measuring the amplitude ratio or phase difference and knowing the effusivities of one backing (reference) and those of the absorbing layer, one can determine the effusivity of the other (experimental) backing sample. The technique then will have the advantage that it is independent of cell parameters and experimental conditions. Moreover, it does not involve any cumbersome frequency analysis of the PA signal. Application of the method to real experiments is described in detail in the next chapter.

References

- [1] A. C. Tam, **Rev. Mod. Phys.** **58**, No.2 381 (1986)
- [2] B. k. Bein, S. Krueger and J. Pelzel, **Can. J. Phys.** **64**, 1208 (1986)
- [3] A. Lachaine, **J. Appl. Phys.** **57**, 5075 (1985)
- [4] P. Charpentier, F. Lepoutre and L. Bertrand, **J. Appl. Phys.** **53**, 608 (1982)
- [5] A. Lachaine and P. Poulet, **Appl. Phys. Lett.** **45**, 953 (1984)
- [6] K. N. Madhusoodanan, M. R. Thomas and J. Philip, **J. Appl. Phys.** **62**, 1162 (1987)
- [7] C. L. Ceasar, H. Vargas, J. Mendes Filho and L. C. M. Miranda, **Appl. Phys. Lett.** **43**, 555 (1983)
- [8] B. Bonne, J. L. Laporte and Y. Rousset, **J. Appl. Phys.** **67**, 2253 (1990)
- [9] U. Zammit and M. Marinelli, R. Pizzo Ferrato, F. Scudieri and S. Martellucci, **J. Phys.E: Sci. Instrum.** **21**, 935 (1988)
- [10] Z. Yasa and N. Amer, in **Topical Meeting on Acoustic microscopy** Ames. Iowa, WA 5 -1 (1979)
- [11] Sheenu Thomas, J. Isaac and J. Philip, **Rev. Sci. Instrum.** **66**, 3907 (1995)
- [12] O. Pessoa Jr., C. L. Ceasar, N. A. Patel, H. Vargas, C. C. Ghizoni and L. C. M. Miranda, **J. Appl. Phys.** **59**, 1316 (1986)
- [13] A. Rosencwaig, **Photoacoustics and photoacoustic spectroscopy**, (John Willy, New York 1980)
- [14] L. C. Aamodt, J. C. Murphy and J. G. Parker, **J. Appl. Phys.** **48**, 927 (1977)

[15] R. Tilgner, J. Baumann and M. Beyfuss, *Can. J. Phys.* **64**, 1287 (1986)

[16] C. A. Bennett, Jr. and R. R. Patty, *Appl. Opt.* **21**, 49 (1982)

CHAPTER 6

THERMAL CHARACTERISATION OF SOLIDS BY A PA SCANNING TECHNIQUE : EXPERIMENT

6.1 Introduction

This chapter of the thesis is devoted to discuss the experimental details and results of applying the PA scanning technique to determine the thermal effusivity of specific solids. In order to test the correctness of the technique we have attempted this method on different sample pairs whose thermal parameters are known. Since this method is different from the existing PA techniques for the determination of thermal parameters, its feasibility has to be studied. This is the reason why samples of known thermal parameters are selected for these experiments. Experimental results are in good agreement with the values of the thermal parameters of the samples used in the experiments and are in good agreement with the theoretical formulae derived in Chapter 5. The present experiments on PA scanning technique have been performed on sample configurations made as outlined in the theoretical formation and the sample surface coated with a very thin layer of lamp black. This sample is scanned in one dimension in a step by step fashion by means of a chopped beam of light by keeping it in the PA cell of the PA scanning system. The details of sample preparation, experimental method, results and a discussion of the results are given in the following sections.

6.2 Sample preparation

For measuring the thermal effusivity of a sample by the PA scanning technique a reference sample is required. The experimental sample and the reference sample should

be attached together as a single sample configuration which has been already discussed in the previous chapter (see Fig. 5.1). This sample configuration consists of a reference sample in which the experimental sample is inserted by drilling a pit in the reference sample. A very thin layer of good light absorbing material such as lamp black is coated over the surface of the entire sample combination after making the surface very flat and uniform. This method has been applied in different sample pairs made with materials of different thermal conductivity such as copper, stainless steel, brass, silicon, nylon, teflon etc.

Two discs of diameter $\approx 2\text{cm}$ and thickness $\approx 2\text{mm}$ are made of the material used as the reference sample in the experiment. One disc is bored at the center with nearly 4mm diameter. This bored disc is mounted symmetrically on the other disc by means of very fine layer of glue like araldite. The experimental sample is made in the form of a cylindrical piece of diameter 4mm and length 2mm. This piece of experimental sample is inserted tightly in the bore of the reference sample disc. The top surface of this sample combination is hand lapped and made perfectly flat so that it has a single uniform surface. The experimental and reference samples can be interchanged by preparing the experimental sample in the form of the outer disc and reference sample in the form of the central piece. The thickness of the experimental and reference samples should be more than the thermal diffusion length of the thermal wave which is generated as the sample configuration is subjected to photoacoustic scanning process. This means that the sample combinations as such should be thermally thick for the chopping frequency selected for modulating the intensity of incident light beam.

The polished surface of the sample combination is coated with a very thin layer of lamp black. Actually this thin layer of lamp black acts as the light absorbing sample and generates PA signals. In order that the thermal properties of the backing

materials, i.e. the reference sample and experimental sample, be reflected in PA signals, the thickness of lamp black coating is made very small. This means that the absorber layer is thermally very thin. Therefore, absorber layer coating should be made on the sample combination with extreme care and should not exceed few microns. A cross sectional view of the sample configuration along with its dimensions is shown in Fig. 6.1.

6.3 Experimental method

The sample thus prepared as above is fixed conveniently in the PA cell and subjected to PA scanning by using the PA imaging setup. Details of the PA imaging setup have already been discussed in Chapter 2 of the thesis. In order to measure the PA amplitude and phase simultaneously, the single phase lock - in amplifier in the PA imaging setup (Fig.2.2) is replaced by a dual phase lock - in amplifier (Stanford Research System, Model SR 830). Auto phase setting arrangement in this lock - in amplifier helps one to read the PA phase as well as amplitude directly from the two digital display panels provided for phase and amplitude on this instrument.

The PA scanning setup is programmed to move horizontally in a step by step fashion. Each step can provide a lateral shift of 0.25mm. All the samples used in this experiment are scanned in a similar manner along the diameter of the sample from one end to the other in about 40 steps. As the light beam scans the absorber surface changing the backing from one to the other (reference sample to experimental sample or vice versa), the PA signal amplitude and phase from each point are recorded after ensuring that the readings are stabilized. The software which control the PA scanning unit has been provided with the required time period between consecutive steps for stabilizing the readings on the lock - in amplifier.

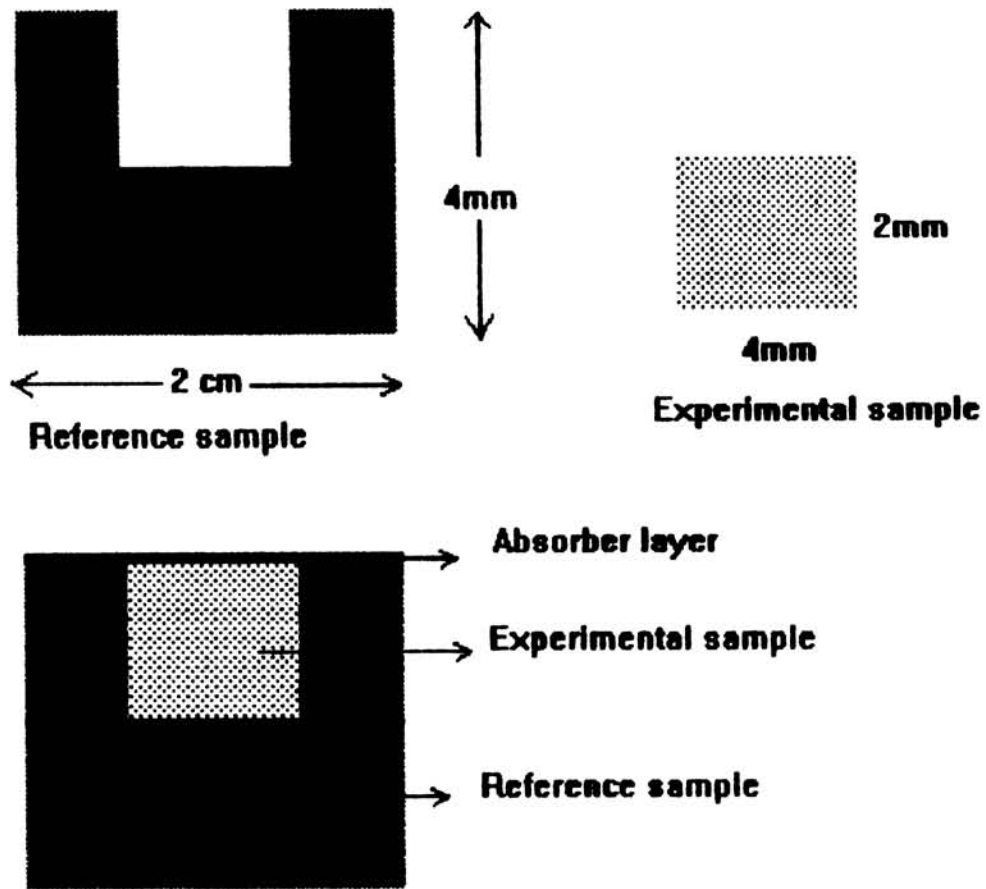


Fig. 6.1 : The sample configuration used in the present experiments.

A 10 mw He - Ne laser of wave length 632.8 nm is used as the source of radiation. The laser beam is chopped at a frequency of 40Hz using the optical chopper as has already been described in Chapter 2. 40 Hz is selected as the chopping frequency because the PA cell has the best response at this frequency. It is made sure that the absorber layer on the sample surface is thermally very thin at this frequency. Since chopping frequency is low, frequency of the acoustic signal produced in the PA cell also is small. Thus the wave length of the PA signal will be large. The change in distance between the point source of the PA signal and detector as the light beam scans the sample surface, which is a few mms, is very small compared to the wavelength of the photoacoustic signal at this frequency. So the corresponding phase change introduced due to shift in the point source of the PA signal can very well be neglected.

The experimental arrangement has been tested several times using a sample configuration in which the reference and experimental samples are made of the same material. In this case the system just sense the boundaries without causing any change in the PA signal amplitude or phase as the backing is changed from the reference to the experimental sample.

6.4 Results

The PA amplitude and phase obtained from each sample pair as it is scanned along a line in step by step fashion are recorded and plotted. Samples which are subjected to this experiment includes copper, brass, stainless steel, silicon, nylon and teflon. Figures 6.2, 6.3, 6.4, 6.5, 6.6, 6.7, 6.8, and 6.9 depict the variation of the amplitude and phase of the PA signals as a function of scanning distance in one dimension for different sample configurations. All the graphs show sharp changes in amplitude and phase at two specific points as the distance is varied. These correspond to the boundaries between reference and experimental samples. As the surface of the absorbing layer of

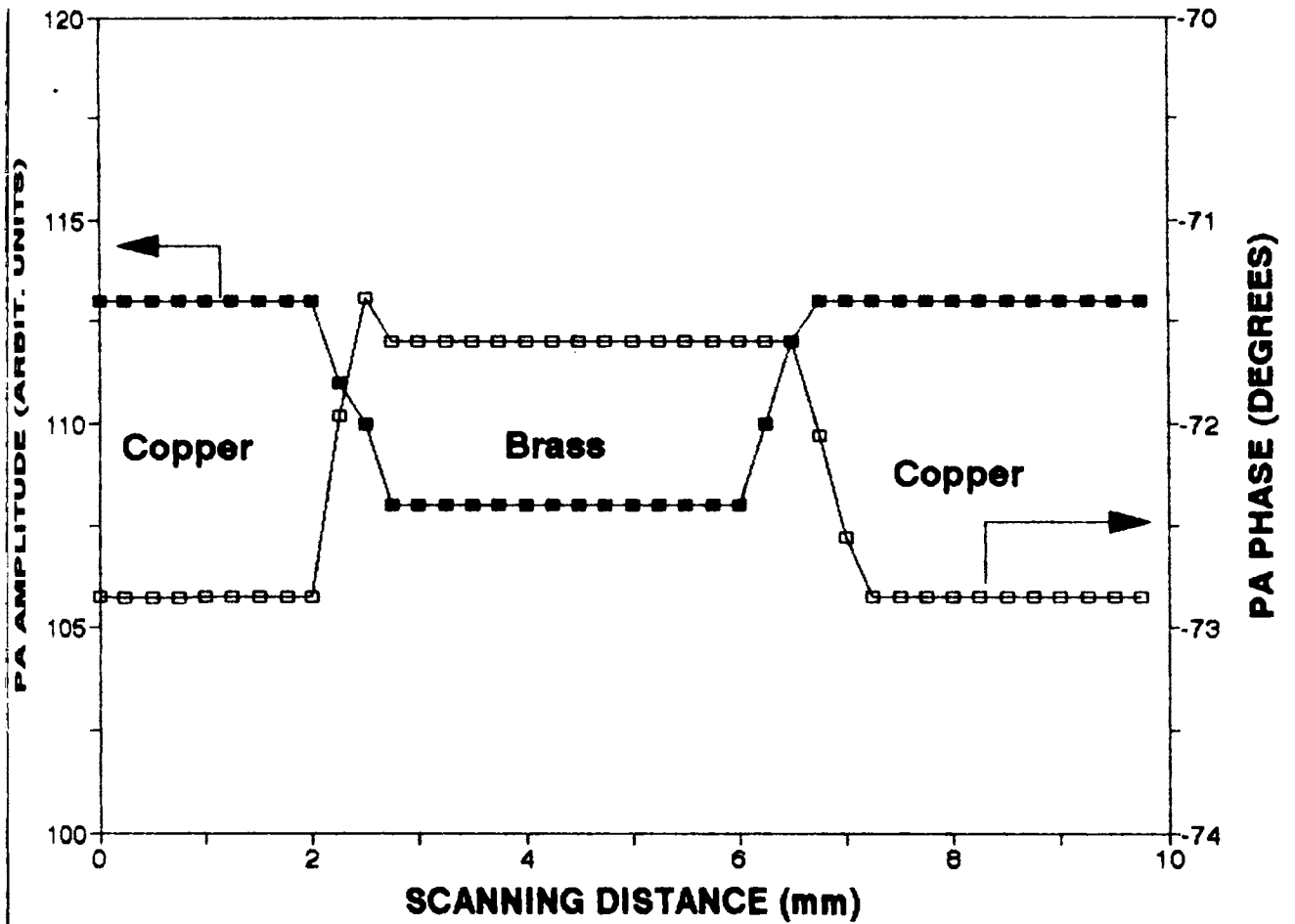


Fig. 6.2 : Variations of PA amplitude and phase with scanning distance in the Copper - Brass sample pair.

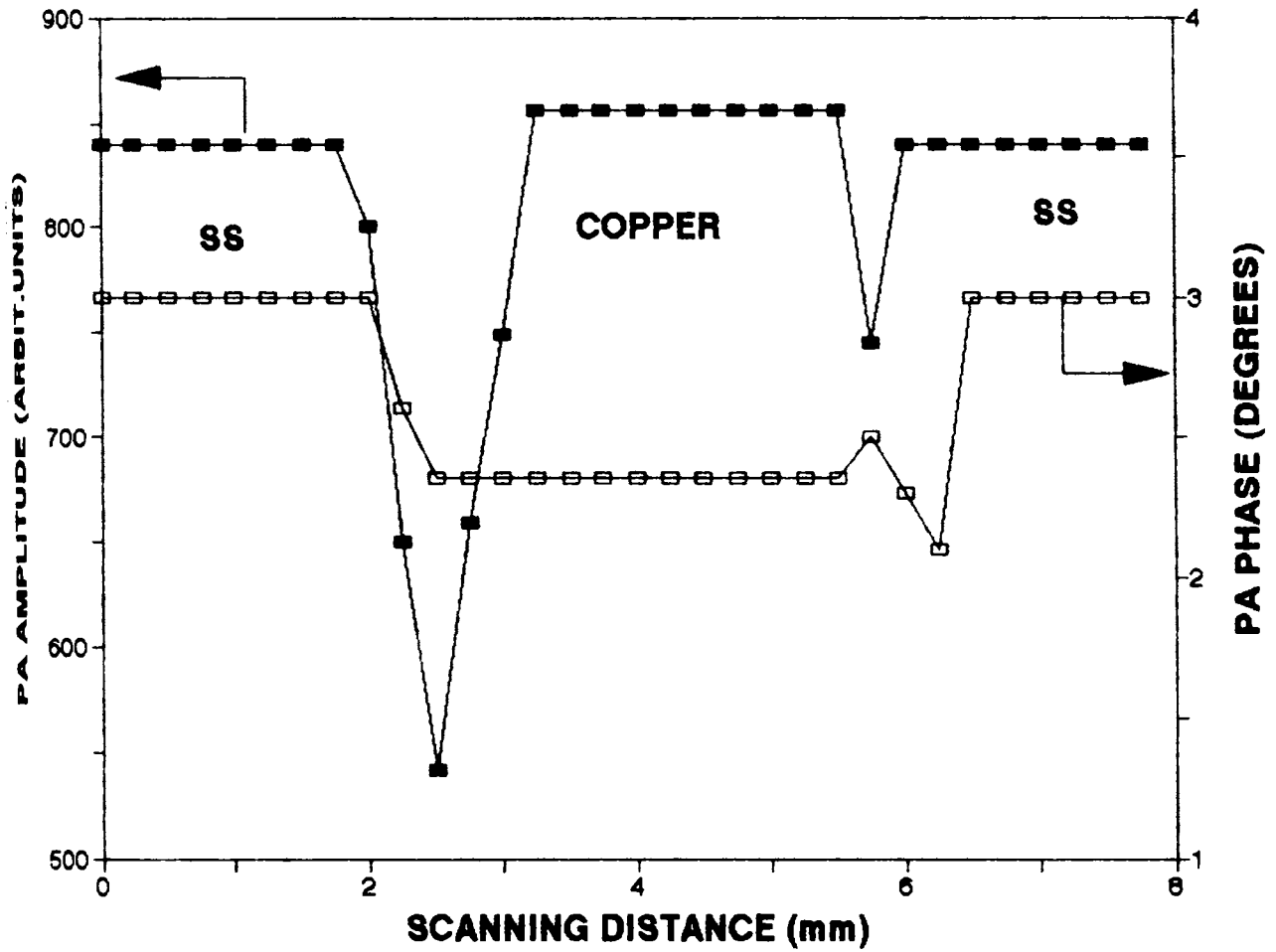


Fig. 6.3 : Variations of PA amplitude and phase with scanning distance in the Stainless steel - Copper sample pair.

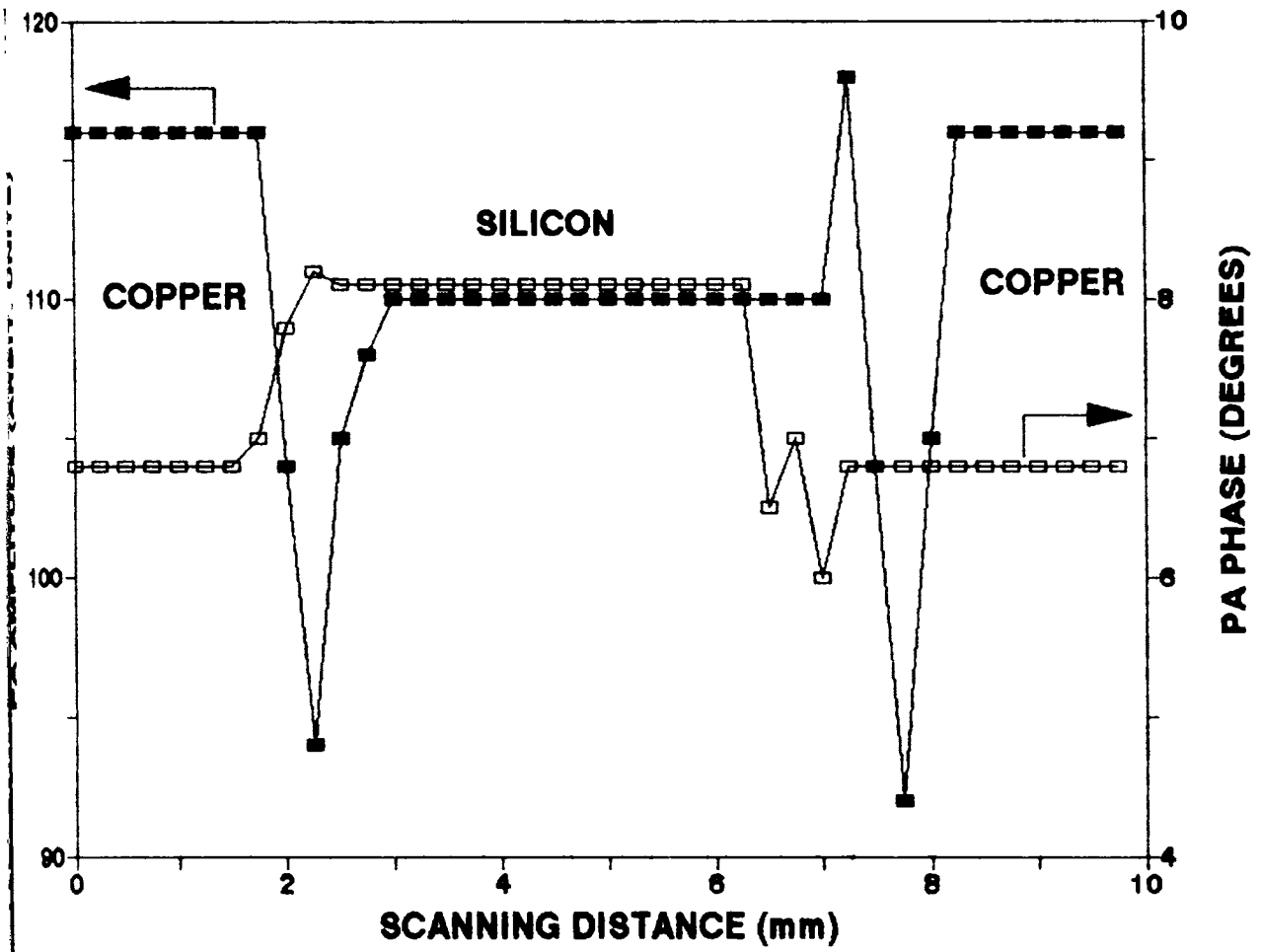


Fig. 6.4 : Variations of PA amplitude and phase with scanning distance in the Copper - Silicon sample pair.

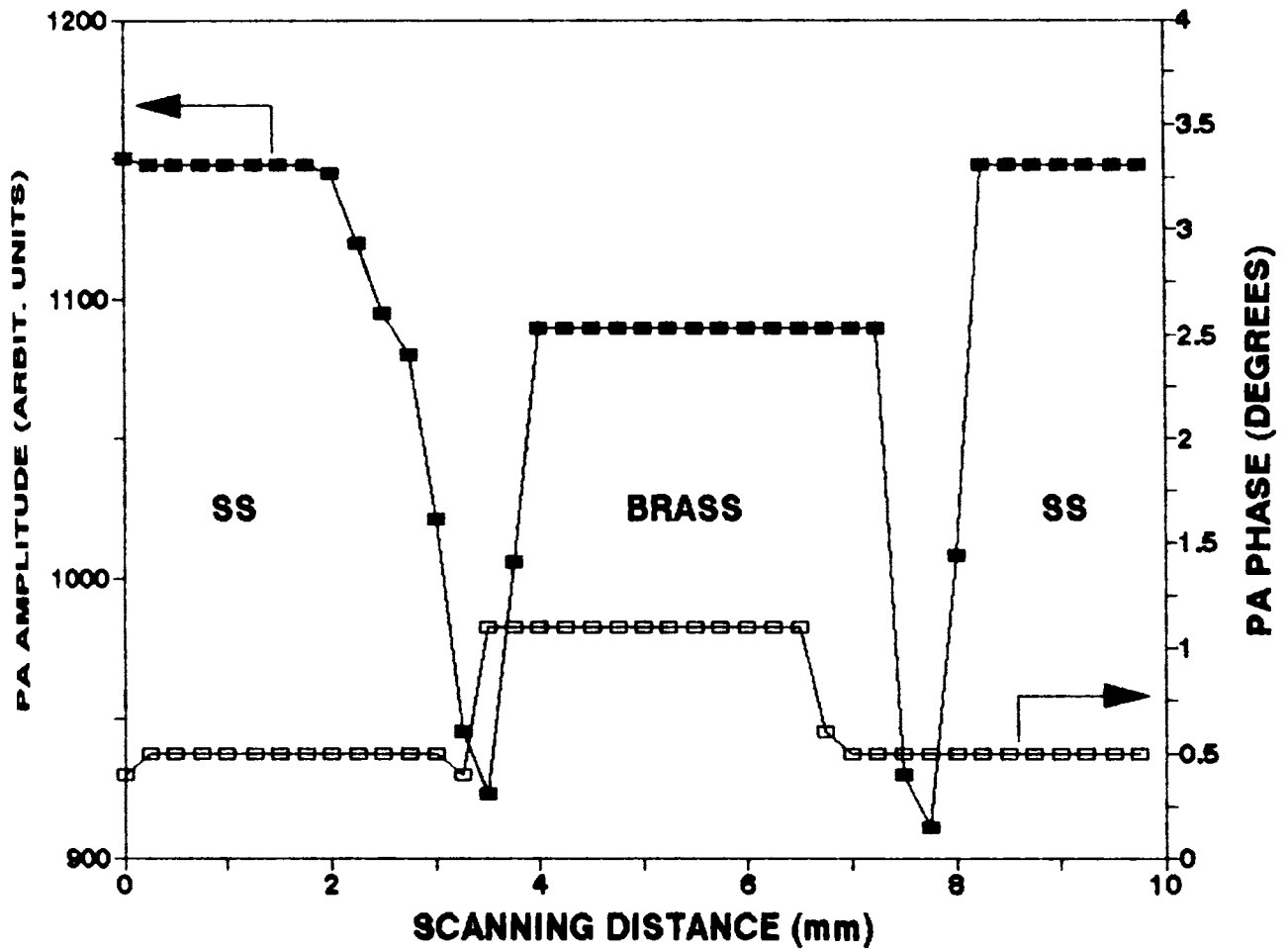


Fig. 6.5 : Variations of PA amplitude and phase with scanning distance in the Stainless steel - Brass sample pair.

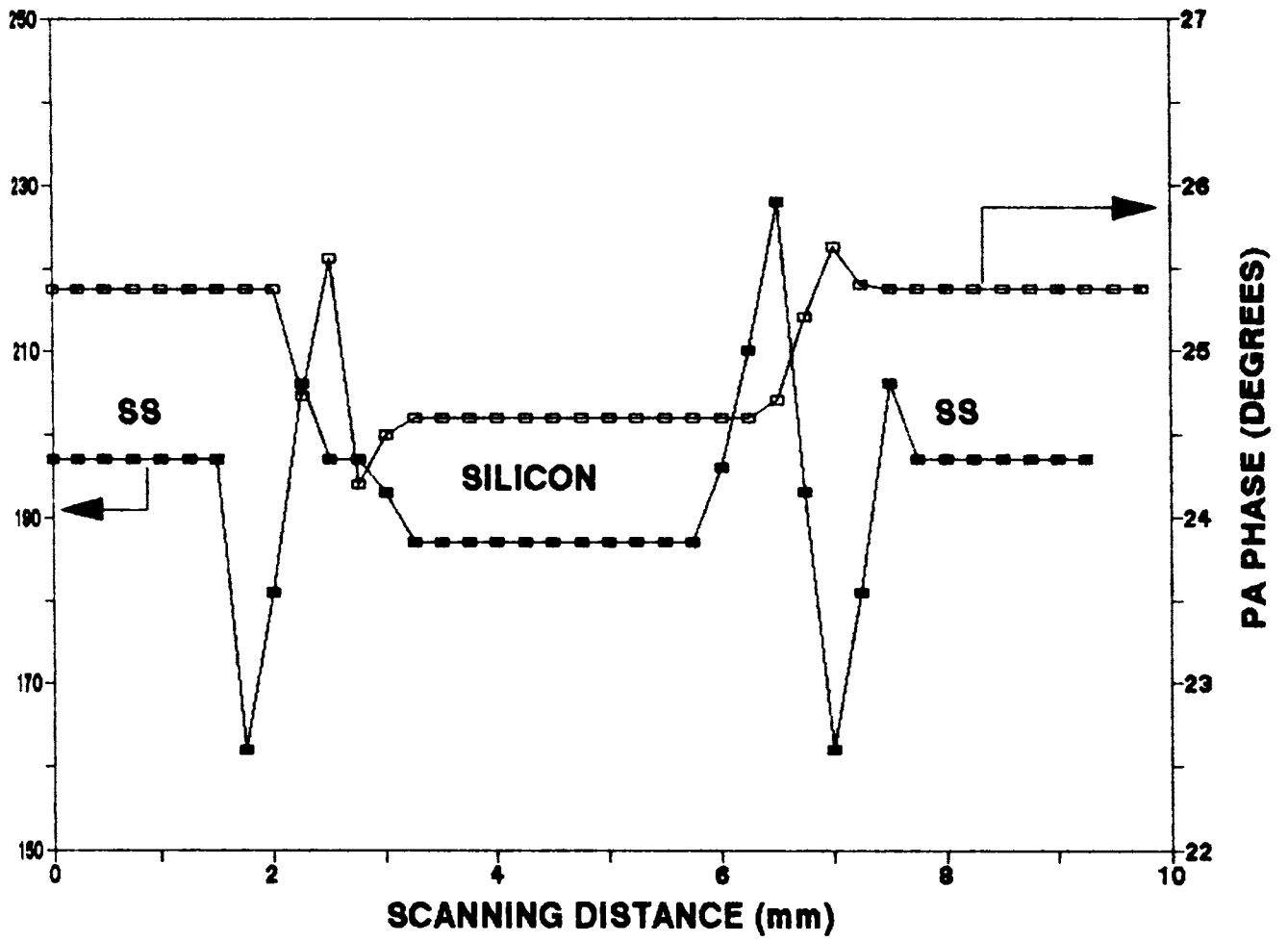


Fig. 6.6 : Variations of PA amplitude and phase with scanning distance in the Stainless steel - Silicon sample pair.

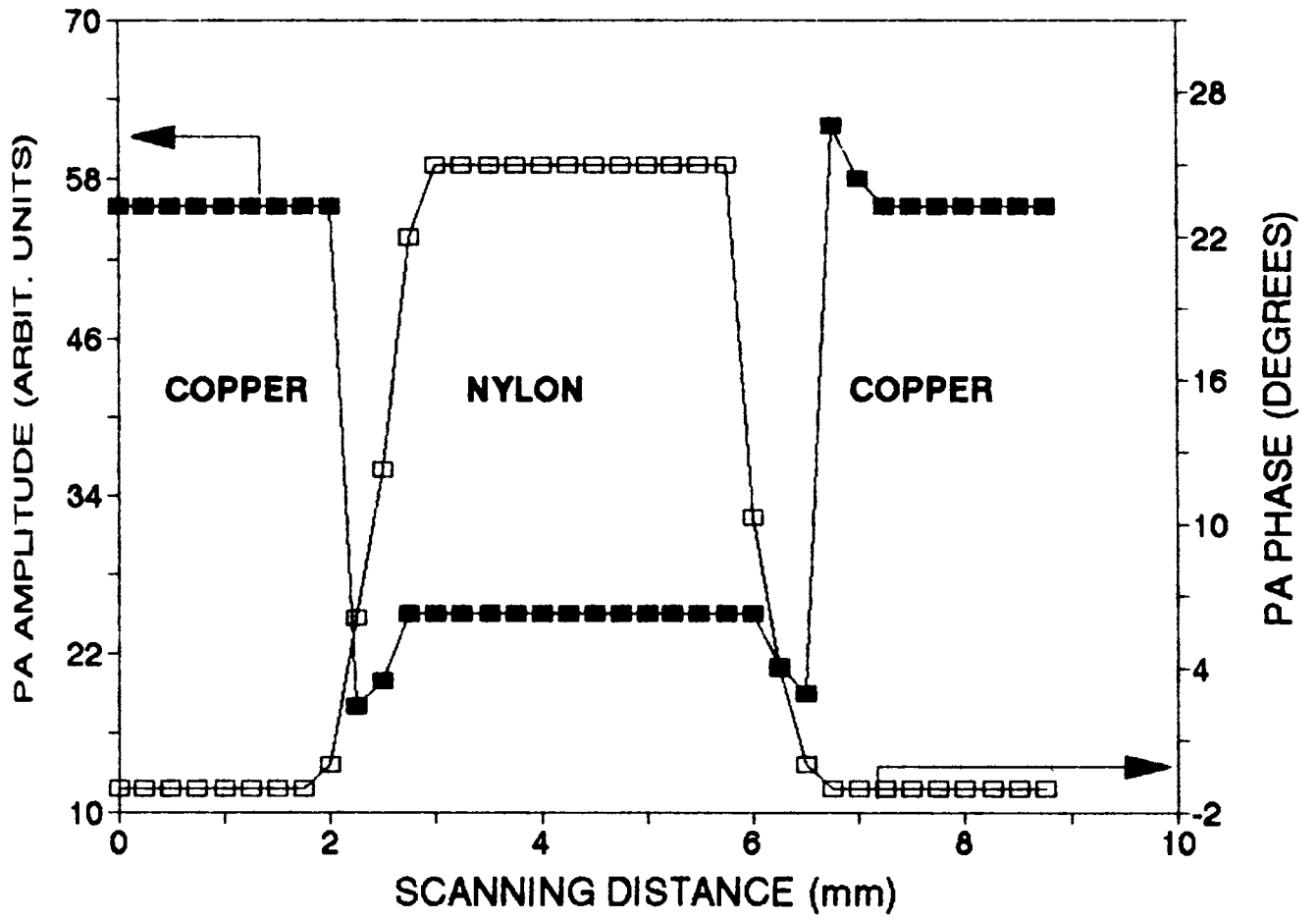


Fig. 6.7 : Variations of PA amplitude and phase with scanning distance in the Copper - Nylon sample pair.

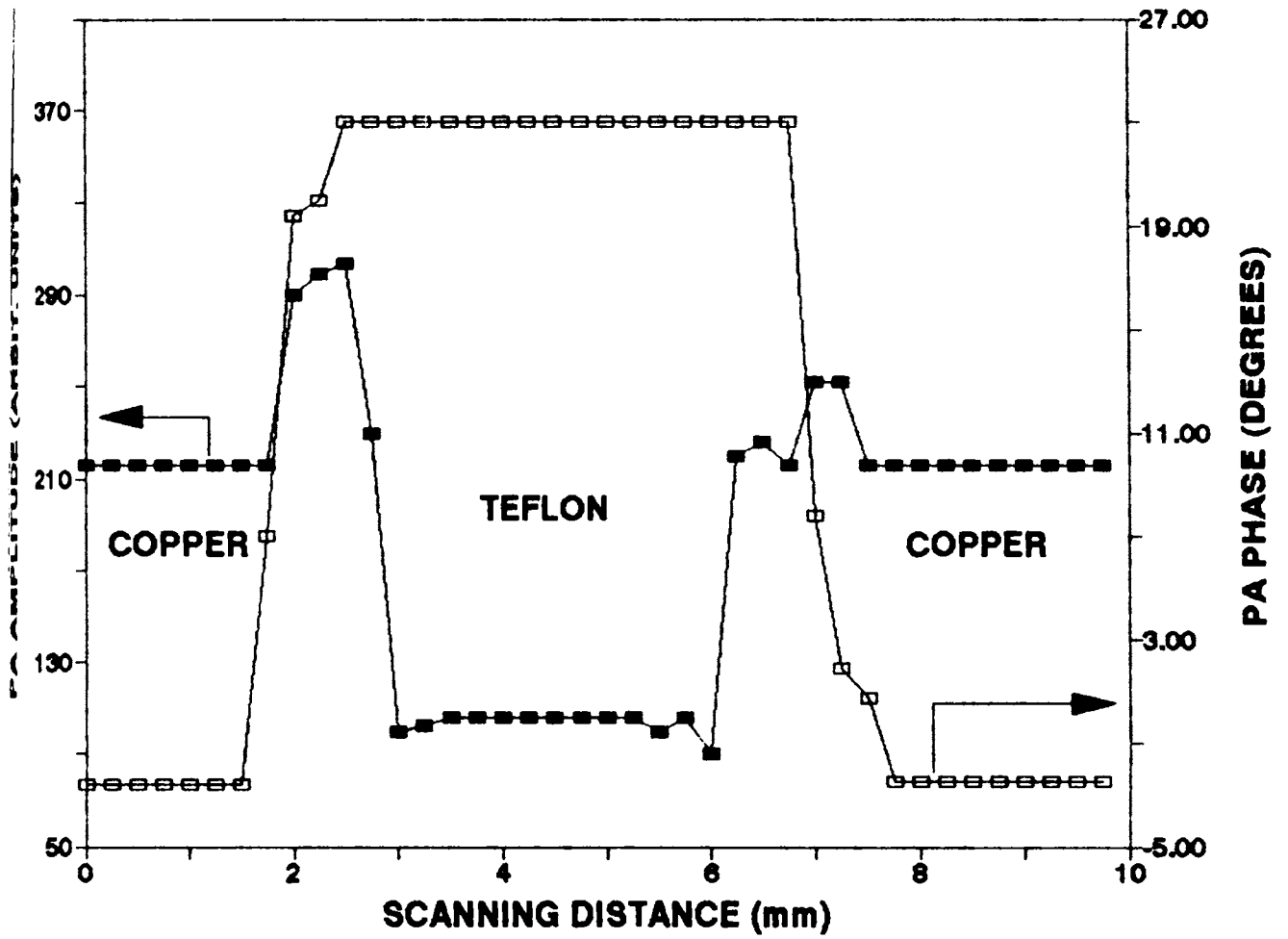


Fig. 6.8 : Variations of PA amplitude and phase with scanning distance in the Copper - Teflon sample pair.

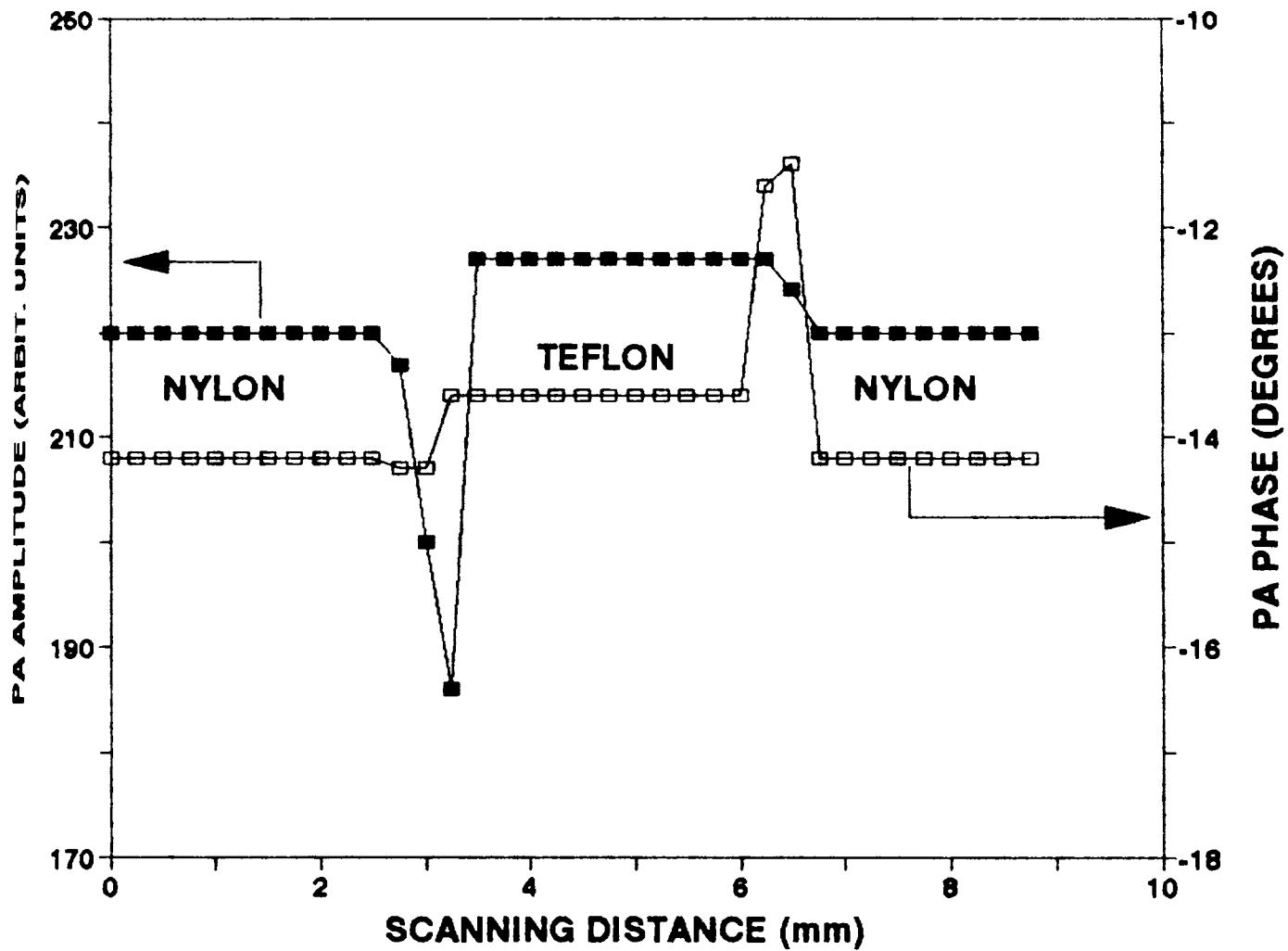


Fig. 6.9 : Variations of PA amplitude and phase with scanning distance in the Nylon - Teflon sample pair.

the sample is scanned from one end to other end, the backing sample changes from the reference sample to the experimental sample and then to the reference sample again. Therefore the middle regions of the all the plots presented in the amplitude and phase of PA signals are from the experimental sample whereas the side regions of the graphs are from the reference sample. The direction in which the PA amplitude or phase change in the experimental sample relative to the reference sample clearly indicates whether the experimental sample has a higher or lower thermal effusivity compared to the reference sample. Obviously, there is no variation in amplitude or phase, except for variations at the boundaries, when the same material is used in places of the reference and experimental samples, leading to a value zero for the phase difference and unity for the amplitude ratio.

The PA amplitude ratio and phase difference have been determined for each sample pairs, from the experimental data. By grouping the sample pairs into three categories which has been discussed in the previous chapter on theory, we have calculated their amplitude ratio and phase difference using equations (5.38), (5.39), (5.40), (5.41) and (5.37) of the previous chapter. For the theoretical calculations, the required thermal parameters of each sample are taken from standard hand books. The experimentally determined and theoretically evaluated amplitude ratio as well as phase difference of different sample configurations are tabulated in Table 6.1. The thermal effusivity of carbon layer used as the absorber is estimated by measuring the amplitude ratio and phase difference in one experiment in which both the backings used have known thermal effusivities. It is found to be nearly $0.02 \text{ cal cm}^{-2} \text{ K}^{-1} \text{ sec}^{-1/2}$.

Using the amplitude ratio and phase difference values obtained from the experiment, we have also determined the effusivities of all the experimental samples. These effusivity values of all the samples are tabulated in Table 6.2. For comparison, the

Table 6.1

Measured and calculated values of phase difference and amplitude ratios for different sample configurations discussed in the text.

Sample configuration E - Exp. sample R - Ref. sample	Thermal wave reflection coefficient	Phase difference (degrees)		Amplitude ratio	
		Measured	Calculated	Measured	Calculated
E- Brass, $\epsilon_{b1} = 0.443$ R - Copper, $\epsilon_{b2} = 0.87$	$R_1 = -0.91$ $R_2 = -0.96$	1.2 ± 0.06	1.2	0.94 ± 0.05	0.97
E- SS, $\epsilon_{b1} = 0.585$ R - Copper, $\epsilon_{b2} = 0.87$	$R_1 = -0.93$ $R_2 = -0.96$	0.60 ± 0.03	0.62	0.98 ± 0.05	0.98
E- Silicon, $\epsilon_{b1} = 0.37$ R - Copper, $\epsilon_{b2} = 0.87$	$R_1 = -0.91$ $R_2 = -0.96$	1.32 ± 0.07	1.4	0.93 ± 0.05	0.95
E- Brass, $\epsilon_{b1} = 0.443$ R- SS, $\epsilon_{b2} = 0.585$	$R_1 = -0.91$ $R_1 = -0.93$	0.70 ± 0.04	0.62	0.95 ± 0.05	0.98
E- Silicon, $\epsilon_{b1} = 0.37$ R- SS, $\epsilon_{b2} = 0.585$	$R_1 = -0.91$ $R_2 = -0.93$	0.75 ± 0.04	0.62	0.95 ± 0.05	0.96
E - Copper, $\epsilon_{b1} = 0.87$ R- Nylon, $\epsilon_{b2} = 0.017$	$R_2 = -0.96$ $R_2 = +0.08$	26 ± 1.3	27.5	2.20 ± 0.11	2.1
E- Teflon, $\epsilon_{b1} = 0.018$ R - Copper, $\epsilon_{b2} = 0.87$	$R_1 = +0.05$ $R_2 = -0.96$	25.6 ± 1.2	26.3	0.49 ± 0.02	0.48
E- Teflon, $\epsilon_{b1} = 0.018$ R- Nylon, $\epsilon_{b2} = 0.017$	$R_1 = +0.05$ $R_2 = +0.08$	0.60 ± 0.03	0.64	1.03 ± 0.05	1.02

Table 6.2

Thermal effusivities of experimental samples measured by PA amplitude ratio and phase difference methods.

Experimental samples	Measured thermal effusivity $\text{cal cm}^{-2} \text{K}^{-1} \text{Sec}^{-1/2}$		Calculated thermal effusivity $e = \sqrt{k\rho C}$ $\text{cal cm}^{-2} \text{K}^{-1} \text{Sec}^{-1/2}$
	Amplitude ratio method	Phase difference method	
Brass	0.40 ± 0.02	0.44 ± 0.02	0.443
SS	0.525 ± 0.026	0.569 ± 0.03	0.585
Silicon	0.38 ± 0.019	0.35 ± 0.02	0.37
Teflon	0.018 ± 0.001	0.018 ± 0.001	0.018

effusivity of each sample determined using the data available in hand books are also tabulated in the same table. In all the examples of sample pairs listed in Table 6.2, there is good agreement between the theoretical and experimental values.

5 Discussion and conclusion

Through this work we have demonstrated a rather simple and direct method for determining the thermal effusivity of solids using photoacoustic technique. In this scanning method, measurements are made relative to a reference sample. Therefore this technique is free of PA cell calibration and other experimental parameters. The only requirement is that the thermal parameters of the reference sample should be known accurately. Experimentally it is found that, giving a uniform coating over the surface of the sample configuration is not difficult. Of course, one must ensure that the samples are made to have the top surfaces flat and have the same level. In a routine experiment, one can have a standard reference sample and the experimental sample can be inserted into an appropriate cavity made in the reference sample.

In some of the plots, PA amplitude and phase increases or decreases abruptly at the boundaries between the two samples. But the regions corresponding to reference and experimental samples are quite clear and explicit. The sharp peaks in PA amplitude and phase at the boundaries in certain cases may be due to the nonalignment of the boundaries of the reference and experimental samples. In the case of samples having perfect alignment at the boundary between experimental and reference samples, one gets a uniform change of PA amplitude and phase as the backing sample changes from the reference to the experimental sample and again to the reference sample.

Analysis of the results presented in Table 6.1 and Table 6.2 show that we have good agreement between measured and calculated values for all the three groups of

sample pairs having thermal wave reflection coefficient, R_1 and R_2 , having the same or opposite signs. Both methods, phase difference and amplitude ratio measurements are found to work well and found to give results which do agree with each other. But phase difference is comparatively small and amplitude ratio is around unity when the thermal wave reflection coefficients of the two samples R_1 and R_2 are either positive or negative. On the other hand, when R_1 and R_2 of the two samples have opposite signs they give rise to large difference in phase and a value away from unity for amplitude ratio. Therefore, although the PA scanning method works well in all sample combinations irrespective of their thermal effusivities, it is convenient to take measurements if sample configuration is made by selecting materials with opposite signs for thermal wave reflection coefficient values.

The errors in the measured values can be attributed mainly to the experimental uncertainties in the measurements. By admitting an estimated 5 % error generally in all the cases, we have evaluated the possible variations in the measured values and recorded them in the two tables. These experimental results also prove that the approximations and assumptions made in the original R - G theory for this new scanning technique are physically realistic and correct.

Since these measurements do not involve any variations in frequency, sample thickness or backing material as in conventional PA experiments, the technique is quite straight forward and fast. This method could be developed in to a standard experimental technique with which thermal conduction analysis of unknown samples could be done in a routine way.

CHAPTER 7

A ONE DIMENSIONAL PHOTOACOUSTIC SCANNING TECHNIQUE TO MEASURE THERMAL EFFUSIVITY OF THIN FILMS

7.1 Introduction

The photoacoustic (PA) technique now finds a wide range of applications in spectroscopy, chemistry, material science, medicine etc. It is extensively used to investigate optical and thermal properties of solid samples[1]. This aspect has been discussed at length in Chapter 1. Its acceptability as an analytical tool is due to the fact that the technique is very sensitive and it works well in samples in which the conventional spectroscopic techniques often fail. Since photoacoustic effect in solids involves an energy conversion process in which the incident light is first converted into thermal waves and then into acoustic waves, the measured photoacoustic amplitude and phase are complex functions of the physical properties such as absorption coefficient, thermal conductivity and heat capacity of the sample. Moreover, the PA amplitude and phase do depend on the photoacoustic cell parameters as well and extraction of desired information from the measured quantities are not so straight forward. One has to adapt special experimental techniques to isolate optical absorption coefficient, thermal conductivity or heat capacity of solid samples.

In PA experiments to determine thermal conductivity of solid samples, one usually measures either the thermal diffusivity or thermal effusivity from which one can evaluate thermal conductivity knowing the density and heat capacity of the sample. The PA technique for measuring thermal diffusivity, defined as $\alpha = k/\rho C$ where k is the thermal conductivity, ρ is the density and C is the heat capacity of the sample, or thermal effusivity, defined as $e = \sqrt{(k\rho C)}$, is essentially a periodic heat flow technique.

The measurement usually involves a chopping frequency analysis of the PA amplitude and phase and determination of the critical frequency, f_0 , at which the sample goes from thermally thick to a thermally thin regime[2,3,4,5]. For a thermally thick sample, $l_s a_s \gg 1$ where l_s is the sample thickness and $a_s = (\omega/2\alpha)^{1/2}$ is the thermal diffusion coefficient where ω is the angular frequency of light modulation. For such a sample, the PA phase ceases to vary beyond the critical frequency corresponding to $l_s a_s = 1$ so that $\alpha = f_0^2 l_s^2$. By measuring the frequency dependence of the PA amplitude, one can determine f_0 as the frequency at which the variation deviates from the ω^{-1} dependence predicted by the Rosencwaig - Gersho (R-G) theory[6] for a thermally thick sample.

The characteristic frequency f_c is determined by measuring the variations of PA signal amplitude with chopping frequency. For this first of all the amplitude of the PA signal for a thermally thick sample (reference sample) is measured as a function of the chopping frequency. This sample should be thermally thick in the entire chopping frequency range used in the measurement. Repeat the same measurement after thinning down the sample (experimental sample) into an appropriate thickness which comes within the range of thermal diffusion length of the thermal waves generated during the frequency analysis. One can observe a distinct deviation of slope of the chopping frequency versus PA amplitude graph from the experimental sample after a particular chopping frequency whereas the graph from the reference sample shows a constant slope throughout the entire range of chopping frequency. The chopping frequency at which the slope of the graph deviate is assumed as the characteristic frequency of the sample.

Swimm[3] has also adapted a similar method for determining the thermal properties of thin film samples. But this technique is dependent mainly on the chopping frequency versus PA phase measurement from a reference sample (thermally thick, optically dense bulk sample) and that from an optically dense thin film sample on a

thermally thick substrate. The calibration phase data are subtracted from the thin film phase data. To the extent that frequency-independent phase shift and systematic phase variation present in both measurements cancel, the resultant phase difference characterizes the thin-film/substrate system alone.

A few other techniques have also been developed to determine thermal diffusivity and effusivity of solid samples. One of them involves measurement of the variation in PA amplitude and phase with distance between the point where the heat is generated and the point at which the thermal oscillations are detected[7]. Another technique involves measurement of the variation in PA phase with frequency for different sample thicknesses. By adopting R - G theory to specific experimental conditions and analysing the generated PA signal amplitude and phase, different workers have determined thermal parameters of different solid samples[9,10]. Still another technique to measure thermal diffusivity of a solid sample employing PA technique involves determination of the amplitude ratio or phase lag of the PA signal between the front and rear surface illuminations at a single chopping frequency[11,12]. This technique has the advantage that the measurement is independent of sample thickness and chopping frequency. Here the authors measured the PA signal phase by illuminating front and rear surfaces of the sample with the same chopped beam of light. For this Pessoa *et al.*[11] have used two beams of light derived from the same source to illuminate the front and rear surfaces of the sample simultaneously, whereas Thomas *et al.*[12] have adopted the technique of illuminating the front surface first and then rotating the PA cell by 180° about the vertical axis to illuminate the rear surface of the sample with the same light beam.

In the last two chapters we have described a photoacoustic scanning technique that has been developed to determine thermal effusivity of solid samples in which the chopped light beam is scanned across a sample configuration in which the experimental

sample is attached to a reference sample whose thermal parameters are known. The samples act as thermally thick backing media for a light absorbing thermally thin film which is coated uniformly above the surface of the two samples. Measurement of the PA amplitude ratio or phase difference as the light beam crosses the boundary enables one to evaluate the thermal effusivity of the experimental sample. This technique has the advantage that the measurement is independent of PA cell parameters and other experimental conditions. The principle and theory of this technique has already been outlined in Chapter 5 and the experimental details are described in Chapter 6 of this thesis.

All the techniques outlined above measure thermal diffusivity or effusivity of solid samples in the bulk form. To the best of our knowledge, no experimental technique exists which enables one to measure thermal effusivity or diffusivity of samples in the thin film form without involving complex frequency analysis of the generated PA signal. In this chapter we report an extension of the PA scanning technique described in Chapter 6 to determine thermal effusivity of thin film samples. The technique has been applied to a specific set of thin film samples as well as to a sample whose thermal parameters are already known. The variation of thermal effusivity with film thickness has been measured to determine the range of thickness over which the technique can be applied. The principle of the technique, experimental method, results obtained and a discussion of the results are outlined in the following sections.

7.2 Principle of the method

Consider the sample configuration shown in Fig 7.1, similar to the one outlined in Chapter 5, in which two solid backing samples (substrates) A and B are kept in close contact so as to have a sharp boundary between them. The top of the two samples are flat and are at the same level. Assume that the thermal parameters, such as thermal

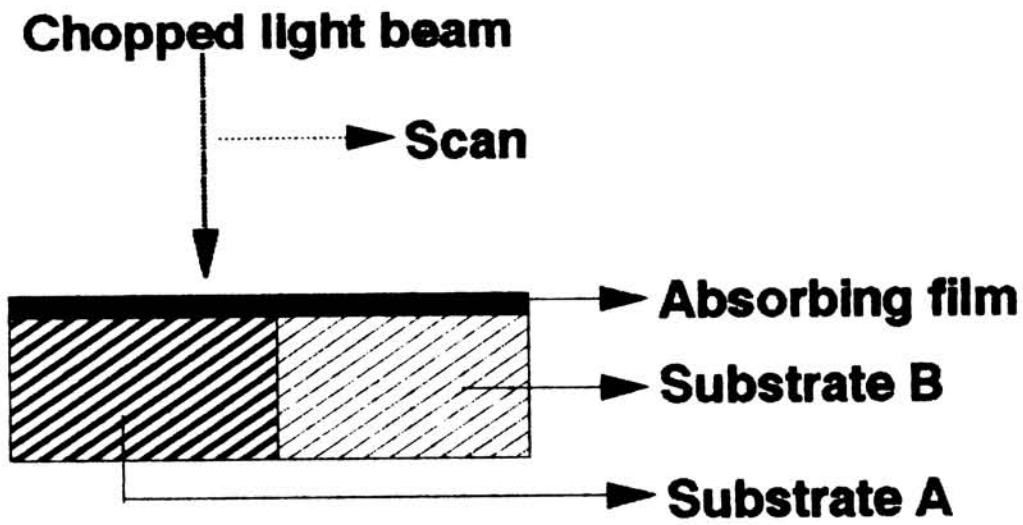


Fig 7.1 : Sample configuration

conductivity and heat capacity of these substrate samples are known. This sample combination acts as the substrate for the thin light absorbing film coated over it. The top surface of the film layer can be scanned with a chopped beam of light in a step by step fashion so that the backing for the film changes smoothly from substrate A to substrate B. The chopping frequency and substrate thickness are so chosen that the film is thermally very thin and the substrate is thermally thick. It is known from R-G theory that for such a sample configuration, the PA signal do depend on the thermal properties of the backing medium [1].

One can apply the Rosencwaig- Gersho one- dimensional theory for the production of photoacoustic signal to the sample configuration shown in Fig.7.1 as has already been outlined in Chapter 5. For an optically opaque and thermally thin sample with a single backing medium, R- G theory shows that the complex envelope of the PA signal is given by

$$P = Ae^{-i\Phi} \quad (7.1)$$

where A and Φ are the amplitude and phase of the generated PA signal. This expression can be written more explicitly as

$$P = Q \left[\frac{(r-1)(b+1)e^{\sigma l_s} - (r+1)(b-1)e^{-\sigma l_s} + 2(b-r)e^{-\beta l_s}}{(g+1)(b+1)e^{\sigma l_s} - (g-1)(b-1)e^{-\sigma l_s}} \right] \quad (7.2)$$

where

$$Q = \frac{\beta I_0 \gamma P_0}{2\sqrt{2} T_0 k_s l_s a_s (\beta^2 - \sigma^2)} \quad (7.3)$$

Here β is the optical absorption coefficient of the sample, I_0 is the intensity of the incident light, γ is the ratio of specific heats, P_0 is the ambient pressure, T_0 is the ambient temperature, k_s , l_s , a_s are the thermal conductivity, thickness and thermal

diffusion coefficient of the sample and

$$\sigma = (1 + i)a_s \quad (7.4)$$

The terms $b, g,$ and r are given by

$$\begin{aligned} b &= \frac{k_b a_b}{k_s a_s} = e_b/e_s \\ g &= \frac{k_a a_a}{k_s a_s} = e_a/e_s \\ r &= \frac{(1 - i)\beta}{2a_s} \end{aligned} \quad (7.5)$$

Here k is the thermal conductivity and $a = [\omega/2\alpha]^{1/2}$ is the thermal diffusion coefficient with the subscripts b, a and s referring to the backing sample, the air medium in front of the sample and the absorber film sample respectively. ω is the angular frequency of light modulation, α is the thermal diffusivity and $e = \sqrt{k\rho C}$ is the thermal effusivity of the corresponding media.

In our experiments we limit the thickness of the absorber film to the very thin regime ($< 10 \mu$ m thick) and the modulation frequency used is small (≈ 40 Hz). Correspondingly, the phase lag caused by the sample to the generated thermal wave, given by $\Phi_s = l_s/\mu_s$ where $\mu_s = 1/a_s$ is the thermal diffusion length, is very small. At the same time it acts as the source of heat at the surface of the backing medium. So there is a direct thermal coupling between the backing medium and the air medium in front of the sample. Under this condition, the effusivity ratio b given in equation (7.5) can very well be written as

$$b = e_b/e_a = k_b a_b/k_a a_a \quad (7.6)$$

Since we have chosen metallic substrates with good thermal conductivity and restrict our experiments to low conductivity film samples, one can see that $k_a a_a < k_s a_s \ll k_b a_b$. This can very well be verified by substituting the values of k and a available

for the different media involved. The above fact tells that the backing medium sees just one source of heat in front of it and it does not distinguish between the absorber layer and the air medium. So from the point of view of PA signal generation at the surface of the backing medium, one can rewrite the ratio g in equation (7.5) as

$$g = e_s/e_a = k_s a_s/k_a a_a \quad (7.7)$$

The expressions for b and g have been rewritten as in equations (7.6) and (7.7) to eliminate the thermal parameters of air from the subsequent derivations. The relative change in thermal effusivity values between different backing samples is accounted for in terms of the thermal wave reflection coefficients at the boundary between the film layer and the backing media as outlined below.

For an optically thick sample, β is very high and the optical absorption length $l_\beta = 1/\beta$ is very small. Moreover, since the film is thermally very thin, $l_s \ll \mu_s$. Therefore we can very well assume that $e^{-\beta l_s} \rightarrow 0$ and we limit to zero order approximation so that $e^{\sigma l_s} \rightarrow 1$. Substituting these in equation (7.2) and simplifying it algebraically, one gets the following expression for the square of the PA signal amplitude.

$$A^2 = Q^2 \left[\frac{b^2(g+b)^2}{4a_s^2[(g^2+b^2)^2 + 4gb[(g+b)^2 - gb]]} \right] \quad (7.8)$$

The algebraic steps involved in arriving at this equation are already given in Chapter 5. Naturally, for higher sample thicknesses one should include higher order terms in the expansion of $e^{\sigma l_s}$. If the first order term is included, $e^{\sigma l_s} \rightarrow 1 + \sigma l_s$ in which case the PA amplitude given by the above equation gets modified and will have dependence on thickness.

Substituting for b and g from (7.6) and (7.7) in this equation, we can rewrite this expression in terms of the thermal effusivities of the film and the backing media.

If subscripts A and B refer to the two backing media, the amplitude of the PA signal from the film with backing medium A works out to be

$$A_A = Q \sqrt{\frac{e_A^2(e_s + e_A)^2}{4a_s^4[(e_s^2 + e_A^2)^2 + 4e_s e_A[(e_s + e_A)^2 - e_s e_A]}} \quad (7.9)$$

A similar expression holds good for the signal amplitude from the film with backing medium B. In one-dimensional PA scanning method, as one changes the backing from sample A to sample B, the ratio between the amplitudes, after algebraic simplification, works out to be

$$\frac{A_A}{A_B} = \left[\frac{e_A^2(e_s + e_A)^2[(e_s^2 + e_B^2)^2 + 4e_s e_B[(e_s + e_B)^2 - e_s e_B]]}{e_B^2(e_s + e_B)^2[(e_s^2 + e_A^2)^2 + 4e_s e_A[(e_s + e_A)^2 - e_s e_A]]} \right]^{1/2} \quad (7.10)$$

where e_s, e_A and e_B are the thermal effusivities of the absorber film, sample A and sample B respectively. Under the same assumptions, as the backing sample is changed from A to B, the phase difference between the generated PA signals works out to be

$$\Phi_A - \Phi_B = \tan^{-1}\left(1 + \frac{e_A}{e_s}\right) - \tan^{-1}\left(1 + \frac{e_B}{e_s}\right) \quad (7.11)$$

The intermediate steps involved in arriving at equations (7.10) and (7.11) are already outlined in Chapter 5. These equations are rederived here for completeness of this chapter. If one uses two metallic samples for A and B, then the thermal wave reflection coefficients at the absorber - substrate boundaries defined by

$$R_A = \frac{(1 - e_A/e_s)}{(1 + e_A/e_s)}$$

$$R_B = \frac{(1 - e_B/e_s)}{(1 + e_B/e_s)} \quad (7.12)$$

would be negative for all nonconducting films because for these $e_s \ll e_A$ or e_B . In such a situation, equation (7.10) simplifies to

$$\frac{A_A}{A_B} = \left[\frac{e_A[e_B + 4e_s(1 - e_s/e_B)]}{e_B[e_A + 4e_s(1 - e_s/e_A)]} \right]^{1/2} \quad (7.13)$$

Squaring both sides of (7.13) and crossmultiplying, we get

$$\left(\frac{A_A}{A_B}\right)^2 e_B [e_A + 4e_s(1 - e_s/e_A)] = e_A [e_B + 4e_s(1 - e_s/e_B)]$$

For further algebraic simplifications, we can write a quadratic equation in terms of thermal effusivity of the absorber film e_s , as given below.

$$4\left[\left(\frac{A_A}{A_B}\right)^2 e_B/e_A - e_A/e_B\right]e_s^2 - 4\left[\left(\frac{A_A}{A_B}\right)^2 e_B - e_A\right]e_s - \left[\left(\frac{A_A}{A_B}\right)^2 e_B e_A - e_A e_B\right] = 0$$

Therefore, one can evaluate the thermal effusivity of the absorber film in the following way

$$e_s = \frac{\left[\left(\frac{A_A}{A_B}\right)^2 e_B - e_A\right] \pm \sqrt{\left[\left(\frac{A_A}{A_B}\right)^2 e_B - e_A\right]^2 + \left[\frac{e_B}{e_A} \left(\frac{A_A}{A_B}\right)^2 - \frac{e_A}{e_B}\right] e_A e_B \left[\left(\frac{A_A}{A_B}\right)^2 - 1\right]}}{2\left[\frac{e_B}{e_A} \left(\frac{A_A}{A_B}\right)^2 - \frac{e_A}{e_B}\right]} \quad (7.14)$$

Retaining the amplitude ratio term intact like this, enables one to eliminate PA cell as well as the experimental parameters. Knowing e_A and e_B and measuring the amplitude ratio, one can evaluate e_s . When either R_A or R_B or both are positive, equations (7.13) and (7.14) take different forms. These cases are not discussed further here, as for nonconducting films R_A and R_B would be negative when samples A and B are metallic. We have limited our investigations to light absorbing low thermal conductivity films in this work.

The values of the PA phases Φ_A and Φ_B appearing in equation (7.11) cannot be separated and treated independently because one doesn't know the absolute phases from the two regions of the sample in the experiment. Equation (7.11) can be rewritten to evaluate e_s , using standard trigonometric formulae.

$$\tan(\Phi_A - \Phi_B) = \tan\left[\tan^{-1}\left(1 + \frac{e_A}{e_s}\right) - \tan^{-1}\left(1 + \frac{e_B}{e_s}\right)\right]$$

$$ie \quad \tan(\Phi_A - \Phi_B) = \frac{(1 + \frac{e_A}{e_s}) - (1 + \frac{e_B}{e_s})}{1 + (1 + \frac{e_A}{e_s})(1 + \frac{e_B}{e_s})}$$

After algebraic simplification one gets

$$2e_s^2 - \left[\frac{(e_A - e_B)}{\tan(\Phi_A - \Phi_B)} - (e_A + e_B) \right] e_s + e_A e_B = 0$$

Therefore the thermal effusivity, e_s , of the thin film absorber is given by

$$e_s = \frac{\chi \pm (\chi^2 - 8e_A e_B)^{1/2}}{4} \quad (7.15)$$

where

$$\chi = \frac{(e_A - e_B)}{\tan(\Phi_A - \Phi_B)} - (e_A + e_B)$$

Knowing e_A and e_B and measuring $(\Phi_A - \Phi_B)$ as the absorber film is scanned across the backing boundary, one can determine e_s .

7. 3 Experimental method

The small volume PA cell and the microprocessor controlled scanning unit already described in Chapter 2 has been used for measurements. In most of our experiments, one step corresponds to a distance of 0.25 mm and the delay between steps is a few minutes which is the time taken for the lock-in amplifier readings to stabilize. The block diagram of the experimental set up is already shown in Fig 2.2. A 120 mW He - Cd laser (Kimmon Electric Co. Ltd, Model 1K 4122 R-F) of wavelength 442nm is used as the radiation source for all the measurements reported in this chapter. A chopping frequency of 40 Hz has been chosen to correspond to the best performance of the PA cell. The PA signal amplitude and phase have been measured with a double phase lock-in amplifier (Stanford SR 830).

The main advantage of the present technique is that the measurements are independent of PA cell parameters and experimental conditions. As one scans the surface

of the film across the substrate boundary, the backing for the film sample is smoothly changed from A to B. The setup has been tested several times by having samples A and B made of the same material and a good light absorber such as carbon black coated as a film. In this case, as expected, there is no change in PA phase or amplitude as the backing is changed from A to B making amplitude ratio unity and phase difference zero.

We have carried out a series of measurements to test the validity of the assumptions made to arrive at equations (7.14) and (7.15). We have carried out measurements with commercially available black enamel paints with the intention of measuring their thermal effusivities. We have chosen a substrate configuration in which substrate A is brass and substrate B is steel. The substrate is a few mm thick, about 15 mm long and 10 mm wide. The paint sample is coated over the substrate with a brush and carefully measured the thickness of the film after drying. It has then been subjected to PA scanning experiment and measured the amplitude ratio and phase difference of the PA signal generated from the two regions of the sample with backings A and B. The experiments have been repeated for different thicknesses of the same sample to find out how far the thermal effusivity measured by this technique vary with thickness and to determine the thickness value below which the technique can be applied without ambiguity. Later, the experiments have been repeated on three more different brands of black enamel paint available in the market and their thermal effusivities have been determined.

Measurements have also been carried out on a thin film sample of polyacetal whose thermal parameters - thermal conductivity and heat capacity - are known. This sample has been prepared on the same substrate to a thickness $\approx 10 \mu m$. Polyacetal is coated on the substrate by the dipping method. For this a dilute solution of polyacetal is prepared by dissolving it in a solvent, Toluene. The substrate is dipped in the solution for a little time and taken out. After a few hours drying at room temperature, the film

formed on the surface of the substrate is hand lapped gently for thinning down to a thickness $\approx 10 \mu m$. Polyacetal is black and is a good absorber of light at all wavelengths. A comparison has been made between the thermal effusivity measured by the present technique and thermal effusivity already reported by previous workers. The results are given below.

7.4 Results and discussion

A typical PA amplitude and phase plot obtained with one brand of black paint (brand 1) as the absorber film sample scanned with the light beam is shown in Fig 7.2. The sharp changes in amplitude and phase correspond to the point where the light beam crosses the boundary between substrates A and B (brass and steel). Some uncertainty in PA signal occurs as the light beam crosses the boundary due to the finite spot size of the beam, but the signal is very clean when the substrate is either A or B. The uncertainties in amplitude and phase measurements are estimated to be less than 2%. The thermal effusivity of this brand of black paint has been evaluated using equations (7.14) and (7.15) from amplitude ratio and phase difference values measured. The effusivity values of the substrate, brass and steel, used in these calculations are 0.443 and 0.34 cal cm⁻² K⁻¹ sec^{-1/2} respectively.

The variation of thermal effusivity obtained for one brand of black enamel paint (Brand 1) using PA amplitude ratio and phase difference techniques with thickness of the film are plotted in Fig 7.3. As is evident from this figure, the effusivity values determined by the two methods do vary with thickness, the variation being more in phase difference measurement. But, in the limit of small thickness, say for thickness less than $\approx 10 \mu m$, the effusivity values obtained by the two methods agree within experimental uncertainties. So for enamel paints we can conclude that the assumptions made in the theory are well valid below a thickness of the order of $10 \mu m$. This limit

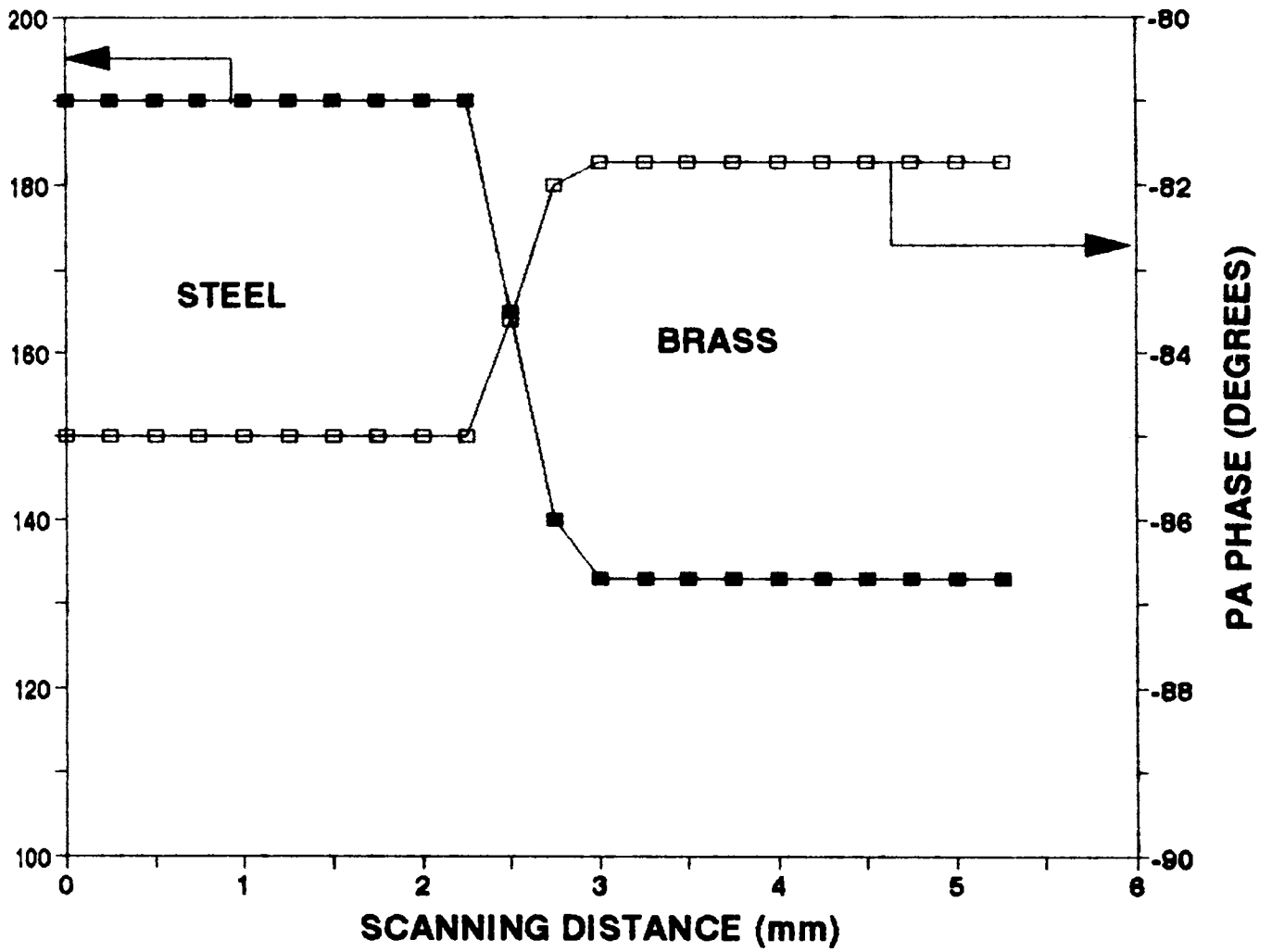


Fig 7.2 : Variations of PA amplitude and phase with scanning distance in the black paint (brand 1).

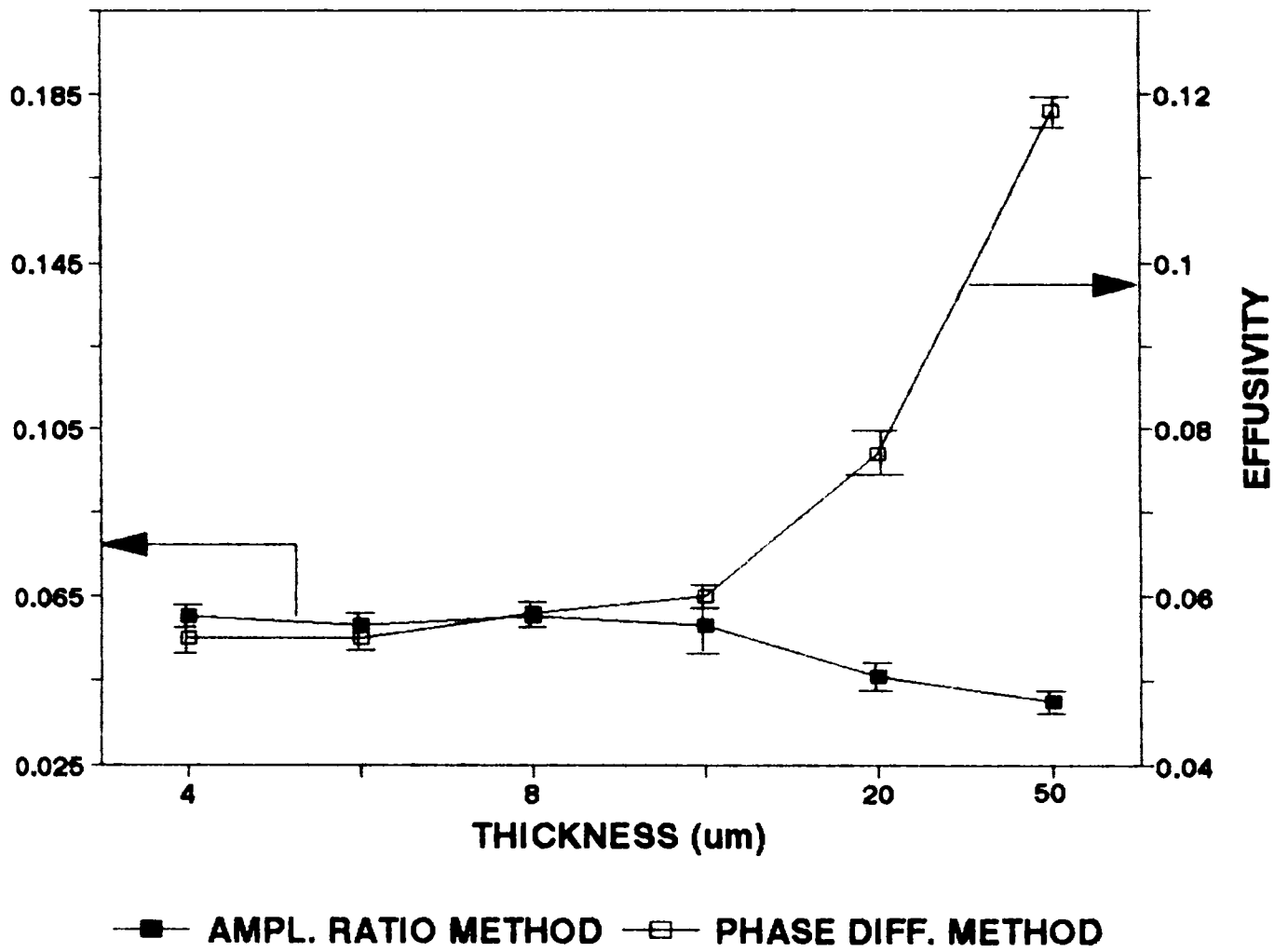


Fig 7.3 : Variations of thermal effusivity (in units of $\text{cal cm}^{-2}\text{K}^{-1}\text{sec}^{-1/2}$) with thickness of the film of black paint (brand 1).

holds good for almost all nonconducting films. Since the thickness of most practical thin films are less than $10\mu m$, the technique works well for all nonmetallic, light absorbing films. The thermal effusivity values determined by the two methods for this brand of black paint are tabulated in Table 7.1.

We have carried out measurements on three more brands of black enamel paints limiting the thickness to less than $10\mu m$ while preparing the films. Amplitude and phase plots obtained from these brands of black enamel paints are shown in figures 7.4, 7.5. and 7.6. Their thermal effusivities have been determined as before. These results are also tabulated in Table 7.1. It can be noted that the effusivity values for different samples, determined by the amplitude ratio and phase difference methods agree well within experimental limits.

It is interesting to note that different brands of paints have different thermal effusivity values. Unfortunately we couldn't cross check the effusivity values for the paints tabulated in Table 7.1 as no such data could be found in literature. The cross checking done with carbon black film is found to give effusivity values agreeing very well with available data which reaffirms the correctness and dependability of the technique.

The meaning of the difference in thermal effusivity of different brands of enamel paints in terms of their durability and stability is an interesting practical problem. This aspect is being studied more carefully. Our interest has only been the development of a photoacoustic technique which enables one to measure the thermal parameters of thin films. The method is independent of film thickness in the limit of thickness less than nearly $10\mu m$, the only limitation being that it should be light absorbing which can to a large extent be got over with a suitable choice of wavelength for many samples.

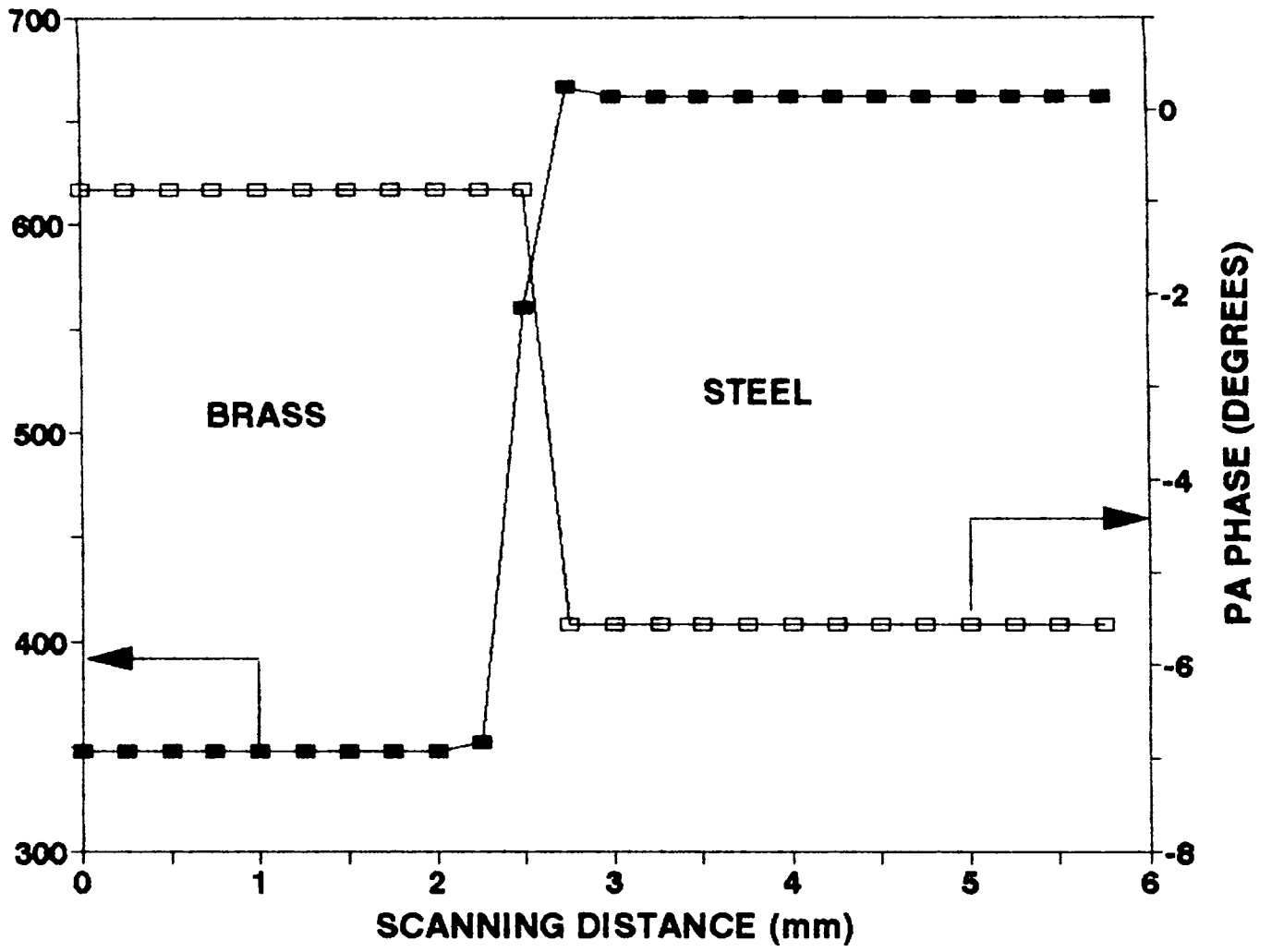


Fig 7.4 : Variations of PA amplitude and phase with scanning distance in the black paint (brand 2).

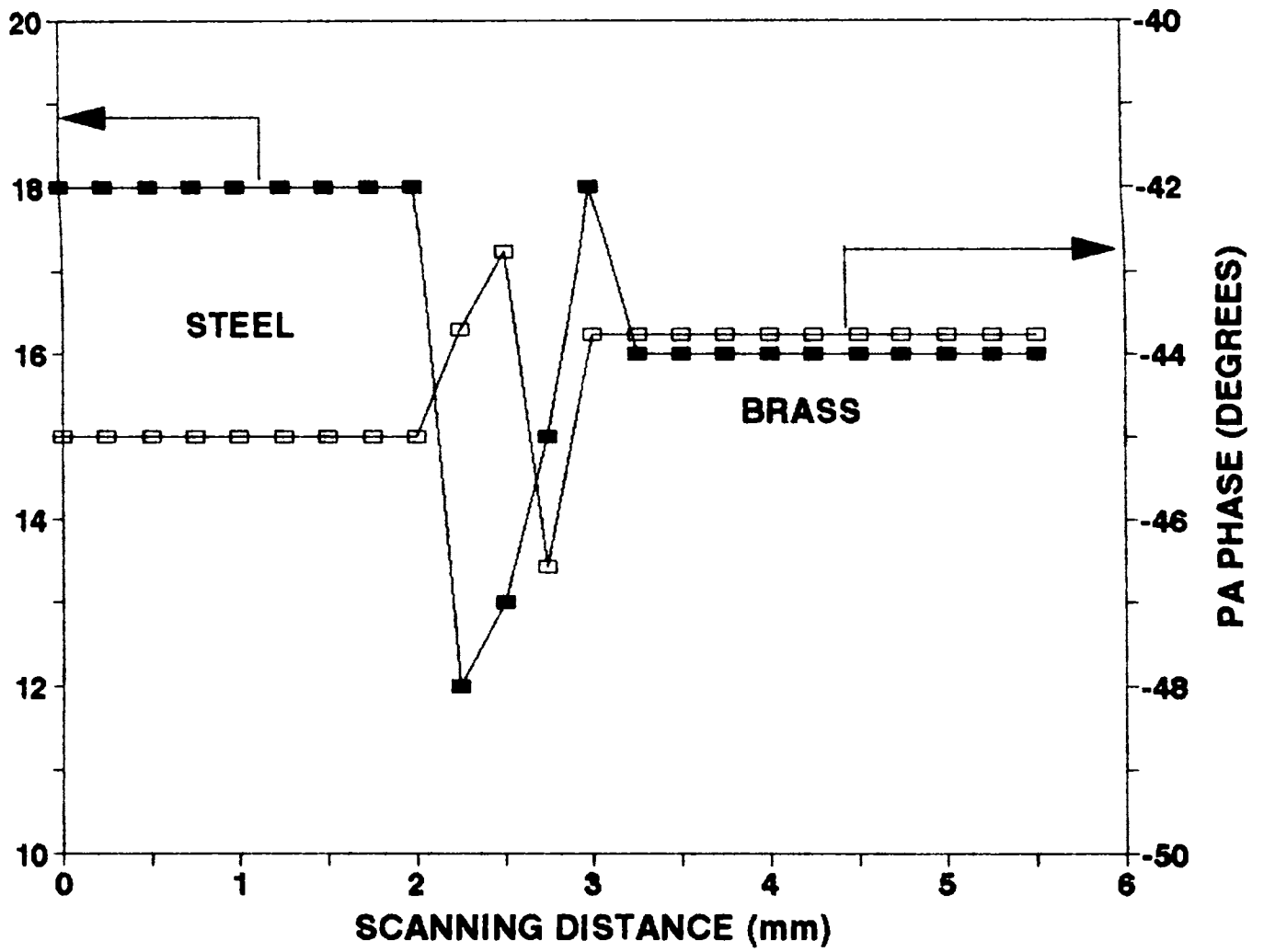


Fig 7.5 : Variations of PA amplitude and phase with scanning distance in the black paint (brand 3).

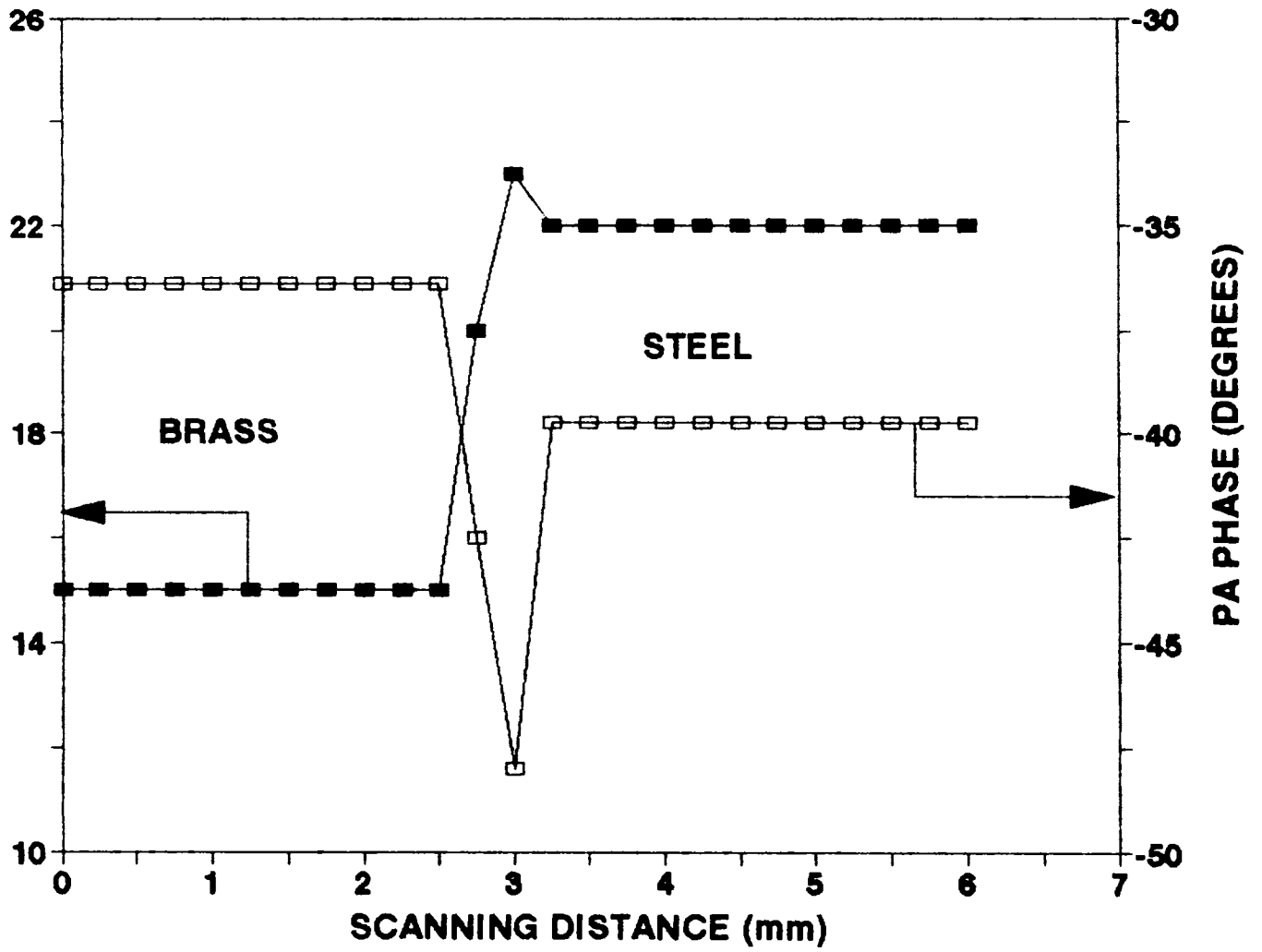


Fig 7.6 : Variations of PA amplitude and phase with scanning distance in the black paint (brand 4).

Table 7.1

Thermal effusivities of four brands of black enamel paints determined from PA amplitude ratio and phase difference measurements

Sample	Thermal effusivity ($\times 10^{-2} \text{ Cal cm}^{-2} \text{ K}^{-1} \text{ sec}^{-1/2}$)	
	Amplitude ratio measurement	Phase difference measurement
Brand 1	5.81 \pm 0.11	6 \pm 0.12
Brand 2	6.49 \pm 0.13	7 \pm 0.14
Brand 3	3.91 \pm 0.08	3.78 \pm 0.076
Brand 4	5.91 \pm 0.11	6.21 \pm 0.11

Table 7.2

Thermal effusivity of polyacetal in units of $\times 10^{-2} \text{ cal cm}^{-2} \text{ K}^{-1} \text{ sec}^{-1/2}$.

Measured values		Value reported in literature *
PA amplitude ratio method	PA phase difference method	
1.75 \pm 0.05	2.03 \pm 0.05	1.84

* Madhusoodanan *et al.* J. Appl. Phys. **62** , 1162 (1987)

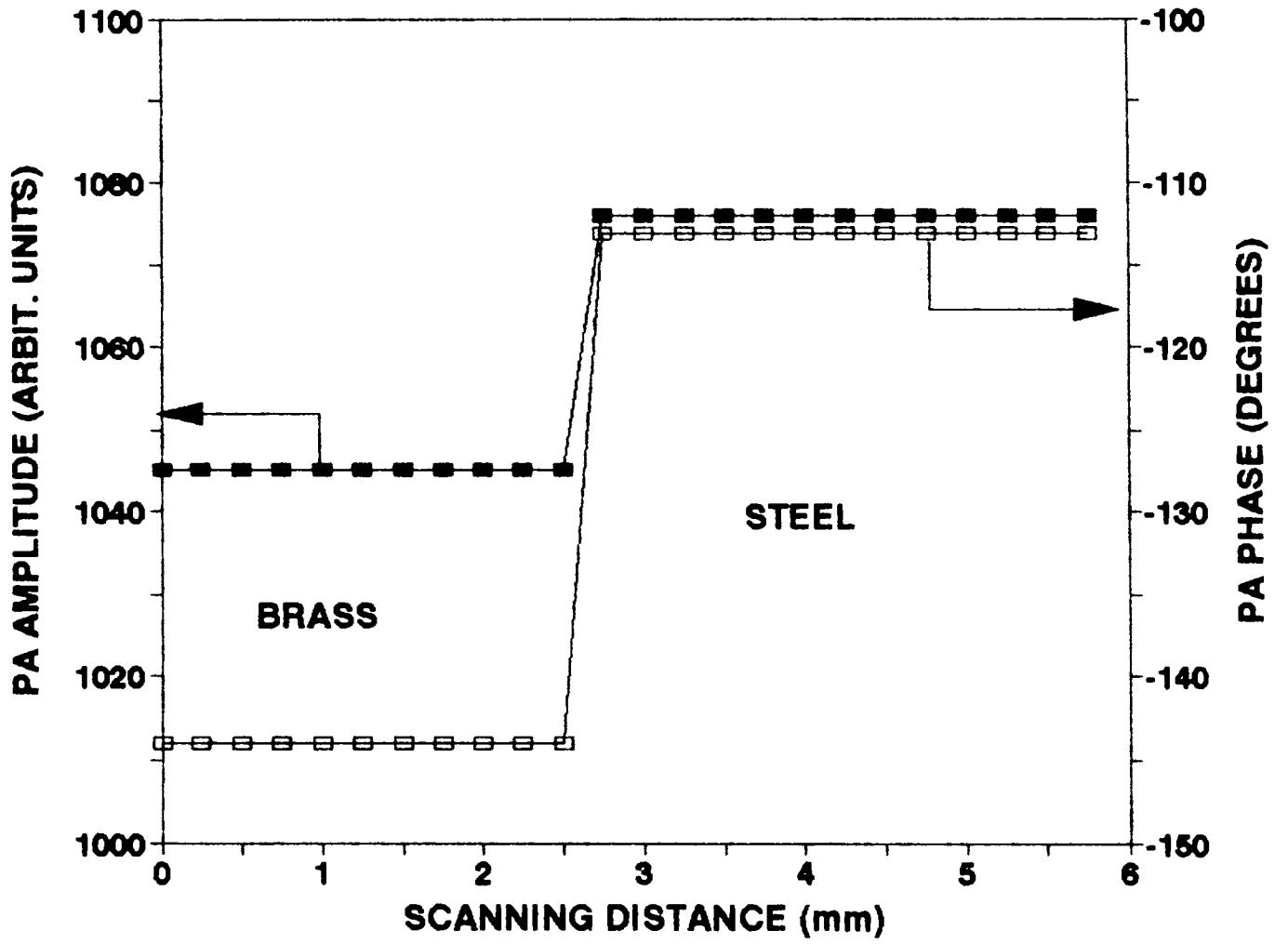


Fig 7.7 : Variations of PA amplitude and phase with scanning distance in the polyacetal film

The PA amplitude and phase plots obtained with polyacetal film having thickness $\approx 10\mu\text{m}$ is plotted in Fig. 7.7. The measured values of the thermal effusivity of polyacetal film by the amplitude ratio and phase difference methods along with the value already reported in literature are tabulated in Table 7.2. A comparison of the values tabulated in this table shows that the agreement between measured and reported values is good within experimental uncertainties.

7.5 Conclusions

Thus we have demonstrated a relatively simple and convenient photoacoustic scanning technique to measure thermal effusivity of light absorbing thin films. The technique is free of PA cell parameters and experimental conditions. It does not involve any complex frequency analysis of the PA signal and is relatively error free. The technique can easily be automated for routine measurement of thermal parameters of thin film samples. Our works demonstrate that the technique works well as long as the thickness is limited to $\approx 10\mu\text{m}$ to comply with the assumptions and approximations made to derive equations (7.14) and (7.15). Moreover, the experiments should be limited to light absorbing and low thermal conductivity films. As long as the thermal conductivity of the material of the film is lower than those of the substrate material, the technique should work. Since there are not many methods developed to measure thermal parameters of thin films, we think this technique is very valuable and will find applications. One can keep the substrate combination shown in Fig. 7.1 in a vacuum coating unit while preparing a film along with the true substrate of the film and measure the thermal effusivity as outlined in this chapter. The limitation that the film should be light absorbing can be got over by choosing appropriate wavelength for the laser or one can use a focused beam of white light. This aspect as well as more experimentation on different films will be undertaken later.

References

- [1] A. Rosencwaig, **Photoacoustics and photoacoustic spectroscopy** (Wiley, New York 1980)
- [2] P. Charpentier, F. Lepoutre and L. Bertrand **J. Appl. Phys.** **53**, 608 (1982)
- [3] R. T. Swimm **Appl. Phys. Lett.** **42**, 955 (1983)
- [4] A. Lachaine and P. Poulet **Appl. Phys. Lett.** **45**, 953 (1984)
- [5] K. N. Madhusoodanan, M. R. Thomas and J. Philip **J. Appl. Phys.** **62**, 1162 (1987)
- [6] A. Rosencwaig and A. Gersho **J. Appl. Phys.** **47**, 64 (1976)
- [7] C. L. Cesar, H. Vargas, J. Mendes Filho and L. C. M. Miranda, **Appl. Phys. Lett.** **43**, 555 (1983)
- [8] A. Lachaine, **J. Appl. Phys.** **57**, 5075 (1985)
- [9] B. Bonno, J. L. Laporte and Y. Rousset, **J. Appl. Phys.** **67**, 2253 (1990)
- [10] U. Zammit, M. Marinelli, R. Pizzo Ferrantto, F. Scudieri and S. Martellucci, **J. Phys. E: Sci. Instrum.** **21**, 935 (1988)
- [11] O. Pessoa Jr, C. L. Cesar, N. A. Patel, H. Vargas, C. C. Ghizoni and L. C. M. Miranda, **J. Appl. Phys.** **59** 1316 (1986)
- [12] S. Thomas, J. Isaac and J. Philip, **Rev. Sci. Instrum.** **66**, 3907 (1995)

CHAPTER 8

SUMMARY AND CONCLUSION

We conclude this thesis by summarising the work already presented in the earlier chapters and by outlining the scope for doing further work in this area.

The photoacoustic technique has emerged as a powerful analytical technique to investigate optical and thermal properties of matter in all forms. Because of its inherent sensitivity and adaptability to analyse samples in any form, it has become a standard spectroscopic tool to analyse a wide variety of samples ranging from superconductors to human blood. We have outlined various aspects of the photoacoustic effect and its applications in the introductory chapter of the thesis. A brief history of the effect and its development as an analytical tool over a period of 100 years is briefly sketched. The theory of the photoacoustic effect in condensed media, mechanism of signal generation and the principles behind using it for optical and thermal characterisation of solid samples are described.

The instrumentation requirements for undertaking photoacoustics work are discussed at length in the second chapter. The technical details of all the instruments and parts used in this work are described.

We have used the photoacoustic technique for two purposes. First, the technique is used to do imaging and depth profiling in solids. We have shown how one can do imaging of surfaces and interiors of solid materials. Our work clearly demonstrates that the technique can bring out features of surface and subsurface inhomogeneities of solid samples. Our experiments indicate that the photoacoustic effect can be used as a convenient nondestructive testing method where the conventional techniques often fail. It is a matter of time that a full fledged photoacoustic imaging unit would be available

commercially. This technique is likely to find applications in thermal wave imaging of solid matter, *in situ* inspection of integrated circuits during fabrication, component testing during micromachining etc.

The second application to which we have used the photoacoustic technique is to measure thermal parameters such as diffusivity and effusivity of solid samples in the bulk and thin film forms. After outlining the available techniques to measure thermal diffusivity and effusivity using photoacoustic technique, we show how a photoacoustic scanning technique with a special sample configuration enables one to measure thermal effusivity of solid samples in the bulk and thin film forms. Being a relative measurement technique, our method is free of many of the drawbacks of the existing techniques. We have shown that the photoacoustic scanning technique can be developed as a standard computerised experimental technique to measure thermal effusivity of bulk solid and thin film samples in a routine way. Since photoacoustic amplitude ratio and phase difference are the measured parameters to evaluate thermal effusivity, the method is free of photoacoustic cell parameters and experimental conditions. We have also demonstrated how this technique can be extended to determine thermal effusivity of light absorbing thin films, which otherwise is very difficult to measure.

Further work and experimentation can easily lead to development of an automated photoacoustic imaging setup which could work as a photoacoustic microscope. We are sure a fully computer controlled setup would soon be available commercially for routine nondestructive testing of solid samples.

The photoacoustic techniques of measuring thermal diffusivity and effusivity have many advantageous over other techniques. By combining diffusivity and effusivity data for a sample, one can determine the thermal conductivity and heat capacity of a sample simultaneously. This makes the photoacoustic technique a unique one which enables one

to determine two fundamental properties of a solid. We are sure more measurements on different samples will be carried out soon to determine their thermal conductivity and heat capacity. We also plan to undertake more work in this direction. Moreover, one can also carry out the above measurements as a function of temperature which would enable one to explore features of thermodynamic changes and phase transitions in solid samples.

In summary, the photoacoustic technique offers tremendous possibilities for carrying out imaging work and thermal characterisation of solids.

* * *

Appendix 1

Assembly Language program for 8085 for the two dimensional PA scanning unit.

Software for forward X directional movement of PA scanning unit.

<u>Location</u>	<u>OP code</u>	<u>Mnemonic</u>	<u>Comments</u>
1000	21	LXI H, 1100	set counter 1
1001	00		at 1100
1002	11		
1003	36	MVI M,00	Initialize
1004	00		counter 1
1005	3E	MVI A,80	load control word
1006	80		in register A
1007	D3	out,03	load control
1008	03		register
1009	21	LXI H, 1105	set counter 2
100A	05		at 1105
100B	11		
100C	36	MVI M,00	initialize
100D	00		counter 2
100E	21	LXI H, 1102	set counter 3
100F	02		at 1102
1010	11		
1011	36	MVI M, 00	initialize
1012	00		counter 3
1013	21	LXI H, 1101	set counter 4
1014	01		at 1101
1015	11		
1016	36	MVI M, 00	initialize
1017	00		counter 4
1018	3E	MVI A, 05	send informations
1019	05		to port A for
101A	D3	out,00	switching on motor 1
101B	00		
101C	CD	Call 1400	Delay for
101D	00		0.5 second
101E	14		
101F	3E	MVI A,09	
1020	09		

<u>Location</u>	<u>OP code</u>	<u>Mnemonic</u>	<u>Comments</u>
1021	D3	out 00	
1022	00		
1023	CD	Call, 1400	
1024	00		
1025	14		
1026	3E	MVI A, 0A	
1027	0A		
1028	D3	out 00	
1029	00		
102A	CD	Call, 1400	
102B	00		
102C	14		
102D	3E	MVI A, 06	
102E	06		
102F	D3	out, 00	
1030	00		
1031	CD	Call 1400	
1032	00		
1033	14		
1034	21	LXI H,1101	add 1 in
1035	01		counter 4
1036	11		
1037	34	INR M	
1038	7E	MOV A,M	
1039	21	LXI H, 1110	
103A	10		
103B	11		
103C	BE	CMP, M	compare content of
103D	CC	CZ , 1050	counter 4
103E	50		
103F	10		
1040	C3	JMP, 1018	
1041	18		
1042	10		
1043	76	HLT	

<u>Location</u>	<u>OP code</u>	<u>Mnemonic</u>	<u>Comments</u>
1050	3E	MVI A,00	
1051	00		
1052	D3	out, 00	initialize
1053	00		Port A
1054	CD	Call, 1420	Delay for
1055	20		1 minute
1056	14		
1057	21	LXI, 1105	
1058	05		
1059	11		add 1
105A	34	INR	in counter 2
105B	7E	MOV A,M	
105C	21	LXI H, 1116	compare content
105D	16		of counter 2
105E	11		
105F	BE	CMP, M	
1060	CC	CZ, 1300	operate
1061	00		Y-motor
1062	13		
1063	C3	JMP, 1310	operate
1064	13		X- motor
1065	10		forward
1066	76	HLT	

Software for Y directional movement of PA scanning unit.

<u>Location</u>	<u>OP code</u>	<u>Mnemonic</u>	<u>Comments</u>
1300	3E	MVI, 80	
1301	80		
1302	D3	out, 03	load control
1303	03		word in
1304	21	LXI H, 1103	control register
1305	03		set counter 5
1306	11		
1307	36	MVI M, 00	initialize
1308	00		counter 5
1309	3E	MVI A, 05	send information
130A	05		to port B for
130B	D3	out,01	switching on motor 2
130C	01		
130D	CD	Call 1400	Delay for
130E	00		0.5 second
130F	14		
1310	3E	MVI A,09	
1311	09		
1312	D3	out 01	
1313	01		
1314	CD	Call, 1400	
1315	00		
1316	14		
1317	3E	MVI A, 0A	
1318	0A		
1319	D3	out 01	
131A	01		
131B	CD	Call, 1400	
131C	00		
131D	14		
131E	3E	MVI A, 06	
131F	06		
1320	D3	out, 01	

<u>Location</u>	<u>OP code</u>	<u>Mnemonic</u>	<u>Comments</u>
1321	01		
1322	CD	Call 1400	
1323	00		
1324	14		
1325	21	LXI H,1103	add 1 in
1326	01		counter 5
1327	11		
1328	34	INR M	
1329	7E	MOV A,M	
132A	21	LXI H, 1111	
132B	11		
132C	11		
132D	BE	CMP, M	compare content of
132E	CC	CZ , 1200	counter 5
132F	00		
1330	12		
1331	C3	JMP, 1309	
1332	09		
1333	13		
1334	76	HLT	

Software for -ve X - directional movement of PA scanning unit.

<u>Location</u>	<u>OP code</u>	<u>Mnemonic</u>	<u>Comments</u>
1500	3E	MVI A,80	load control
1501	80		in register A
1502	D3	out,03	load control
1503	03		register
1504	21	LXI H, 1102	place 01
1505	02		in counter 3
1506	11		
1507	36	MVI M,01	
1508	01		
1509	21	LXI H, 1106	set counter 6
150A	06		at 1106
150B	11		
150C	36	MVI M, 00	initialize
150D	00		counter 6
150E	21	LXI H, 1104	set counter 7
150F	04		at 1104
1510	11		
1511	36	MVI M, 00	initialize
1512	00		counter 7
1513	3E	MVI A, 06	send information to
1514	06		port A for switch on
1515	D3	out,00	motor 1 in reverse
1516	00		direction
1517	CD	Call 1400	Delay for
1518	00		0.5 second
1519	14		
151A	3E	MVI A,0A	
151B	0A		
151C	D3	out 00	
151D	00		
151E	CD	Call, 1400	
151F	00		
1520	14		

<u>Location</u>	<u>OP code</u>	<u>Mnemonic</u>	<u>Comments</u>
1521	3E	MVI A, 09	
1522	09		
1523	D3	out 00	
1524	00		
1525	CD	Call, 1400	
1526	00		
1527	14		
1528	3E	MVI A, 05	
1529	05		
152A	D3	out, 00	
152B	00		
152C	CD	Call 1400	
152D	00		
152E	14		
152F	21	LXI H,1104	add 1 in
1530	04		counter 7
1531	11		
1532	34	INR M	
1533	7E	MOV A,M	
1534	21	LXI H, 1112	
1535	12		
1536	11		compare content of
1537	BE	CMP, M	counter 7
1538	CC	CZ , 1070	go to
1539	70		subroutine
153A	10		
153B	C3	JMP, 1513	repeat
153C	13		
153D	15		
153E	76	HLT	

<u>Location</u>	<u>OP code</u>	<u>Mnemonic</u>	<u>Comments</u>
1070	3E	MVI A,00	
1071	00		
1072	D3	out, 00	initialize
1073	00		Port A
1074	CD	Call, 1420	Delay for
1075	20		1 minute
1076	14		
1077	21	LXI, 1106	
1078	06		
1079	11		
107A	34	INR	add 1 in counter 6
107B	7E	MOV A,M	
107C	21	LXI H, 1117	compare content
107D	17		of counter 6
107E	11		
107F	BE	CMP, M	
1080	CC	CZ, 1300	operate
1081	00		Y- motor
1082	13		
1083	C3	JMP, 150E	operate
1084	0E		X- motor
1085	15		reverse
1086	76	HLT	

<u>Location</u>	<u>OP code</u>	<u>Mnemonic</u>	<u>Comments</u>
1200	21	LXI H, 1100	
1201	00		
1202	11		add 1 in
1203	34	INR	counter 1
1204	7E	MOV A, M	
1205	21	LXI H, 1113	
1206	13		compare content
1207	11		of counter 1
1208	BE	CMP	
1209	DC	CC, 1210	
120A	10		
120B	12		
120C	CD	CALL, 036E	display
120D	6E		end signal
120E	03		
120F	76	HLT	
1210	21	LXI H, 1102	compare content
1211	02		of counter 3
1212	11		
1213	7E	MOV A, M	
1214	FE	CPI, 01	
1215	01		
1216	CC	CZ, 1005	operate
1217	05		X- motor
1218	10		forward
1219	C3	JMP, 1500	operate
121A	00		X - motor
121B	15		reverse
121C	76	HLT	

Software for 0.5 second delay after each step of stepper motors

<u>Location</u>	<u>OP code</u>	<u>Mnemonic</u>	<u>Comments</u>
1400	0E	MVI E,00	set delay
1401	00		0.5 second
1402	11	LXI D, FFFF	
1403	FF		
1404	FF		
1405	7B	MOV A, E	
1406	15	DCR	
1407	A2	AND D	
1408	C2	JNZ, 1405	
1409	05		
140A	14		
140B	0C	INR	
140C	79		
140D	21	LXI H, 1114	
140E	14		
140F	11		
1410	BE	CMP, M	
1411	C2	JNZ, 1402	
1412	02		
1413	14		
1414	C9	RET	

<u>Location</u>	<u>OP_code</u>	<u>Mnemonic</u>	<u>Comments</u>
1420	21	LXI H, 1120	set delay
1421	20		of 1 minute
1422	11		
1423	36	MVI M, 80	
1424	80		
1425	23	INX H	
1426	36	MVI M, 80	
1427	80		
1428	23	INX H	
1429	36	MVI M, 80	
142A	80		
142B	35	DCR, M	
142C	C2	JNZ, 142B	
142D	2B		
142E	14		
142F	2B	DCX, H	
1430	35	DCR, M	
1431	C2	JNZ, 1428	
1432	28		
1433	14		
1434	2B	DCX, H	
1435	35	DCR, M	
1436	C2	JNZ, 1425	
1437	25		
1438	14		
1439	C9	RET	